2016

Computation Of Acoustic Ressure Fields Produced In Feline Brain By High-Intensity Focused Ultrasound

Nazanin Omidi
University of Mississippi

COMPUTATION OF ACOUSTIC RESSURE FIELDS PRODUCED IN FELINE BRAIN BY HIGH-INTENSITY FOCUSED ULTRASOUND

A Thesis
presented in partial fulfillment of requirements
for the degree of Master of Science
in the Department of Physics and Astronomy
The University of Mississippi

by

NAZANIN OMIDI

August 2016

ABSTRACT

In 1975, Dunn et al. (JASA 58:512-514) showed that a simple relation describes the ultrasonic threshold for cavitation–induced changes in the mammalian brain. The thresholds for tissue damage were estimated for a variety of acoustic parameters in exposed feline brain. The goal of this study was to improve the estimates for acoustic pressures and intensities present in vivo during those experimental exposures by estimating them using nonlinear rather than linear theory. In our current project, the acoustic pressure waveforms produced in the brains of anesthetized felines were numerically simulated for a spherically focused, nominally f1-transducer (focal length = 13 cm) at increasing values of the source pressure at frequencies of 1, 3, and 9 MHz. The corresponding focal intensities were correlated with the experimental data of Dunn et al. The focal pressure waveforms were also computed at the location of the true maximum. For low source pressures, the computed waveforms were the same as those determined using linear theory, and the focal intensities matched experimentally determined values. For higher source pressures, the focal pressure waveforms became increasingly distorted, with the compressional amplitude of the wave becoming greater, and the rarefactional amplitude becoming lower, than the values calculated using linear theory. The implications of these results for clinical exposures are discussed.

LIST OF ABBREVIATIONS AND SYMBOLS

P Pressure

I Intensity

∇ Gradient Operator

∇^2 Laplacian Operator

r Position vector in radial direction

x Position vector in axial direction

t Time

ρ Density

β Nonlinearity coefficient

α Absorption coefficient

c Speed of Sound

a Radius of transducer

∂ Partial derivatives

δ Diffusivity of sound

ω Angular frequency

f Frequency

ACKNOWLEDGEMENTS

I would like to express my sincere gratitude to the Department of Physics and Astronomy, for letting me fulfill my dream of being a student here. A special acknowledgment is forwarded to Dr. Luca Bombelli for his kindness, all tremendous helping, and advising during the years of my study. Most of all, I am fully indebted to Dr. Cecille Labuda, my advisor and mentor, for her understanding and patience. This project would never have been completed without her persistent support, help, and intellectual guidance. I would also like to thank deeply my research and thesis advisor, Dr. Charles C. Church for giving me this opportunity to work on this project and all his guidance and continual support throughout this research work and writing process. To my committee, Dr. Cecille Labuda, Dr. Charles C. Church, and Dr. Joel Mobley, I am extremely grateful for your assistance and suggestions throughout my project and taking the time to review this thesis. Thanks also go out to all of the members of the Physical Ultrasonic research group, the staff of the National Center for Physical Acoustics, all my friends, and my classmates at the University of Mississippi for the positive influence and assistance during my work.

Most importantly, my loveliest and deepest appreciation goes to my best parents and siblings for their encouragement and unconditional support especially during my unbearable times and for pushing me farther than I thought I could go. All my love to them, for finding me the light, whenever it was far away.

TABLE OF CONTENTS

LIST OF TABLES

LIST OF FIGURES

CHAPTER I: INTRODUCTION

1.1 Ultrasound

The American National Standards Institute defines ultrasound (US) as a mechanical pressure waveform that oscillates at frequencies greater than 20 kHz, i.e., frequencies higher than the upper perception limit of human hearing. Figure 1.1 shows the frequency spectrum of acoustic waves, and phenomena and applications affiliated with different regions. Specifically, the ultrasonic range utilized in biomedical applications is between 0.5-10 MHz.

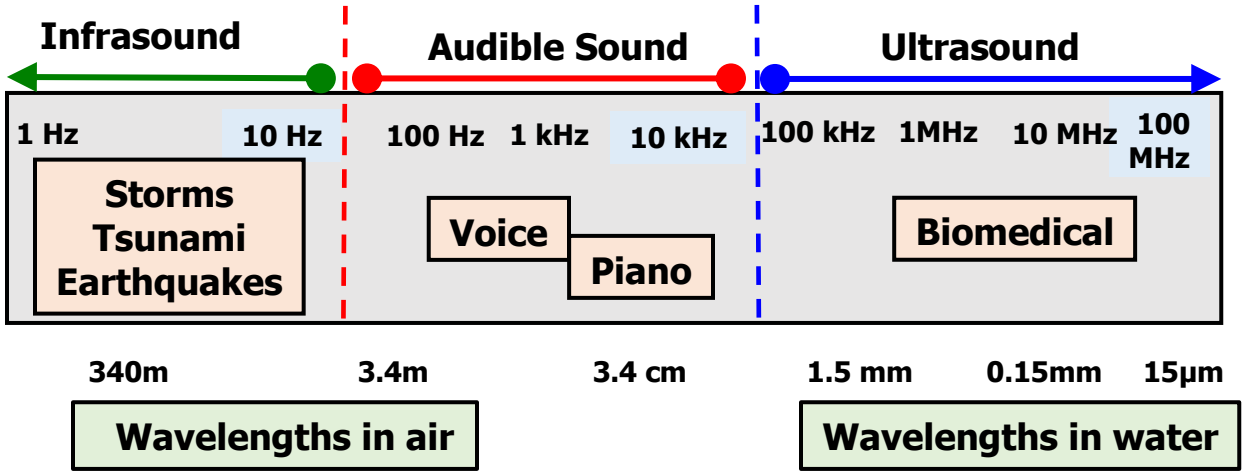

Figure1.1: The frequencies between 20 Hz-20,000 Hz are the normal range of human audibility. Sound at frequencies above the human hearing detection range is called ultrasound. Frequencies below 20 Hz are designated as infrasound (*Courtesy of Joel Mobley*).

Dunn and Fry [1] explained further that the ultrasound pressure waveform is similar to audible sound, considering its physical properties, only that it cannot be heard by humans. By 1893 a whistle was made by Sir Francis Galton that could produce ultrasound waves [2]. The

detection of submarines by Paul Langevin in 1917 [3] was the first attempt to apply the acoustics of ultrasound. In 1945, the adaptation of radar techniques resulted in the construction of pulsed ultrasonic instruments that could operate on a higher range of frequencies. A number of techniques were developed in which ultrasound in the frequency range of 0.02MHz could be used in Brillouin scattering applications [4] which uses the scattering of the light in a biomedical medium due to the interaction of the light with medium inhomogeneities which can result in thermal fluctuations in the medium.

The advanced possibilities of ultrasound technology in medical applications date back to the mid-20th century after the end of World War II [5]. Ultrasound techniques became widely used to visualize the internal body for diagnosis of tissue disease; ultrasound imaging became an important tool for treatment planning. Progress in the field of ultrasound in medicine was widely embraced not only as a diagnostic imaging tool but also as a therapeutic modality; it was capable of producing destructive and modification effects on living tissue [6],[1]. The most significant examples of ultrasound therapy are drug delivery and focused ultrasound surgery which have been demonstrated clinically in the past few years [7]. In addition, construction of piezoelectric materials, lens-focusing systems, as well as field quantifying systems have encouraged the application of high intensity ultrasound in the production of reversible and irreversible effects in a living medium [8]. Further, scientific developments have led to the emergence of two distinct modes of operation [4]. First is passive use, a mode in which the sound field does not significantly change the structure or the functionality of the examined system. The second method involves active use, an application in which reversible or irreversible alteration of the medium is the objective. For the active use, motivation for more research was energized by the observation that

ultrasound was capable of giving a deeper heating effect in biological media than the common superficial irradiation by infrared and other radiations [8].

1.2 Literature review:

Auditory response to ultrasound pressure waveforms*:* The hearing pathway through which ultrasonic pressure waveforms perceived by the ear are sensed and interpreted as sound in the brain was established [9]. Several studies done on this have been focused on determining whether the electrophysiological response of the hearing pathway to ultrasound is the same as that of audible acoustic stimuli. Research demonstrations in animals have shown that ultrasound induces auditory responses such that the ultrasonic pressure waveforms interact with the auditory system [10].

Taylor and Ashleman [11] measured the electrophysiological responses in cats with undistorted cochleae at three successive levels of the cat's auditory nervous system, the eighth cranial nerve, the medial geniculate nucleus as well as the primary auditory cortex. They showed that by destroying the cochlea, the auditory information cannot be registered in the hearing pathway.

Chou et al [10] reported electrical responses out of single auditory neurons in cats during pulsed microwave irradiation fields and acoustic clicks. Guy et al [12] also did further studies to demonstrate that the electrophysiological responses of the auditory pathway to the brains of cats is similar to the responses cats give to radiofrequency pulses.

Ultrasonic hearing was supported by a theoretical breakdown of acoustic vibrations induced in the heads of humans and animals [13] so that the perceived frequency of the induced sound is a function of head size. For example, for a man-sized head or a small animal head

consisting only of brain matter exposed to pulse microwave radiation, the acoustic pitch registered by a given animal is the same for all of its kind, regardless of the frequency of the induced ultrasound.

Diagnostic Historical Background: Medical ultrasound imaging has now been applied for at least six decades. The discovery of the piezoelectric effect by Pierre Curie in 1880 marked the beginning of the revolution of ultrasound imaging technology [14]. Many applications were made, e.g., applications in ships to detect depth and in metallurgy to detect fractures and other flaws in metals. A very important application followed the introduction of submarines during WW I. Prof. Langevin developed the use of sonar as a new means for detecting them and determining their locations by echo ranging in water [14].

The ability of ultrasound to have an impact on bio-media was initially observed in 1917 [15]. During the 1920's, Wood and Loomis demonstrated that ultrasound is capable of causing damage to various animal species [14]. Later Langevin demonstrated that small fish can die in a tank when subjected to ultrasound. The thermal impacts of ultrasound were utilized to burn tissues in the late 1940's when performing surgery, and also when destroying cancerous cells [16]. The detrimental effects of ultrasound when focused on neural tissues were examined by Fry et al [17]. The examination included reversible and irreversible damage to nerves as well as nerve conduction abnormalities. According to Fry et al., an exposure of 43.5 seconds to an ultrasound exposure intensity (I) rated at 35 W/cm^2 would cause a transient conduction obstruction in the ventral abdominal ganglion of crayfish. An ultrasound beam of the same intensity when exposed briefly to the neurons found in the lumbar enlargement of intact frogs would cause complete paralysis. These observations justified the idea that ultrasound has the capacity to produce thermal effects

that can hamper the conduction of nerves just as would be observed with other kinds of heating [18]. These observations as well as other severe bio-effects of ultrasound in animal laboratory specimens were officially recognized as potentially significant for diagnostic exposures in 1983 in the Safety Standard for Diagnostic Ultrasound Equipment [19], a joint effort by the American Institute of Ultrasound in Medicine (AIUM) and the National Electrical Manufacturers Association (NEMA). Other scholarly studies brought to the development of ultrasound equipment detailed information on important exposure parameters, including power, Spatial-Peak Temporal-Average Intensity (I_{SPTA}) and the Spatial-Peak Pulse-Average Intensity (I_{SPPA}). These averages were identified as being significant in determining severe bio-effects in animal experiments.

In 1976, the Food and Drug Administration (FDA) began monitoring safety issues of medical devices which included regulating diagnostic ultrasound equipment. The 1976 output levels were considered to be safe, but these were historically based and not scientifically determined. Therefore, in addition to the FDA, the AIUM's Bioeffects Committee adopted an ultrasound safety statement that reported no adverse patient bioeffects with diagnostic ultrasound exposure, or no significant biological effects on mammalian tissues exposed to intensities below 100 $\mathrm{mW/cm^2}$ in the low megahertz frequency range [5], [19].

***Therapeutic Historical Background*:** The early history of the investigation of ultrasound in medical applications for treatment was begun as early as the 1930's [5], [16]. The application involved the depositing of ultrasonic energy in tissues to stimulate desired biological effects. These early applications included trials on various conditions that could be treated by tissue heating [20], [21]. Scientific studies over the following years saw improved methods for effectual therapy of Meniere disease (a disorder in the inner ear that leads to loss of hearing and balance) through the

damaging of the vestibular nerve [1]. Scientific research demonstrated that trans-cranial ultrasound could stimulate or restrain neural activity at low intensities during a short exposure time in the brain without significant neural damage [9]. For this idea, trans-cranial stimulation was used as a therapy when diagnosing neurological disorders, for instance, epilepsy. This was recommended after some laboratory findings that demonstrated ultrasound can relieve seizure activity [11].

The application of ultrasound continued to develop under William J. Fry along with his brother Francis. J. Fry after World War II [5]. William had a strong passion for doing research on various aspects of ultrasound with particular attention to applications in biology and medicine. Immediately after the war, he left the Naval Research Laboratory in Washington DC where he had been designing piezoelectric transducers. He was seeking an opportunity to lead his research activities in a more dynamic atmosphere. Eventually, he obtained a position as a physicist at the University of Illinois working in the Bioacoustics Research Laboratory [5].

In the 1950's, the Fry brothers performed detailed theoretical and experimental analyses of the mammalian central nervous system [17] toward two related goals; first, using ultrasound exposure as a neuroanatomical method to better understand the close, detailed structure and function of biological tissue, and second to examine the influence of high intensity focused ultrasound (HIFU) on biological tissue and brain (brain was the priority point of interest) as a clinical surgical method [17],[23]. In the late 1950's, this study was publicized successfully and led to treatment of a series of human patients suffering from hypokinetic disorders. Particularly noteworthy was Parkinson's disease which also was treated using ultrasound directed towards localized tissues in the brain which behave abnormally before applying the HIFU. It was found

that the Parkinson tremor disappeared virtually immediately with the cessation of the sound pulse [5], [1].

Animal studies conducted at Illinois showed that HIFU can produce histological (structural) and functional (physical mechanisms) changes on the living tissue [1]. In other words, a focused beam of ultrasound can create a restricted lesion on the desired area of the nervous system with no damage to intervening tissue such as damage to blood vessels, etc. [17]. However, injuries are sometimes unavoidable and may represent a serious hazard for healthy tissue. For this and other reasons that showed ultrasound doesn't present a hazard as employed for medical purposes, the Fry brothers indicated that applying ultrasound waves to neurosurgery may assist more brain surgeries and protect some of the issues during standard surgery [24].

As the result of animal experimentation, the Illinois researchers showed that formation of the lesion basically depends on the sound intensity and the duration of exposure, i.e., the minimum time required to produce an effect on the tissue [25], [26]. Focused ultrasound of 1, 3, and 9 MHz was employed with intensities ranging from $10^2 - 2 \times 10^4$ W/cm^2, and corresponding pulse durations of the exposure from $2.5 - 5 \times 10^{-4}$ sec [6], [26]. The sound, transmitted to the tissue through water acting as a propagation path, created permanent changes after a brief exposure. As the intensity increased, the time of irradiation required for the changes on tissue decreased. These changes produced an irreversible effect of ultrasound on tissue [26]. The lesions were produced by three different mechanisms: thermal, mechanical (focal), and cavitation. At lower intensities and longer durations of exposure, the lesion was produced by a thermal mechanism due to temperature increases. At the highest intensities and shortest durations, the lesion was produced

by a cavitation mechanism, while at intermediate levels, the lesion was formed by a mechanical (focal) mechanism which appeared at the focus of the ultrasonic waves.

In the first of a series of animal experiments, spinal cords of frogs and rats were examined; subsequently various parts of the brains of monkeys and cats, such as the cortex, were exposed by focusing the sound beam on desired areas without damaging the adjoining tissue. The description of exact conditions under which physical changes could be induced was reported by Fry et al. [27], [28].

The histological study of frogs was made with three different dosages: light, medium, and heavy. It was reported that by careful control of the dosage of radiation, only the large cells were destroyed while the small neurons, glial cells, nerve fibers, and blood vessels could be left unaffected [17]. Experimental results under increased hydrostatic pressure indicated that cavitation was not an important factor in the mechanism of production of paralysis of the hind legs of the frogs based on a quantitative relation (linear relation) between the minimum time required for paralyzing the hind legs and the pressure amplitude. [28]

The same result was also evidenced in animal experiments in which a small section of the adult cat brain, the limbic system, was examined in the central and lateral side of the brain [5], [17]. In the experiments on cats, the top of the skull bone was removed because of its high absorption for ultrasound. The sound entered the brain and irradiation was performed with the brain temperature fixed at $37^{o}C$ [6]. The effect of ultrasound on nerve tissue was assessed from the coordination of movement, muscle control, etc.

Histological studies on exposed cats indicated that the structural changes occurred 10 min after exposure [1] [6]. The nerve cell bodies were more sensitive than nerve fibers, and in addition,

the white matter was more affected by ultrasound than gray matter which required a higher dosage (about 30% more) for the same effect [29], [23].

In all experiments, the first thought was that the changes in temperature created by high intensity could be considered for these effects. Therefore the increase in temperature was measured by embedding thermocouples into tissue in order to determine acoustic absorption coefficients and heat conduction processes [30]. It was found that: “the temperature changes in tissue by absorption of focused ultrasound (1-10MHz) was essentially independent of frequency for a single pulse duration of 1 to 10 sec [31], because of the frequency dependence of both the absorption coefficient in the tissue and the focal region geometry”. A complete discussion of the temperature factor and experimental protocols can be found in a paper by Fry and Herrick [32], [21].

Later studies and reports revealed that the temperature cannot be the only reason for these effects. Evidence of this was taken from the study of the time interval between two exposures from 5 minutes up to 30 days to destroy nerves of the brain so that the temperature of the tissue returned to normal between exposures [24]. From the result of dosage studies on a series of animals, three factors appeared most important: the geometry of the focal region, the focal intensity, and the physical mechanisms involved in tissue [33]. This information allowed a more optimal choice of exposure conditions during the study and improved comprehension of the result after. For instance, a multiple-beam focusing transducer [4] was replaced by a single beam focusing instrument in order to produce localized lesions, small in all three dimensions (cross sections), so that in the region where the beam converges, the sound level will be high and focused enough to produce desired changes in the tissue.

During the 50's and 60's, additional effects of ultrasound on biological media were discovered and investigated by the Fry brothers together with Floyd Dunn, who was part of the research team at the Bioacoustics Research Laboratory. Experimental animal studies at the Illinois laboratory showed that there exist reversible and irreversible effects produced in nerve tissue by ultrasound which are not the result of temperature change [1], [6]. From the point of view of functional (physical) mechanisms on the tissue, cavitation was investigated as having an important non-thermal role. Cavitation is considered as an interaction of small gas bodies in the biological medium with the propagating ultrasound wave. The incidence of cavitation varies with exposure conditions, nature and state of the medium, the hydrostatic and acoustic pressures, and the presence of gas bodies prior to the exposure [30], [32].

Later in 1970's, extensive studies on cavitation events *in vivo* were described in detail. As previously mentioned, the threshold regime at which ultrasound produced irreversible effects in the mammalian central nervous system was found to be described by the empirical relation: $It^{1/2} = c'$, where I was the intensity at the focus of the beam *in situ* in watts per square centimeter, t was the duration of exposure of the single pulse in seconds, and c' was a constant. In the threshold region where cavitation events were expected to occur, there was no time delay for the lesion to occur, compared to the thermal events in which lesions appeared approximately 10 min after exposure. Moreover, the temperature growth as defined by absorption was almost zero for cavitation events. Lesions might not be found at the focus of the transducer, however, at different positions such as interfaces between neural tissue and fluid-filled blood vessels and ventricles. [1], [6]. Therefore the biological effect produced by cavitation resulted from: "the collapsing gas body

during transient cavitation could occur within a few hundred acoustic pressure cycles, and that event could produce irreversible tissue damage".

More recent developments in ultrasound applications: Applications of ultrasound energy in medicine continue to diversify. For instance, transcranial focused ultrasound is an advantageous non-invasive therapeutic modality used to treat a number of brain conditions. In this case, the ultrasonic wave is used to evoke brain actions through neuromodulation, lesioning of particular tissues and structures, or in blood-brain barrier opening [35]. In that last application, the modality can help in localized administration of medications via the opened blood-brain barrier [36]. It is worth noting, however, that overheating of the cranium and other tissues during clinical exposures is a challenge to the advancement of thermal lesioning in the brain when a high intensity focused ultrasound (HIFU) beam is involved. A number of applications of ultrasound in the field of medicine have been accepted for therapeutic purposes due to their beneficial biological effects. For instance, ultrasound of low power and approximately 1 MHz has been widely applied since the 1950's for physical therapy of medical conditions like tendinitis and bursitis [34]. In the 1970's, applications of ultrasound in therapy were established for physiotherapy and neurosurgery [34]. Cancer treatment also received attention for the use of ultrasound, initially for hyperthermia [37]. The passage of time saw accelerated development of therapeutic ultrasound, with a wide range of techniques currently in use. In 1980's came the application of high-pressure-amplitude shock waves in resolving kidney stone problems with a mechanical approach. As a result "lithotripsy" became the most frequent choice of treatment, quickly replacing surgery [38]. Approved applications of ultrasound now include uterine fibroid ablation, removal of cataract (phaco-emulsification), surgical tissue cutting, and born fracture healing amongst others [34].

Studies have shown the possibility that undesirable bio-effects may occur during treatment, including burns from thermal-based treatments as well as hemorrhage that can result from mechanical-based treatments [35]. But in all areas of ultrasound applications and their bio-effects, standardization and risk management are taken into account to ensure a maximum benefit-to-risk ratio for the patient. Conventional therapeutic ultrasound has been shown to have benefits and well-defined hazards which are manageable. However, the safety information sometimes can be lost or manipulated depending on commercial conflict of interest. The key concern can be therefore to have a more centralized communication of the practical safety information through authoritative agencies, for instance, the American Institute of Ultrasound in Medicine.

1.3 Project objective and motivation

In the early 1970's a group of researchers at the University of Illinois studied the safety of ultrasound and ultrasonic threshold dosages (acoustic intensity and time duration of a single pulse) for the mammalian central nervous system [1], [6], [26], [31]. In this study, feline brains *in vivo* were exposed to focused ultrasound beams, and the threshold for tissue damage was evaluated for a variety of acoustic parameters. The values of the acoustic parameters spanned the range from diagnostic to therapeutic output level and frequencies. The transducer used in their study was a planar x-cut quartz crystal 12.7-cm in diameter faced with a Fresnel lens having a focal length of 13-cm [39] . Based on their results, the threshold *in situ* intensities (*I*) for lesion formation in the brain tissue at each of several frequencies of 1.0, 3.0, 4.0, 4.5, and 9.0 MHz were found to be equal to a constant which was a moderate function of frequency (*f*) and temperature (*T*) divided by the square root of exposure duration (*t*), $I = \frac{C'(f,T)}{\sqrt{t}}$ [26]. The researchers divided the lesions into 3 categories [1], [6] (thermal, cavitation, and mechanical), and the acoustic intensities were quantified using linear extrapolation. During their study, more than 1100 cats were sacrificed, and all animals were examined functionally and histologically in the focal region of the sound beam and intervening tissue between the focal region and the port of entry of the sound into the brain. From all these data, they did not report any tissue abnormalities produced in the sound path through intervening tissue [1].

Although for the purpose of our current project, we attempted to make use of these data, this procedure made our work difficult to support scientifically for several reasons:

In the experiments performed, it was not obvious how to determine ultrasound pressure waveforms in the brain of a cat. In other words, there were no accurate measurements of the

acoustic pressure field due to a lack of appropriate theoretical knowledge and experimental techniques.

In the experimental research, the study of cavitation in tissue was not expressly aimed and therefore the distribution of cavitation lesions was not exactly understood. The simple relationship between the intensity and time duration of exposure ($I\sqrt{t}$) was not, and is still not, well understood especially for the lesions expected to be produced by inertial cavitation at threshold exposure.

The frequency dependence was not that expected for cavitation, and the cavitation resulting from theses exposures was not necessarily at the focus; often an increase in cavitation threshold with increasing frequency is expected from theoretical consideration of the mechanism for cavitation induced in liquid media [1].

While the computed intensities for the focal region and the ultrasound exposure parameters were published, it was not possible to determine the acoustic pressures of acoustic fields at high output powers at that time. The source pressures were unknown, or at least not reported, and the pressure waveforms of the exposure fields were unknown. Thus, most of the experimental results were effectively lost to the scientific community since the acoustic fields could not be reliably compared to outputs from modern instruments.

Therefore, the goal of our research was to recover the acoustic field parameters so that the published data will be made useful. In particular the objective of our study was numerically simulating the acoustic pressure waveforms that occur in the brain of anesthetized cats produced by a spherically focused transducer as a source, given transducer parameters from published papers, initial source pressure amplitude, and frequency using a Finite Difference Time Domain (FDTD) technique. Moreover the focal intensities that correspond to the computed focal pressures

were calculated in order to compare them to the numbers in the published results [26]. In an event of low pressure, the focal intensity was mapped on empirically determined values in which computed waveforms were expected to be the same as those arrived at using linear theory. In situations involving higher source pressures, intensities were expected to match, but the pressure waveforms can only be determined using nonlinear theory. Since the distortion of an acoustic wave increases with increasing source pressure and frequency, the pressure waveforms were expected to be nonlinear. The waveforms were computed using a FDTD technique for nonlinear propagation.

Having the results of our present work, first, we were able to calculate the true shape of the curves of acoustic threshold intensity versus exposure time, as presented in previous study by Dunn et al [26]. Then that information was used to estimate the true shape of threshold curves for the acoustic pressure (positive and negative) versus exposure time to estimate the cavitation threshold. Second, with the information from the first part, we tried to provide a theoretical understanding model for all those shapes which could be reliable in general. The implications of these results could be used for clinical safety exposures. In addition, this will help us to look at heating, radiation force, and maybe some other mechanisms that might be helpful for future work.

CHAPTER II:

NUMERICAL SIMULATION AND EXPERIMENTAL METHOD

In this chapter, the theory of sound waves and our numerical model is presented, followed by the description of the simulation, experimental setup, and methods. Then the calculation data in water is presented in chapter III along with a comparison with tissue calculations as well as the experimental results. This is followed by a discussion and the conclusions of the study at the end.

2.1 Theory for propagation of sound waves

Ultrasound waves are mechanical disturbances that move through a medium. Ultrasound waves have the same properties as normal sound waves. The one-dimensional wave equation for pressure moving in the x-direction at time t and speed *c* is denoted as [40]:

$$\partial^2 p/\partial^2 x = 1/c^2 \, \partial^2 p/\partial^2 t \qquad 2.1)$$

One of the solutions that can satisfy the one-dimensional wave equation is the sinusoidal function:

$$p(x,t) = \sin k(x - ct) \qquad 2.2)$$

When solved with respect to *t* and holding *x* fixed, we see that the pressure around a fixed location varies sinusoidally with a radial frequency $\omega = kc$ which gives a cyclic frequency f with unit of Hz:

$$f = kc/2\pi \qquad 2.3)$$

Likewise, when solved with respect to *x* and holding *t* fixed, we observe that the pressure around a particular time varies sinusoidally with a quantity k known as the wave number that is proportional to the number of oscillations per unit length. We know that the wavelength of the sinusoidal wave can be written as:

$$\lambda = 2\pi/k \qquad 2.4)$$

By substituting and solving the equations, the important relationship between the speed of sound (c), the frequency (f) and wavelength (λ) can be obtained:

$$\lambda = {}^{c}/_{f} \qquad 2.5)$$

where λ is the distance from one crest to the next or one trough to the next. The high crest and low trough represent specific amplitude values of the wave and correspond to peak compressional and peak rarefactional values, respectively [41].

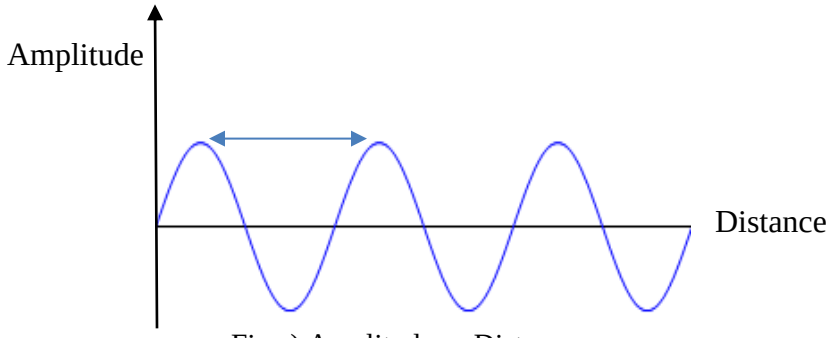

Fig a) Amplitude vs Distance
(Referenced to [41])

The time that it takes for one cycle to occur is called the period *T*, and it is related to the frequency by:

$$T = {}^{1}/_{f} \qquad 2.6)$$

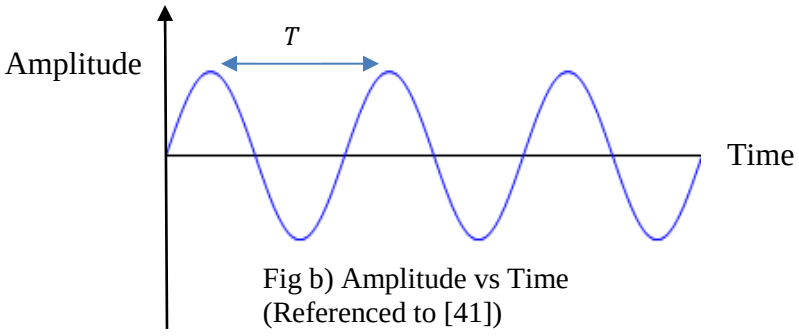

Fig b) Amplitude vs Time
(Referenced to [41])

The horizontal axis, either distance or time, is an important concept in diagnostic ultrasound. Distance information can be converted to time values and time values converted to distance information to display data on a specimen's structure. The propagation speed is an important factor in this conversion process. It is assumed to be constant at 1540 $^{m}/_{s}$, an accepted value for all soft tissue in medical applications [42].

As an ultrasound wave propagates through a medium, it transports energy through the medium. The rate of energy transport is known as "power". Medical ultrasound is produced in beams that are usually focused on a small area, and the beam is described in terms of the power per unit area, defined as the beam's "intensity".

- Energy (*E*) = Ability to do work in joules
- Power (*P*) = Rate of change in energy in watts (joules/sec)
- Intensity (*I*) = power per unit area (*A*)

$$I = P/A \tag{2.7}$$

Ultrasound wave intensity is related to the maximum pressure (P_m) in the medium, and can be defined as [41]:

$$I = {P_m}^2/2\rho c \tag{2.8}$$

which is only true for sinusoidal wave, where ρ is the density of the medium in kg/m^3. The density and speed of sound values for water are given as $\rho=10^3$ kg/m^3 , c= 1500 m/s, respectively [43].

2.1.1 Linear propagation:

If we assume a homogeneous and lossless medium with a negligible viscosity, the sound pressure p, the particulate velocity v and the density ρ can be represented as two linearized Euler equations and an equation of states [43] which are used to derive the wave equation.

- The continuity equation for conservation of mass $\partial \rho / \partial t + \rho \nabla . v = 0$ 2.9)
- Conservation of momentum $\rho \, \partial v / \partial t + \nabla p = 0$ 2.10)
- The equation of state $p = c^2 \rho$ 2.11)

Thus, the homogeneous plane wave equation is described by: [43]

$$\nabla^2 p - 1/c^2 \, \partial^2 p / \partial^2 t = 0 \quad 2.12)$$

This is the pressure wave equation moving in the x, y, and z directions at time t and speed c. This may be compared to equation 2.1 for the pressure wave moving only in the x-direction.

If we consider the acoustic disturbance to be a small perturbation to an ambient state; then $p = p_0 + p'$ where p_0 is the ambient pressure and p' is the acoustic pressure so that p is the total pressure. The same idea is applied for the density and velocity respectively, $\rho = \rho_0 + \rho'$ and $v = v_0 + v'$. Since all the quantities in a homogeneous medium are independent of position, the primes can be ignored, therefore the wave equation can be written as equation 2.12 above.

2.1.2 Nonlinear propagation:

When a wave no longer satisfies the linear wave equation, it is called ‘nonlinear’. This condition can arise from the interaction of different frequencies, or high amplitude (or high intensity) sound waves or the cumulative effect of propagation over large distances. This leads to distortion of the waveform and growth of harmonics in the pressure wave.

If we take into account an inhomogeneous wave equation along with all dissipative term, the nonlinear wave equation would be [44]:

$$[\nabla^2 p - {}^{1}\!/_{c^2}\ {}^{\partial^2 p}\!/_{\partial^2 t}] - {}^{1}\!/_{\rho}\ \nabla p \,.\nabla \rho + {}^{\delta}\!/_{c^4}\ {}^{\partial^3 p}\!/_{\partial\, t^3} + {}^{\beta}\!/_{\rho\, c^4}\ {}^{\partial^2 p^2}\!/_{\partial t^2} = 0 \qquad 2.13)$$

This is a second-order wave equation describing the acoustic pressure in terms of space, time, and the fluid's material properties. In this equation p is the acoustic pressure, ρ and c are the ambient density and sound speed (dropping the primes), δ is the diffusivity of sound defined as how much energy spreads out and diffuses to the surroundings instead of propagate and it is corresponding to thermoviscous absorption, which accounts for both thermal and viscous losses, $\beta = 1 + B/2A$ is the local coefficient of nonlinearity with *B/A* being the nonlinear parameter of the medium [44]. In this equation, the first two terms (in the brackets) on the left hand side of the equation is the D'Alembertian, which exists in all wave equations that illustrate the propagation of a wave in space and time, the second term explains the ambient inhomogeneity in the medium's density, the third term is the loss term due to viscosity of the medium, and the last term defines the nonlinearity during propagation [45].

2.2 Computer simulation method; FDTD

The program used in this study to calculate the pressure and intensity fields is an example of a Finite Difference Time Domain (FDTD) simulation. In this case, FDTD is a numerical technique for predicting the steady state fields produced by the ultrasound transducer. In other words, it is a technique used to find approximate solutions to the associated system of differential equations. Since it is a time domain method, its solution can cover a wide frequency range with a single simulation run and treat nonlinear material properties in a natural way.

The FDTD method belongs in the general framework of grid space. The time-dependent partial differential equations are discretized to space and time partial derivatives. The x-axis vector components in a volume of space are solved at a given instant of time; the radial vector components in the same spatial volume are solved at the next instant in time; and the process of time-stepping is continued over and over again until the desired transient or sinusoidal steady state field behavior is fully achieved.

This method has two advantages over other simulation methods: it is simple to fulfill for complex structures, and its memory and running time requirements are such that solutions for many unknown field components can be obtained within a few hours on a digital computer.

Two numerical FDTD simulations using this particular computer program have been reported. Ibrahim Hallaj implemented a finite difference method to investigate the nonlinear acoustic in underwater and biomedical applications [44]. More recently Jinlan Huang chose the finite difference representation to simulate the heat equation in vascular tissue by exposed to focused ultrasound [46].

2.2.2 The theory of our numerical model (FDTD)

A nonlinear model of acoustic wave propagation using a discretized version of the nonlinear wave equation was employed in our study in two parts to calculate the pressure and intensity fields respectively in the spatial and time domains. First, the 2D steady state pressure field was computed using an axially symmetric system to keep the computation time short; the pressure was only computed in the upper half of the volume, i.e., above the acoustic axis. Second, the 2D steady state intensity simulation was also applied to capture the distribution of

focal intensity over a desired region. The sound wave was propagated in the positive direction, and the space was formatted in cylindrical coordinates [47].

The source used in the study was a spherically focused, nominally f1-transducer with a diameter of 12.7 cm, 13-cm focal length, and frequencies of 1, 3 and 9 MHz; the acoustic axis was defined as the z-axis and *r* was the radial position. [39]

For our numerical model, Eq. 2.13 was expanded into two terms using Taylor expansion, and the wave equation was discretized and solved in the following form, [44]

$$\nabla^2 p - {}^{1}\!/_{c^2}\ {}^{\partial^2 p}\!/_{\partial^2 t} - {}^{1}\!/_{\rho}\ \nabla p \,.\nabla \rho + {}^{2\alpha}\!/_{c\omega^2}\ {}^{\partial^3 p}\!/_{\partial\, t^3} + {}^{2\beta}\!/_{\rho\, c^4}\left[p\, {}^{\partial^2 p}\!/_{\partial t^2} + \left({}^{\partial\, p}\!/_{\partial t} \right)^2 \right] = 0 \qquad 2.14)$$

This differential equation can be reduced to its simplest form considering polar cylindrical coordinates in a homogeneous medium. Therefore Eq. 2.14 can be written in this form: [46]

$${}^{\partial^2 p}\!/_{\partial\, r^2} + {}^{1}\!/_{r}\ \ {}^{\partial\, p}\!/_{\partial r} + {}^{\partial^2 p}\!/_{\partial\, z^2} - {}^{1}\!/_{c^2}\ {}^{\partial^2 p}\!/_{\partial^2 t} - {}^{1}\!/_{\rho}\left[{}^{\partial\, p}\!/_{\partial r}\ {}^{\partial\, \rho}\!/_{\partial r} + {}^{\partial\, p}\!/_{\partial z}\ \ {}^{\partial\, \rho}\!/_{\partial z} \right] + {}^{2\alpha}\!/_{c\omega^2}\ {}^{\partial^3 p}\!/_{\partial\, t^3} + {}^{2\beta}\!/_{\rho\, c^4}\left[p\, {}^{\partial^2 p}\!/_{\partial t^2} + \left({}^{\partial\, p}\!/_{\partial t} \right)^2 \right] = 0 \qquad 2.15)$$

α is the absorption coefficient, which is related to the acoustic diffusivity δ in this form:

$\alpha = {}^{\delta\omega^2}\!/_{2c^2}$ [43] for angular frequency ω and it has the units of [Np/m].

For a plane wave with constant angular frequency, the time average term $\left({}^{\partial\, p}\!/_{\partial t} \right)^2$ is equal to $\omega^2 p^2$ or $\omega^2 \rho c I$ where *I* is the intensity in the direction of propagation. Therefore, the energy dissipated per unit volume and time (the heat generation rate per unit volume and time) at the center of the focus is given by: [43]

$$q = 2\alpha I = \frac{2\alpha}{\omega^2 \rho c} < \left(\frac{\partial p}{\partial t}\right)^2 > \quad 2.16)$$

Using a linear impedance relation between the sound pressure and particle velocity $p = \rho c v$

$$I = \frac{1}{\rho c} \langle p^2 \rangle = \frac{1}{\omega^2 \rho c} \left(\frac{\partial p}{\partial t}\right)^2 \quad 2.17)$$

Since for a plane wave propagating in the z-direction $\frac{dI}{dz} = q$, the axial variation of the intensity of sound in a plane wave using Eq.2.16 is [43]:

$$I(z) = I_0 e^{-2\alpha z}. \quad 2.18)$$

2.3 2D pressure filed calculation:

The computation procedure can be summarized in three parts:

- Generate the simulation parameters using a Matlab script
- Generate the coordinate and indices of the transducer surface using a Matlab script
- Simulate the steady state pressure and intensity using a Fortran script

In order to find the solution to Eq. 2.15, a Fortran code was written by Hallaj [44] was used to calculate the steady-state nonlinear pressure and intensity. The description of the code and all scripts will be found in the Appendix.

Solving Eq. 2.15 using the finite difference method required distributing the space and time domain into discrete grids. The discrete representation of the pressure field is $p = (z_i, t_n)$ or p_i^n with integers $i = [1,2, \dots, i_{max}]$ and $n = [1,2, \dots, n_{max}]$. Then the grid positions are:

$$z_i = (i-1)dz \quad (2.19)$$

$$r_j = (j-1)dr$$

$$t_n = (n-1)dt$$

Where *dz*, *dr*, and *dt* indicate the distance between grid points and the time step respectively.

The second order differential equations applied for Eq.2.15 can be written as: [46]

$$\partial\,\rho\,/_{\partial r} = \frac{1}{2dr}\left(\rho^{n}_{i,j+1} - \rho^{n}_{i,j-1}\right),$$

$$\partial\,\rho\,/_{\partial z} = \frac{1}{2dz}\left(\rho^{n}_{i+1,j} - \rho^{n}_{i-1,j}\right),$$

$$\partial\,p\,/_{\partial r} = \frac{1}{2dr}\left(p^{n}_{i,j+1} - p^{n}_{i,j-1}\right),$$

$$\partial\,p\,/_{\partial z} = \frac{1}{2dz}\left(p^{n}_{i,j+1} - p^{n}_{i,j-1}\right),$$

$$\partial^2 p\,/_{\partial r^2} = \frac{1}{dr^2}\left(p^{n}_{i,j+1} - 2p^{n}_{i,j} + p^{n}_{i,j-1}\right),$$

$$\partial^2 p\,/_{\partial z^2} = \frac{1}{dz^2}\left(p^{n}_{i,j+1} - 2p^{n}_{i,j} + p^{n}_{i,j-1}\right),$$

$$\partial\,p\,/_{\partial t} = \frac{1}{2dt}\left(3p^{n}_{i,j} - 4p^{n-1}_{i,j} + p^{n-2}_{i,j}\right),$$

$$\partial^2 p\,/_{\partial t^2} = \frac{1}{dt^2}\left(p^{n+1}_{i,j} - 2p^{n}_{i,j} + p^{n-1}_{i,j}\right),$$ "*centered formulation*"

$$\partial^2 p\,/_{\partial t^2} = \frac{1}{dt^2}\left(2p^{n}_{i,j} - 5p^{n-1}_{i,j} + 4p^{n-2}_{i,j} - p^{n-3}_{i,j}\right),$$ "*backward formulation*"

$$\partial^3 p\,/_{\partial t^3} = \frac{1}{2dt^3}\left(6p^{n}_{i,j} - 23p^{n-1}_{i,j} + 34p^{n-2}_{i,j} - 24p^{n-3}_{i,j} + 8p^{n-4}_{i,j} - p^{n-5}_{i,j}\right), \qquad (2.20)$$

The boundary conditions: A boundary condition was applied at the edges of the simulation domain, i.e. on the outer surfaces of the mesh, to reduce reflections from the edges of the domain. Boundary conditions of this type are called absorbing boundary conditions (ABC) [48]. The ABC is useful for the first approximation and low order, using Mur's radiation condition [48]:

$$\partial p/\partial x - 1/c\, \partial p/\partial t = 0 \quad (2.21)$$

where *x* represents the *z* or *r* axis. For this symmetric simulation, the reflected boundary condition was applied to compute only the upper half of the two-dimensional domain or $r = [0, r_{max}]$. So the ABC was applied on all the edges except the symmetry axis where a symmetric boundary condition was used:

$$\partial p/\partial r = 0. \quad (2.22)$$

Determining the spatial and time steps: For accurate results from FDTD modeling, an adequate resolution in space and time with respect to the proper length and time scales was required. The resolution was determined by the separation of the grid points and the time steps. Therefore a spatial step size was chosen in which 10-12 points were required per wavelength and a time step was selected for which the Courant- Friedrich- Lewis number (CFL number) was 0.25<CFL<0.5 [46]. The CFL number is defined as $CFL = cdt/dx$ where *c* is the local wave propagation speed, dt is the time step of the FDTD simulation, and dx is the distance separating adjacent grid points. In practice, most simulations are performed with CFL≈ 0.5 and dx set such that there are around 8 mesh points per wavelength. Therefore for a frequency of 1MHz, and speed of sound 1500 m/s in water, setting $dx = 1.5 \times 10^{-4}$ and $dt = 5 \times 10^{-8}$ would be appropriate. Then if we set the time step to give us a CFL number of 0.5 in the *z* or *r* direction, we obtain [49]:

$$dt = CFL \cdot \frac{dz}{c} = 0.5 \times \frac{1.5 \times 10^{-4}}{1500} = 0.05\ \mu s \quad (2.23)$$

The representation of the spatial domain and time step are shown in Figure 2.1.

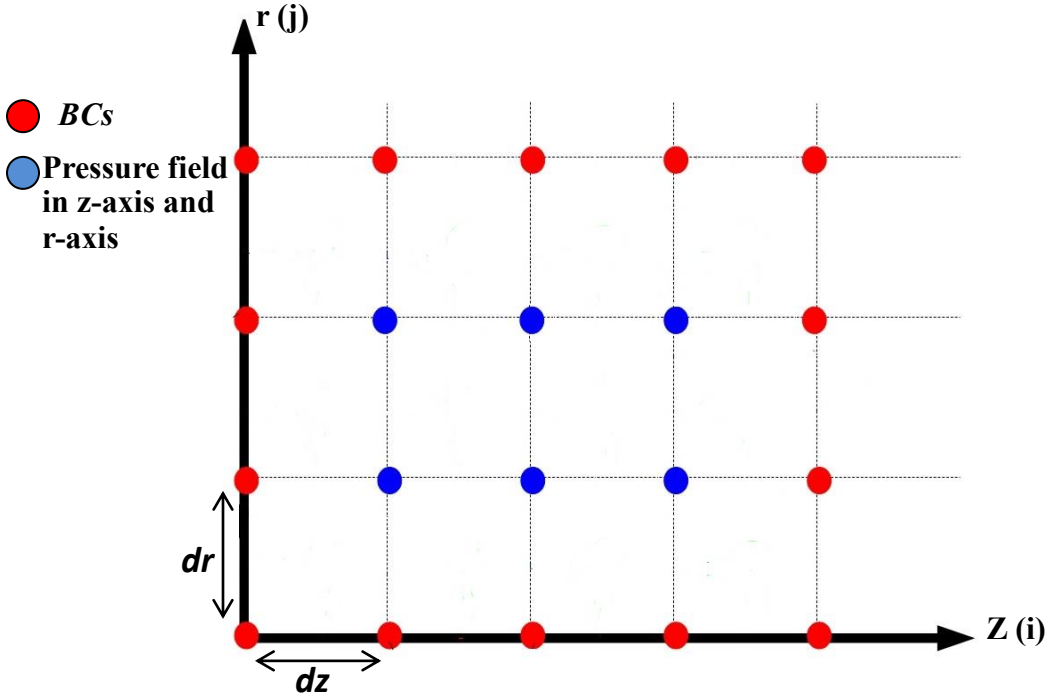

Figure 2.1: Discretized spatial domain and time step using FDTD method

A Fortran 90 script was used to calculate the spatial and time steps needed along with other parameters for the simulation.

Figure 2.2 shows the geometry of the spatial domain for the simulation. It indicates a curve along the axial and radial axes. The curve illustrates the location of the source transducer face with a radius of 6.5-cm and a focal length of 13-cm. The source pressure values were specified along the curve as a function of time. The light pink region represents the location of tissue and the remaining portion of the domain is water.

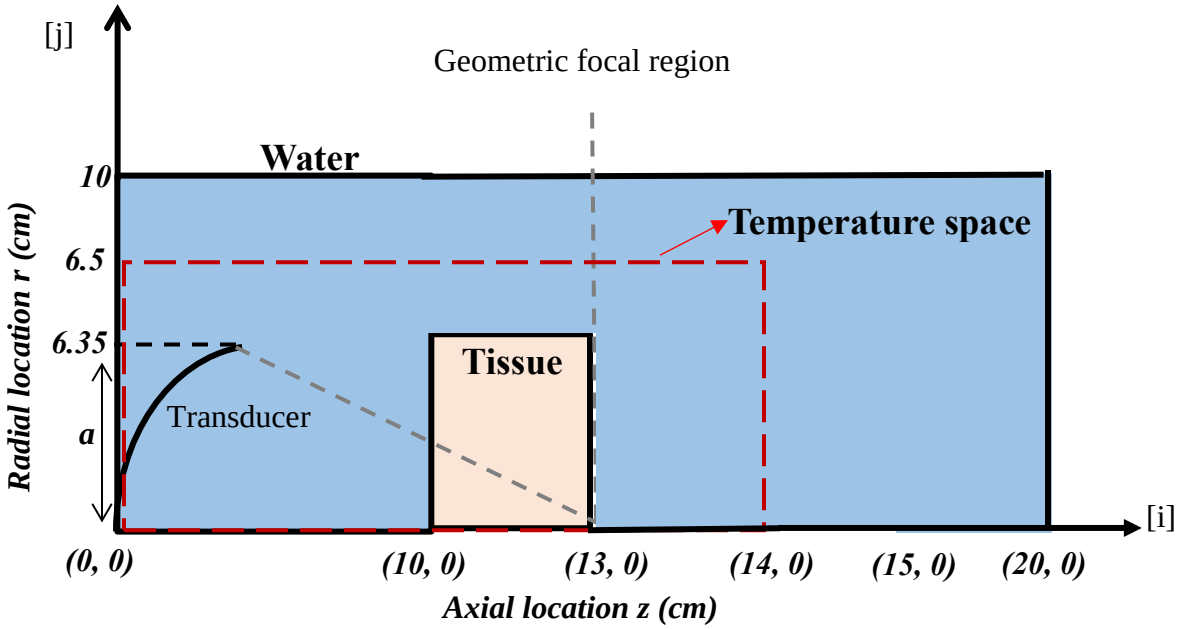

Figure 2.2: The geometry of the 2-D FDTD pressure solution domain.

As mentioned before, the system was always set up in an axially symmetric way to save computation time, so the radial coordinate of the transducer focus is always set to be zero. The spatial steps for r and x were set to be equivalent to the 2D code as will be shown in chapter III. To generate the coordinate and indices of the transducer surface, an input file of point sources with coordinates defining the shape of the transducer was given. The coordinate depends on the spatial grid size, so a new file named "bowlarray_Sonostat" must be created every time the grid size is changed using script "bowlarraysonostat". The bowl coordinate indices and focal index are plotted in Figure 2.3 for a 1-MHz transducer.

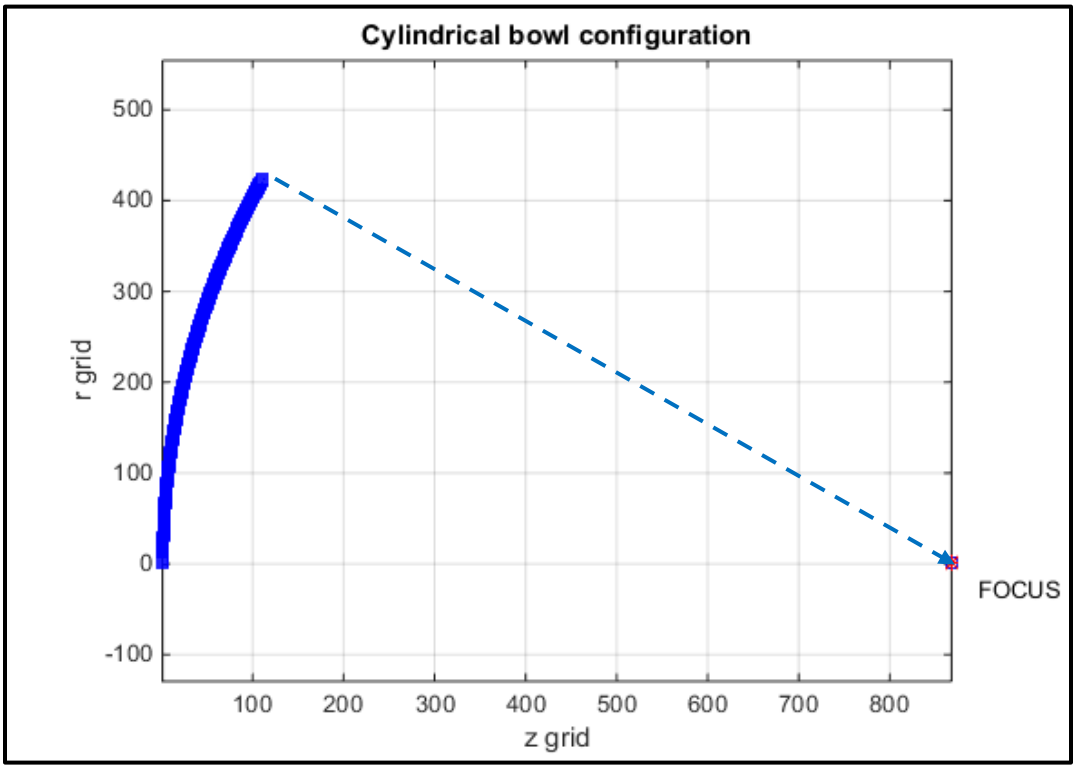

Figure 2.3: Coordinate of transducer surface

A source pressure waveform for the transducer was generated for each frequency of interest, using a script named “sinewave” in Matlab with the series of source pressure outputs named “Wtrn”. Both files “bowlarray_Sonostat.dat” and “Wtrn.trn” must be placed in the same folder with the pressure FDTD code as input files to the code, along with other required parameters that are used by the Fortran code to calculate the pressure waveforms.

To compute the steady-state pressure field, a large solution spatial domain was needed to include all the variations in the wave propagation path, therefore the problem could be solved for a long insonation time where a steady state pressure field was reached long before the full insonation time expired. The pressure solution reached steady state approximately in the time it takes for the wave to propagate to the farthest distance from the source transducer in the solution

domain. In most simulations, the pressure solution reaches steady-state in 100 acoustic cycles for a frequency of 1MHz. The pressure field was calculated for a given source pressure in the water-tissue medium with specified material properties (speed of sound, attenuation coefficient, and density). The water and tissue properties at 1MHz are given in Table 2.1 [50].

Table 2.1: Water and cat brain acoustics properties at 1MHz.

Material	**Speed of sound** $(\frac{\mathbf{m}}{\mathbf{s}})$	**Density** $(\frac{\mathbf{kg}}{\mathbf{m^3}})$	**Attenuation** $\left(\frac{\mathbf{Np}}{\mathbf{m}}\right)$	**Nonlinearity parameter**
Water	1500	1000	0.025	4.96
Tissue	1554	1030	6.6	6.55

For 3MHz, the attenuation is changed to 20 $\mathrm{Np.\,m^{-1}}$. Since the attenuation is dependent to the frequency, the attenuation coefficient at 3MHz is much larger than at 1MHz.

2.4 2D Intensity field calculation

The discrete form that was used to calculate the intensity from the Equations 2.16 and 2.17 is [46]:

$$I_{i,j} = \frac{1}{\rho c\, \omega^2} \left({}^{1}/_{2dt} \right)^2 \sum_{n=1}^{N} \left(3p_{i,j}^{n} - 4p_{i,j}^{n-1} + p_{i,j}^{n-2}\right)^2 \qquad 2.24)$$

where N is the number of time steps averaged. The last 10 acoustic cycles of the pressure simulation were taken as an appropriate base to determine the steady state intensity. For a frequency of 1 or 3 MHz in the intensity computation, the same spatial steps and parameters as the pressure simulation were used to obtain the intensity profile.

2.5 Physical experiment

The experiments performed as part of this study were motivated by the goal of verifying the numerical models we developed in section 2.2. This project made use of a 1.21 MHz transducer

of diameter 5-cm having an actual focal length of 5.20-cm with a Fresnel lens which can focus the ultrasound beam. The pressure field produced by this transducer was measured in the laboratory's scan tank. Thus an important attribute of our experimental arrangement was the ability to measure and to control the acoustic parameters and physical properties of the medium. In addition, the object of the measurements with the lens was to compare them with calculations we made for water only (i.e., no tissue in the field) for those transducer-lens parameters.

At this point it is important we stress that, although we liked to employ materials and experimental arrangements that closely simulate biological media, that is, in fact, a secondary consideration. Our primary goal was to validate our numerical model. Therefore, we choose experimental arrangements that facilitate precise measurements and unambiguous comparison with model predictions. This also was to make sure that the field used by Fry and Dunn (1971), which also employed a Fresnel lens, was not likely to have had odd hot spots off axis. The focal plane was examined at the focus and also a bit beyond that to determine the field and whether there were any hotspots. A photo of Fresnel lens used in our experiment shows in Figure 2.4.

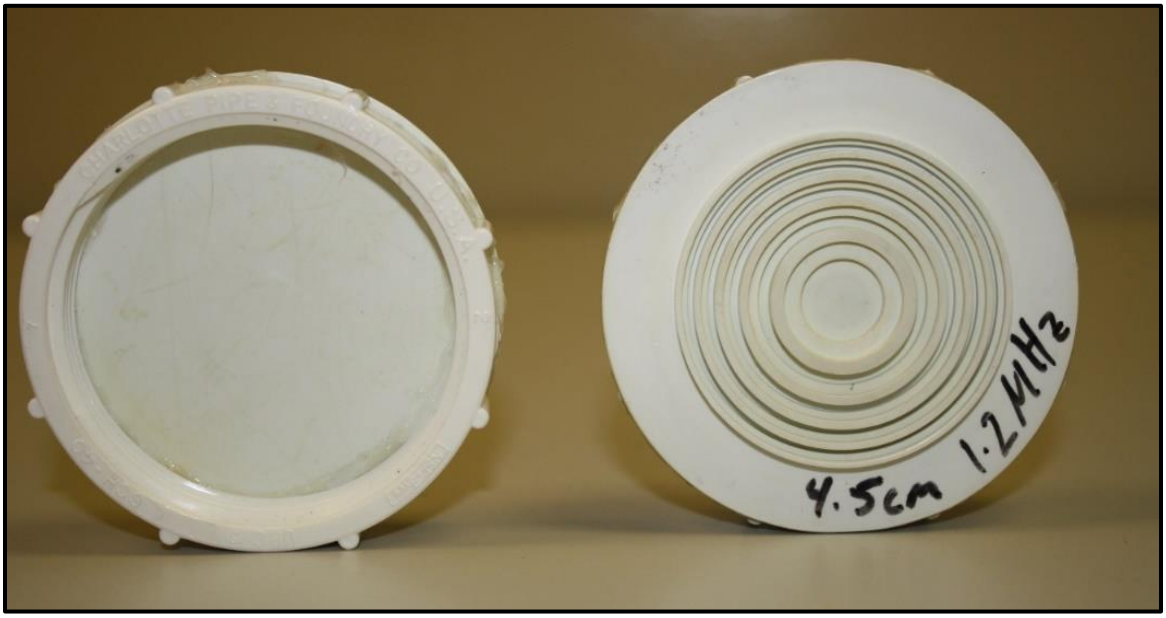

Figure 2.4: A photograph of Fresnel lens used to focus the ultrasound beam

2.5.1 Experimental setup

The data were acquired using the system shown in the schematic diagram in Fig. 2.5 The transducer was mounted in the tank open to the atmosphere and filled with filtered degassed water and driven in pulsed mode to emit a low- intensity acoustic pulse. Normally in HIFU experiments, discontinuous waves are used since there is no problem with overlapping of waves. The hydrophone (0.2-mm Needle, Precision Acoustics Ltd, SN 869) was mounted on a motorized three-dimensional translation system (Centroid Motion Controller) that moved visually into the general vicinity of the transducer focal region. This 3-axis system was used for moving the calibrated hydrophone throughout the acoustic field.

As can be seen in the schematic diagram, the signal from the function generator (Wavetek, Model 395) which generated the source wave, was amplified (boosted) by 10 dB gain with an ENI A150 RF Amplifier. The output of the amplifier was routed to both the transducer and the Agilent

54622A Oscilloscope in order to display the transducer signal on oscilloscope screen. The transducer uses the piezoelectric effect to convert the electrical signal coming from the amplifier to mechanical vibrations. The hydrophone is also piezoelectric and converts the pressure variations of the ultrasonic wave to an electrical signal. The hydrophone signal was boosted by a pre-amplifier (Precision Acoustics LTD Hydrophone Booster Amplifier), and then fed to the input of the oscilloscope where is was captured, digitized, and downloaded to the computer for further analyses by Matlab programming. The oscilloscope was triggered by the waveform generator which allows the absolute propagation time to be collected. Figure 2.6 shows a photograph of the experimental setup.

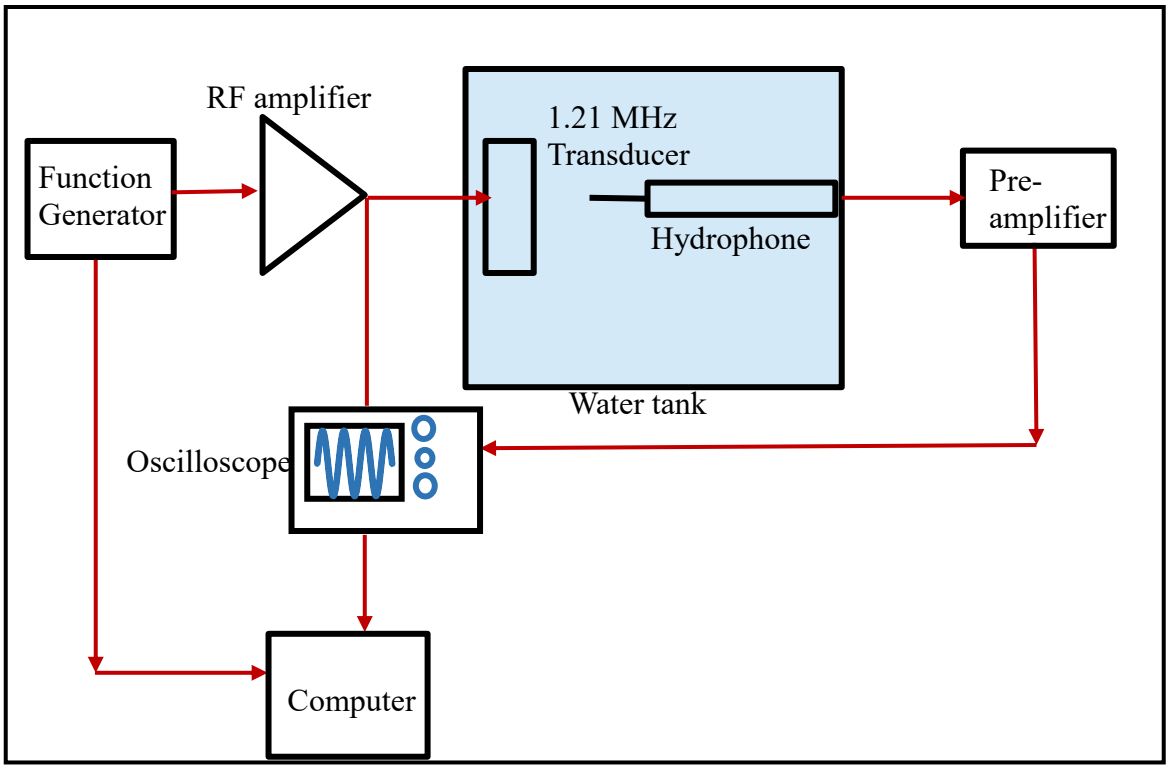

Figure 2.5: Schematic diagram of the experimental setup

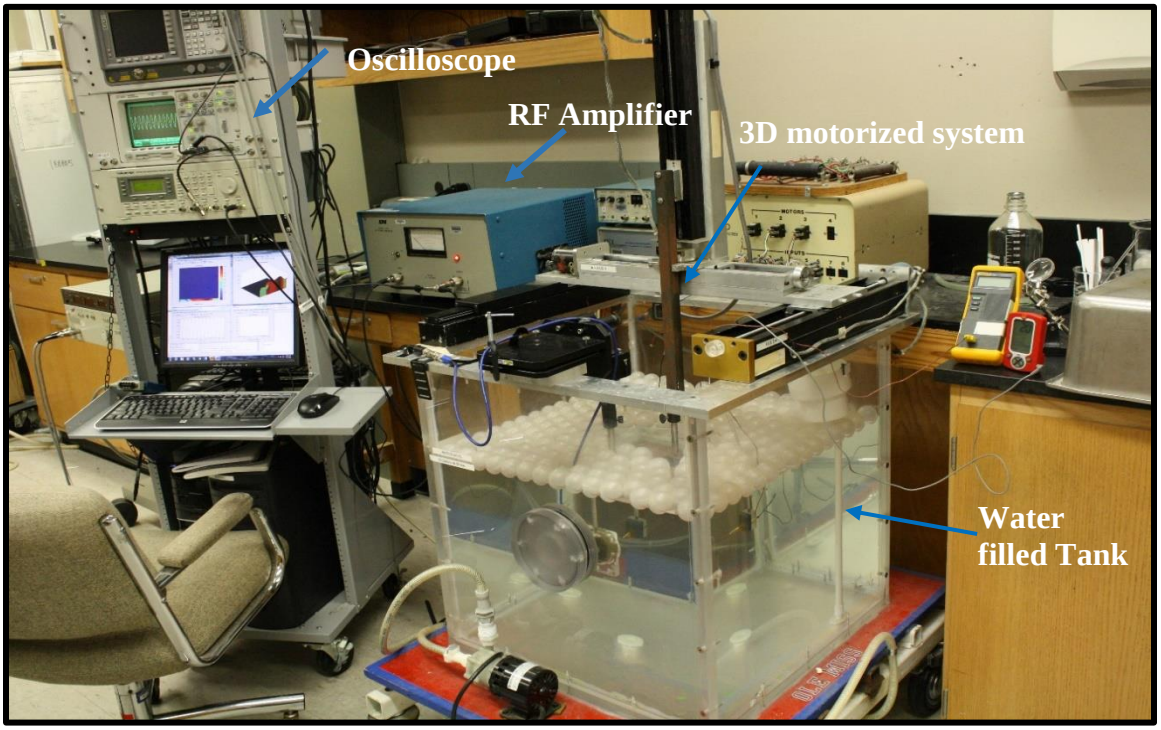

Figure 2.6: A photograph of experimental setup

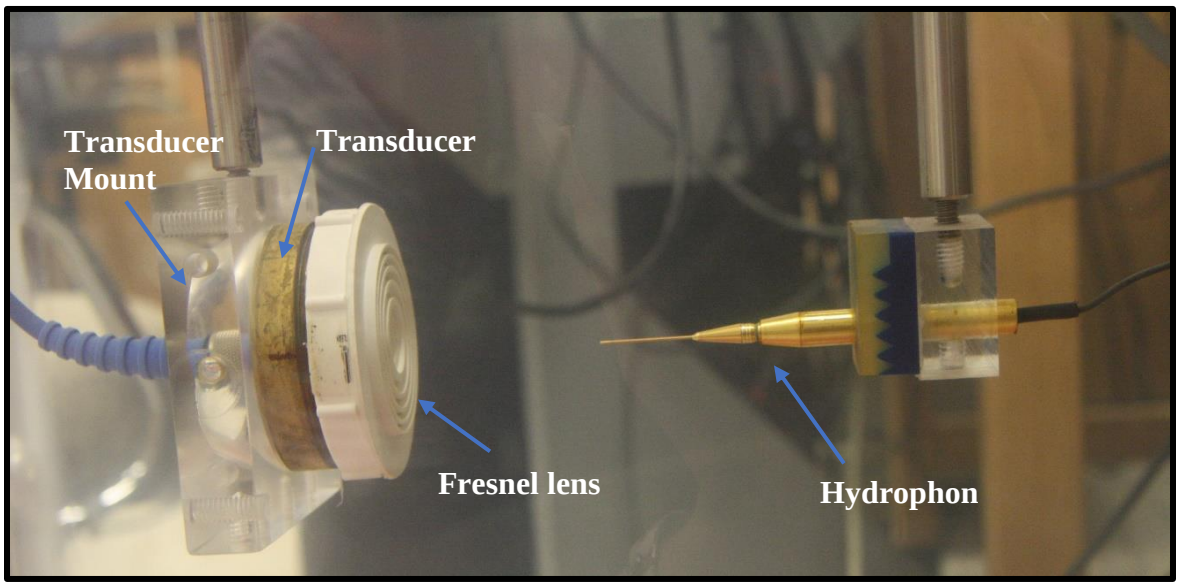

Figure 2.7: A close-up photograph of transducer, Fresnel lens, and hydrophone

2.5.2. Pressure field measurement

The hydrophone and transducer are both placed in the water bath. For the experimental measurements, the waveform generator was set to output a single cycle of a 1.21-MHz sine wave. The amplified pulse excited the transducer, and the resulting pulse propagated through the water and was sampled by the hydrophone. By slowly scanning the hydrophone through the x, y and z-planes (with the z plane along the acoustic axis) which was controlled by a program running in Matlab on the computer and observing the change in the amplitude of the received signal on the oscilloscope, the hydrophone could be positioned at the focus of the transducer. When the largest amplitude voltage response was obtained from the hydrophone, the hydrophone was considered to be in the center of the focal region of the transducer.

The smallest step size of the positioning system was 0.05 mm. A low voltage was applied to the transducer by using a low setting on the function generator and the hydrophone voltage response along with the voltage of transducer was measured. The lowest applied voltage was 100 mV (positive amplitude). The calibration data for the hydrophone are given from 1 to 20 MHz in the hydrophone calibration certificate. All these data were inserted to give the calibration result at 1.21 MHz shown below in Table 2.2.

To determine the pressure distribution in the acoustic field generated by the 1.21 MHz transducer, an axial and radial scan were performed with given ranges for x, y, and z-axis as well as step size using Matlab script. With a lower voltage amplitude of 100 mV applied to the transducer, the hydrophone was located in the focal plane of the transducer perpendicular to the transducer axis. Then the voltage was increased up to 250 mV until a smooth waveform was obtained without noise. The voltage was set on 100mV, the hydrophone was moved in small steps

of about 0.1mm from one side of the field to the other side. At each location, the hydrophone and transducer voltage response were measured peak to peak. Using the calibration, the pressure field was calculated at each location. This procedure was repeated moving the transducer along its central axis through the focal region as well as some points before and after the focal zone. This range included both the near and far field regions, including the focal zone which lies in between.

Images of the experimental data for all acquired plane scans were produced for each propagation. These experimental results will be shown in chapter III.

Table 2.2: Calibration data interpolated from the data of hydrophone certificate

Frequency (MHz)	**dB (mV/MPa)**	**Sensitivity (V/Pa)**
1.21	220.574	52.26×10^{-8}

2.6 Acoustics property measurements

We needed to know the acoustical properties of the materials we were using (including water) to ensure that these properties remained stable during our study.

2.6.1 Sound speed measurement

The sound speed can be determined using a technique, where the speed is calculated by the ratio of a known distance and the time needed for an acoustic pulse to travel that distance. The time delay can be obtained directly from the digital oscilloscope using the time cursor by measuring the time difference between the first zero crossings of the input waveform to the transducer and the output waveform from the hydrophone.

When conducting ultrasound experiments, monitoring the temperature is very important. Since the speed of sound changes with temperature, and because the scans used in this experiment

lasted several hours, any fluctuations in the temperature of the tank water could cause unwanted timing variations across the scan plane. The tank temperature was measured using a thermocouple probe (Fluke 50S K/J Thermometer) as T^0=21.4^o C.

In our experiment setup, the time delay between two signals Δt was measured as 35μs. However since in our case, the focal distance of the transducer covering by a Fresnel lens was unknown, this relative measurement required the information on the sound speed of water, which was obtained by measuring the temperature of the water, and using the following formula [41]:

$$c(T') = 1402.7 + 488T' - 482T'^2 + 135T'^3 \text{ where } T' = {}^{T^0}/_{100} \ , \qquad 2.25)$$

where T^0 is in degrees Celsius. From this formula the speed of sound was calculated as:

$c(T')$ = 1486.38 $^{\mathrm{m}}/_{\mathrm{s}}$.

To determine the actual focal length of the Fresnel lens, the values of Δt and c were utilized to calculate the actual focal length of the Fresnel lens using the relationship between the speed of sound and distance.

$$x = c\Delta t \ => 1486.38\, {}^{\mathrm{m}}/_{\mathrm{s}} \times 35\mu\mathrm{s} = 5.20 \text{ cm} \qquad 2.26)$$

2.6.2 The electrical impedance of the transducer

The impedance of the 1.21 MHz transducer was measured directly over several days to see if it varied in time at an average temperature of 21.5 C^{O} using an HP 4193A Vector Impedance Meter connected to the transducer. Measuring the complex impedance means to measure its magnitude and phase angle. Technically at the frequencies below 100MHz, the impedance magnitude can be determined by voltage and current measurement. First, it was observed that the impedance of the transducer was increasing during the observation. We found an issue in the cable, replaced it with a new cable and did the measurement again. This time it was found that the

impedance of the transducer remained constant at an average value of 27.5Ω during the measurement. The values of the measurement at different temperatures are shown in Table 2.3.

Table 2.3: The impedance measurement of transducer mounted into the water

Number of days	Temperature of water (C^O)	Range of measured values (Ω)
1	21.6	27.5Ω
2	21.5	27.5Ω
3	21.4	27.5Ω

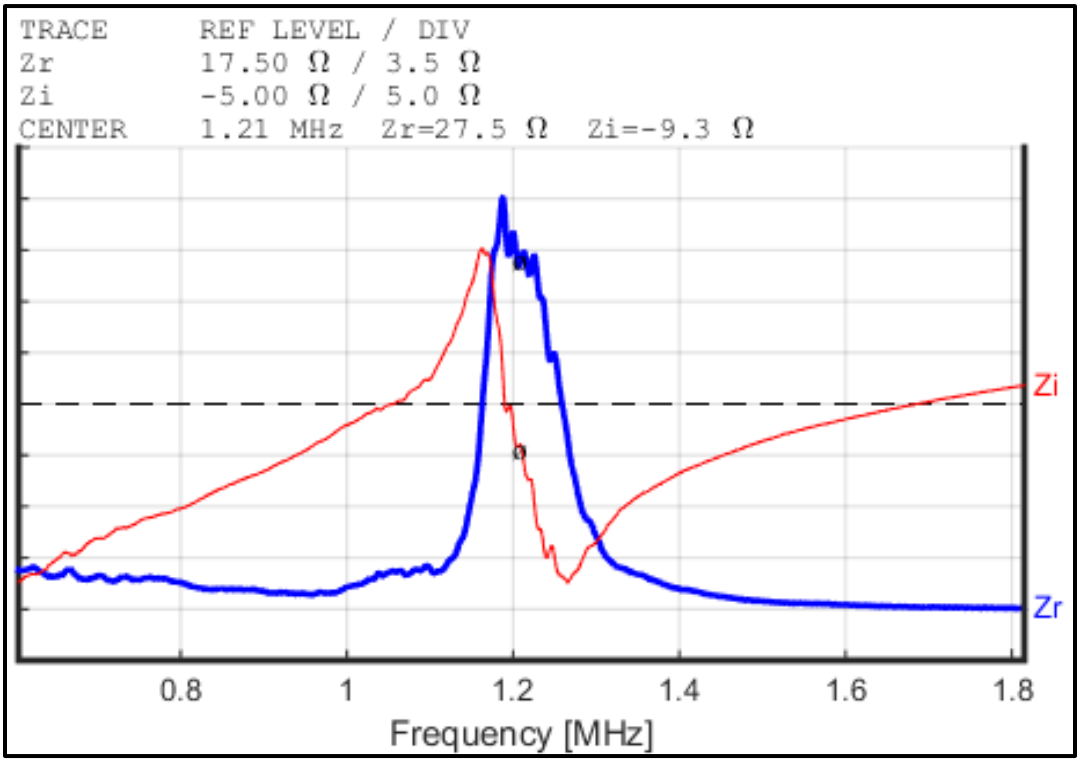

Figure.2.8: The complex impedance magnitude for 1.21MHz transducer in water

2.7 Pressure field simulation for the transducer-lens assembly

The acoustic pressure field inside the scan tank was determined by two methods:

1. *In situ* measurement of the pressure using a calibrated hydrophone as described in section 2.5;

2. FDTD calculation for the acoustic pressure in the water, based on the known physical properties of the medium and the transducer calibration in water. Therefore, the pressure field was calculated for the 1.21-MHz transducer-lens assembly in water using the FDTD code. The goal of the calculation of the pressure field for the transducer-lens in water was to compare it with the measurements we made for the transducer-lens set up in the scan tank.

2.8 Intensity calculation in water and tissue

The goal of the intensity calculations was to compare them to the published intensity numbers in the papers. The calculations at frequencies of 1 and 3 MHz were done in water only to get the intensities at the geometric focus and the actual focus. We assumed that the published results were measured intensities at the actual focus. The intensities were calculated using the linear relationship between pressure and intensity in equation $I = P^2/2\rho c$.

In addition, in order to obtain additional results for maximum pressures and make sure the code was running correctly, the curves of pressure vs. time were calculated for the actual focus. Then the intensities in water were calculated by manually integrating the time-varying pressure over a complete cycle. The intensities obtained as an average from the waveforms at several positions in order to make sure that we find the maximum in each of calculations. The equation used to calculate the intensities was:

$$I = 1/\rho c(t_2 - t_1) \int_{t1}^{t2} p^2 \, dt \qquad 2.27)$$

When $p = Asin\omega t$ and $\omega = 2\pi/T$, i.e., in the linear case, substituting into Eq. 2.27 leads to:

$$I = \frac{A^2}{T\rho c}\left(\frac{T}{2\pi}\right)\int \sin^2 x dx = A^2/\rho c(\frac{1}{2\pi})\int [\frac{1}{2}(x - \sin(2x)] = A^2/2\rho c \quad 2.28)$$

$$I = A^2/\,2\rho c \quad 2.29)$$

In addition, in both diagnostic and therapeutic applications of medical ultrasound, it is necessary to know the values of acoustic field parameters in the tissue region exposed to ultrasound. These values were estimated using the calculations performed in water in a process called derating. To obtain values of *in situ* acoustic parameters, the intensity calculations in water was multiplied by an exponential term to account for losses that occur in tissue over the propagation path. This method was used in the paper by Dunn et al [26] such that the ultrasound intensity in tissue, *I*, at the depth *d* is derated as $I = I_0 \exp(-\mu d)$ with I_0 equal to the wave intensity in water at the same location linearly scaled from low to high source pressures at each frequency, $\mu = 0.20f$ cm^{-1}, the intensity absorption coefficient per unit path length of the tissue, *f* is the frequency in megahertz.

For each value of derated intensity, the corresponding exposure time that Dunn would have found for the threshold at that intensity were determined using the formula in Table II of Dunn paper [26] which described as: $I = \frac{c'(f,T)}{\sqrt{t}}$ where $t = \left(\frac{c'(f,T)}{I}\right)^2$.

Then the intensity values in tissue were calculated by integrating the pressure waveforms of tissue from the simulation over a complete cycle using the trapezoid method in Matlab.

These numbers were correlated to the numbers in the papers to find what exact exposure parameters needed to be used in the calculations to match the intensities in the papers. The results of the intensity calculations in tissue are shown in chapter III.

CHAPTER III

RESULTS AND ANALYSIS

RESULTS OBTAINED FROM 2D PRESSURE AND INTENSITY SIMULATION FOR 1 AND 3 MHZ FREQUENCIES IN WATER USING FDTD CODE

For frequencies of 1 and 3 MHz with the same spatial domain in the pressure and intensity computation, the parameters shown in Table 3.1 were determined using Matlab script. These parameters were used in the Fortran code to simulate the 2D steady state pressure as a function of axial distance from the transducer. The steady state pressures along the transducer axis and the steady state focal intensities were obtained for a series of source pressures from 10-140 kPa in water for both 1 and 3 MHz frequencies respectively. The data presented in figures 3.1 and 3.2 contain the steady state pressure amplitude and positive and negative focal pressures at both 1 and 3 MHz frequencies in water. The steady state pressures for the complete signal can be seen in Fig. 3.1 at source pressures ranging from 10 to 70 kPa for both 1 and 3 MHz. In order to make sure the pressure waveform reached the steady state, different simulation times were applied, and the behavior of the waves was tracked. If the waveform looked the same with different time lengths it has to be steady state because it is not changing; otherwise it is not steady state. In our case, we ran our code with different simulation times, and we reached a steady state result at each time. So we made sure that the waveform looks good, as can be seen in Figs. 3.1 (a) and (c) for different frequencies of 1 and 3 MHz. The windowed signal is shown in Figs. 3.1 (b) and (d) which indicate the expanded waveforms, just to better track the signal's behavior. As can be seen from the peaks, the focal pressures are increased as source pressures increase. Distortion of the waves increases with increasing source pressures as well as increasing frequency.

For a frequency of 1MHz, the source pressures ranging from 10 to 140 kPa yielded higher peak positive focal pressures of 0.77 to 12.80 MPa and lower peak negative focal pressures of 0.76 to 9.41 MPa when the simulated space is water as shown in Fig 3.2 (a) and (b). Similar results are given for 3 MHz in Figs. 3.2 (c) and (d). For example, the peak positive focal pressures increased from 2.23 to 56.71 MPa in the water, while the corresponding values for peak rarefactional pressures range from 2.11 to 24.76 MPa. From the simulation results, it can be concluded that the pressure amplitudes at 3MHz are higher than the pressure amplitudes at 1MHz due to the sharper and narrower focus at 3MHz. The positive focal pressure was almost 3 times higher for the highest source pressure of 140kPa in the focal region compared to 70kPa at 3MHz, and it almost doubled at 1MHz for those source pressures. Likewise the negative focal pressure almost doubled for the highest source pressure of 140kPa compared to 70kPa at both 1 and 3 MHz.

Generally, by looking at the focal pressure waveforms for both 1 and 3 MHz, it can be seen that the peaks and the focal pressures are increased as source pressures increase. Distortion of the waves increases with increasing source pressures as well as increasing frequency, as we expected. When frequency grows, more harmonics and increasingly distorted waves will appear. It is also obvious that the actual acoustic focal length is shorter (12.3cm) than the geometric focal length (13 cm) because of water refraction in the FDTD solution, which is expected.

Table 3.1 Simulation Parameters for 2-D pressure code at 1and 3MHz frequencies in water

Simulation Parameters	***Values for* 1MHz**	***Values for* 3MHz**
Max distance in z-direction- zmaxP	20cm (0.2 m)	20 cm (0.2 m)
Max distance in r-direction- rmaxP	10cm (0.1 m)	10 cm (0.1 m)
Max distance in z-direction- zmaxT (temperature space)	15cm (0.15m)	15cm(0.15m)
Max distance in r-direction- zmaxT(temperature space)	10cm (0.1m)	2cm (0.02m)
Spatial step in z direction- dzp	1.5×10^{-4} m	5.0×10^{-5} m
Spatial step in r direction- drp	1.5×10^{-4} m	5.0×10^{-5} m
Time step- dtp	5×10^{-8} s = 0.05μs	1.6667×10^{-8} s
Number of acoustic cycles- Nptspercycle	20	20
Max index in z-direction- Imaxp	1334	4001
Max index in r-direction - Jmaxp	668	2001
Max index in z-direction temp- ImaxT	1001	3001

Max index in r-direction temp-JmaxT	668	401
Distance from front face of transducer to front surface of tissue – Iskin	68	201
Coordinate of geometric focus of transducer in z-axis - Ifocusp	868	2601
Coordinate of geometric focus of transducer in r axis-Jfocusp (symmetry)	1	1
Tend to end time index	$2.7 \times 10^{+3}$ s	$7.99 \times 10^{+3}$ s
Max index in time- Nmaxp	3000 (each unit equivalent to 0.05μs)	8000 (each unit equivalent to 0.016 μs)

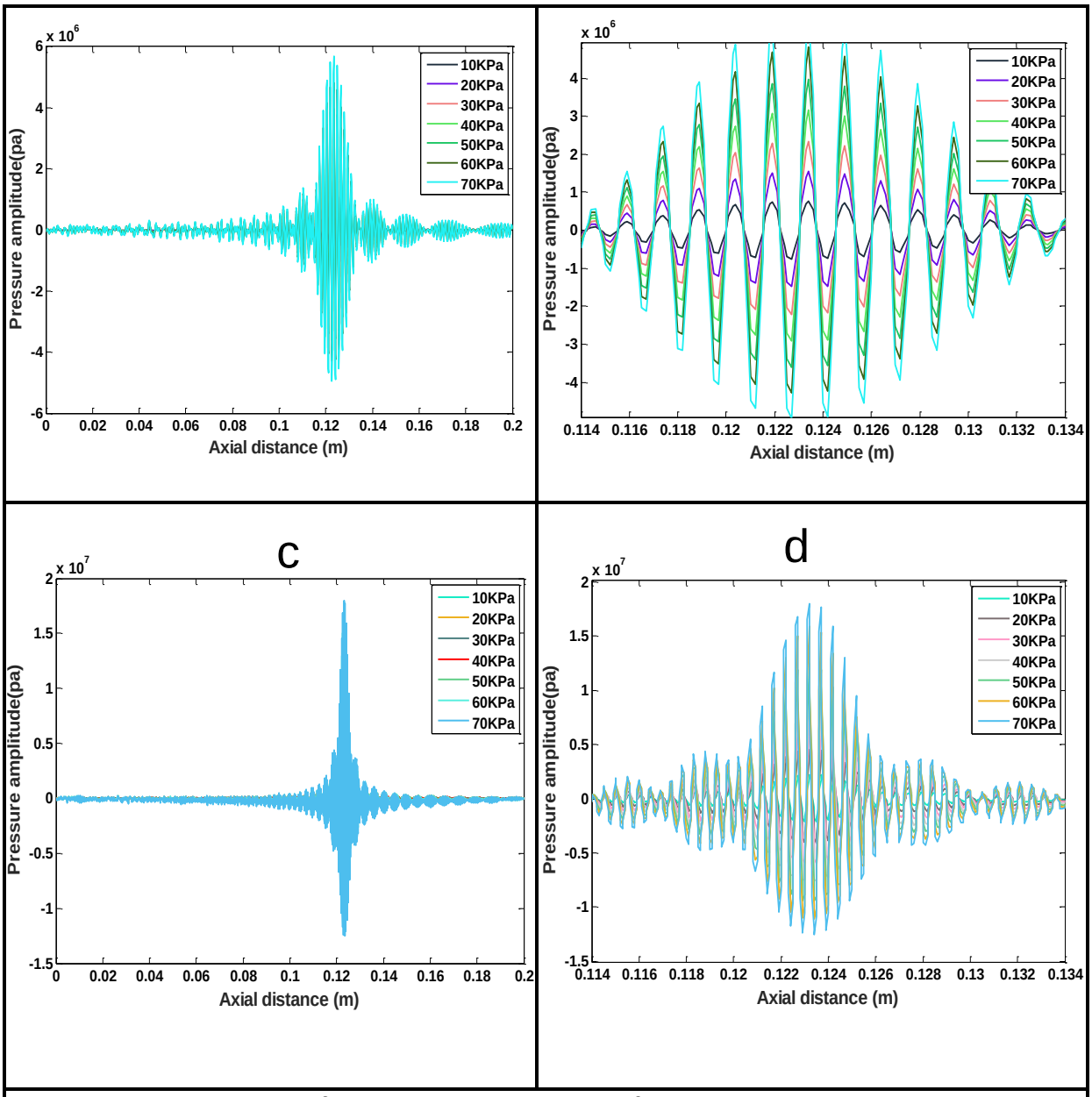

Fig.3.1: Characterization of steady state pressure waveforms showing (a) pressure along axial distance of 1 MHz transducer (b) windowed waveforms vs. axial distance of 1 MHz transducer (c) pressure along axial distance of 3MHz transducer (b) windowed waveforms vs. axial distance of 3 MHz transducer

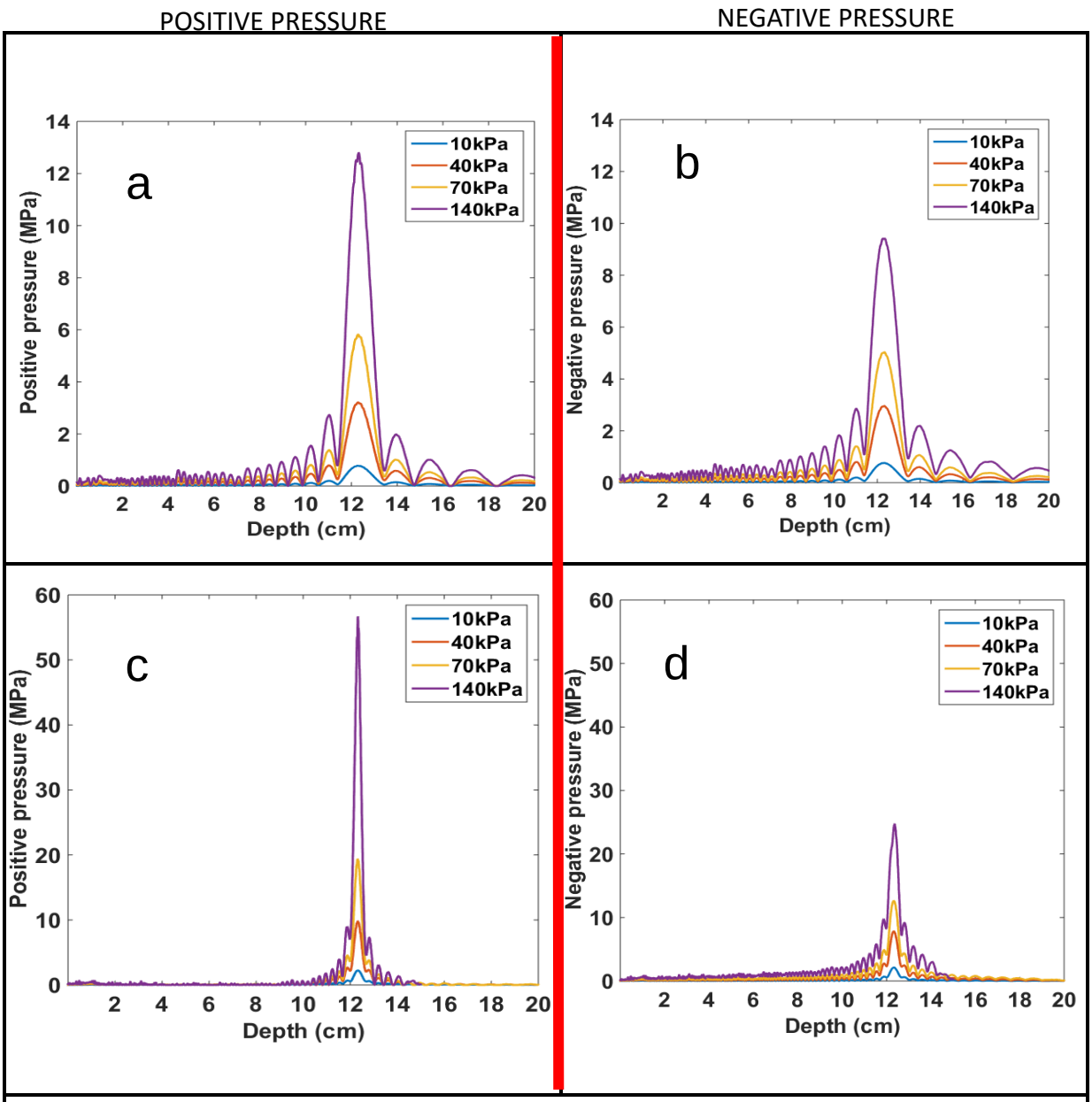

Fig.3.2: Characterization of 1 and 3 MHz transducer in water showing (a) steady state compressional pressure vs. depth at 1MHz (b) steady state rarefactional peak pressure vs. depth at 1MHz (c) steady state compressional pressure vs. depth at 3MHz (d) steady state rarefactional peak pressure vs. depth at 3MHz.

In order to confirm that our calculation results for 3MHz are still consistent, the FDTD code was applied for a smaller step size ($dx = 4 \times 10^{-5}, dt = 8 \times 10^{-9}$) in our numerical model. The reason for this implementation was to obtain additional higher harmonics and the resulting extra distortion of the waveforms beyond that which was observable from our calculation outputs and pressure profiles with the larger step size.

The peak positive and negative pressures for the source pressures of 10, 40, and 70 kPa are shown in the water in figure 3.3. The positive peak amplitudes are 2.23, 9.81, and 19.4MPa, respectively, for 10, 40, and 70 kPa, while the negative peak pressures are 2.08, 7.50, and 11.81 MPa. Both compressional and rarefactional peak amplitudes are in a good agreement with previous calculations we made at 3MHz frequency to verify the stability of our results.

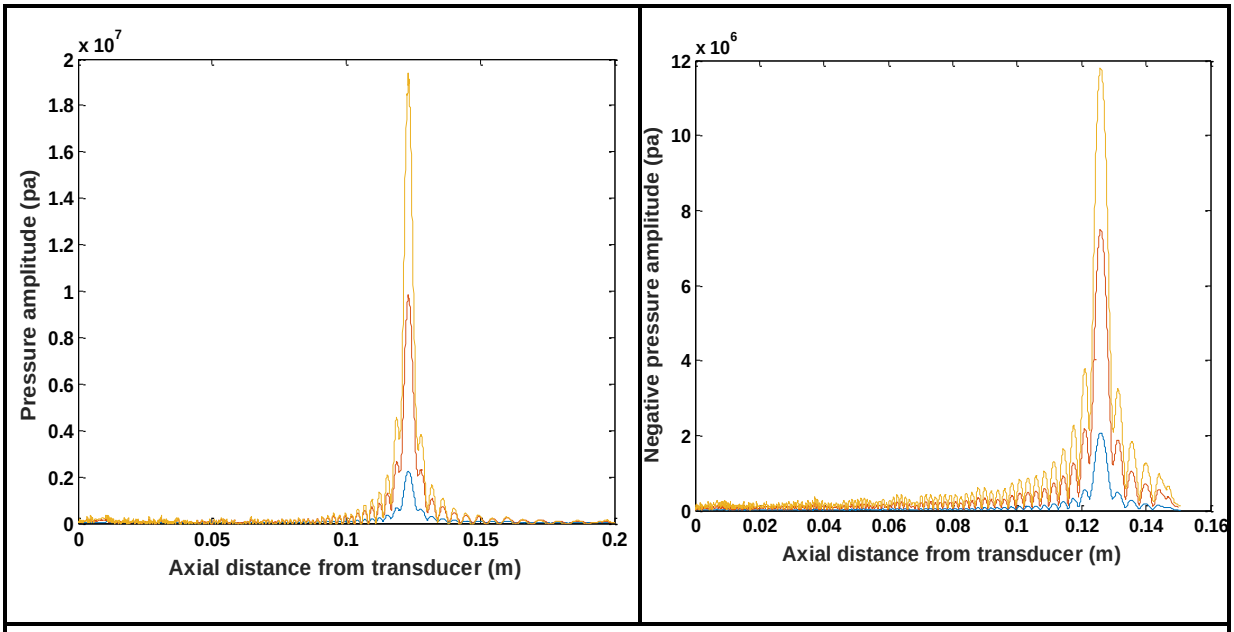

Figure 3.3: Smaller step size simulation for (a) positive amplitude and (b) negative amplitude at source pressures of 10, 40, and 70 kPa for 3MHz frequency in water.

The simulated spatial intensity profile as a function of axial and radial distance was plotted in Fig. 3.4. The spatial acoustic intensity in water was computed in 2D in the simulation space as shown in the figure. In order to save computation time in the simulation, the intensity space was mapped only in a subsection of the space containing the region of interest. This space is also axially (cylindrically) symmetric, and it only shows half of the focal zone, not the entire focal region. As can be seen from figures (a) and (b), the intensity was found at the real focus of the transducer, which has a shorter length than geometric focus due to the water refraction. Moreover, comparing the color distribution for the simulated intensity (dark red means high intensity and dark blue means low intensity) at 1 and 3 MHz, it is shown that the simulated intensity values for 3 MHz are much greater than 1MHz due to the sharper focus at the higher frequency. For instance, a source pressure of 10 kPa gives an intensity of $1194\mathrm{W/cm^2}$ at 1MHz compared to $12338\,\mathrm{W/cm^2}$ at 3 MHz, the latter being about 10 times higher than the intensity at 1MHz. These ranges of intensities were compared to the intensity numbers we obtained from the numerical simulation shown in the next chapter.

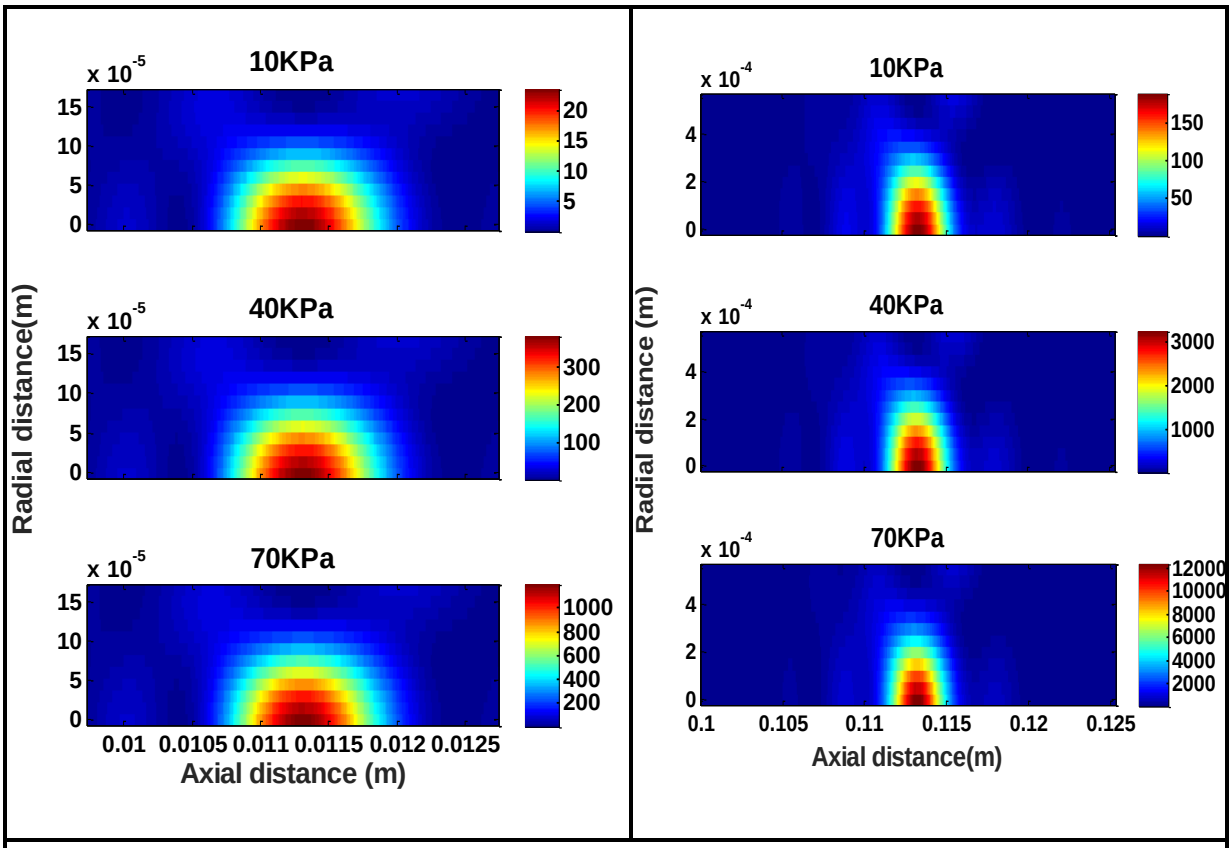

Fig.3.4: Acoustic intensity as a function of axial and radial location for FDTD solution to the wave equation. The peak intensity at the focus is 1194 W/cm^2 for (a) 1MHz and 12338 W/cm^2 for (b) 3MHz at 70 kPa source pressure.

RESULTS OBTAINED FROM 2D PRESSURE SIMULATION FOR TRANSDUCER LENS ASSEMBLY BOTH CALCULATION AND MEASUREMENT

As explained before, we need to verify that our sound propagation model accurately predicts the spatial pressure distribution generated by a planner transducer covering with a focusing lens. Pressure is the most conveniently measurable quantity and thus will be used for comparison. As described in Section 2.6, the pressure field was calculated using the Fortran code to compere our calculations with the measurements we made in the scan tank. This can be achieved in pure water with the hydrophone fixed in place. Results for the simulation parameters using the code are presented in Table 3.2.

Figure 3.5 shows the pressure profile as a function of the radial and axial distance from the acoustic axis of x, y, and z for the 1.21 MHz transducer in water and the peak voltages (pressure) are 277, 279, and 275 mV, respectively.

Figure 3.6 shows computed and measured results obtained in water at 30°C for the sound sources. The pressures shown at (a) and (b) are all peak positive quantities of calculation and measurement that have been normalized to the spatial maximum value present at the real focal point. The axial distance in plot (b) shows the shifted axis by some amounts in order to have the same range and unit as (a). The plot (c) shows the solid red and blue lines which correspond to calculation and measurement respectively. Except for the peripheral regions of the field, we see that our model is able to predict all the detailed structure, and good agreement was found in the focal region (real focus of 5.20 cm) and beyond and also we observed no odd hotspot in the field.

Table 3.2: Simulation parameters for 1.21-MHz transducer-lens assembly

FDTD Simulation Parameters	***Value***
Max distance in z-direction- zmaxp	10 cm (0.1 m)
Max distance in r-direction- rmaxp	5 cm (0.05 m)
Spatial step in z direction- dzp	1.5×10^{-4} m
Spatial step in r direction- drp	1.5×10^{-4} m
Time step- dtp	5×10^{-8} s = 0.05μs
Number of acoustic cycles- Nptspercycle	17
Max index in z-direction- Imaxp	668
Max index in r-direction - Jmaxp	334
Max index in z-direction temp- ImaxT	401
Max index in r-direction temp- JmaxT	201
Distance from front face of transducer to tissue front surface – Iskin	68
Actual focal length	5.20 cm
Geometric focal length	5.5 cm
Coordinate of geometric focus of transducer - Ifocusp	386
Coordinate of focus of transducer- Jfocusp (symmetry)	1
Tend to end time index	$1.3 \times 10^{+3}$ s
Max index in time- Nmaxp	1500 (each unit equivalent to 0.05μs)

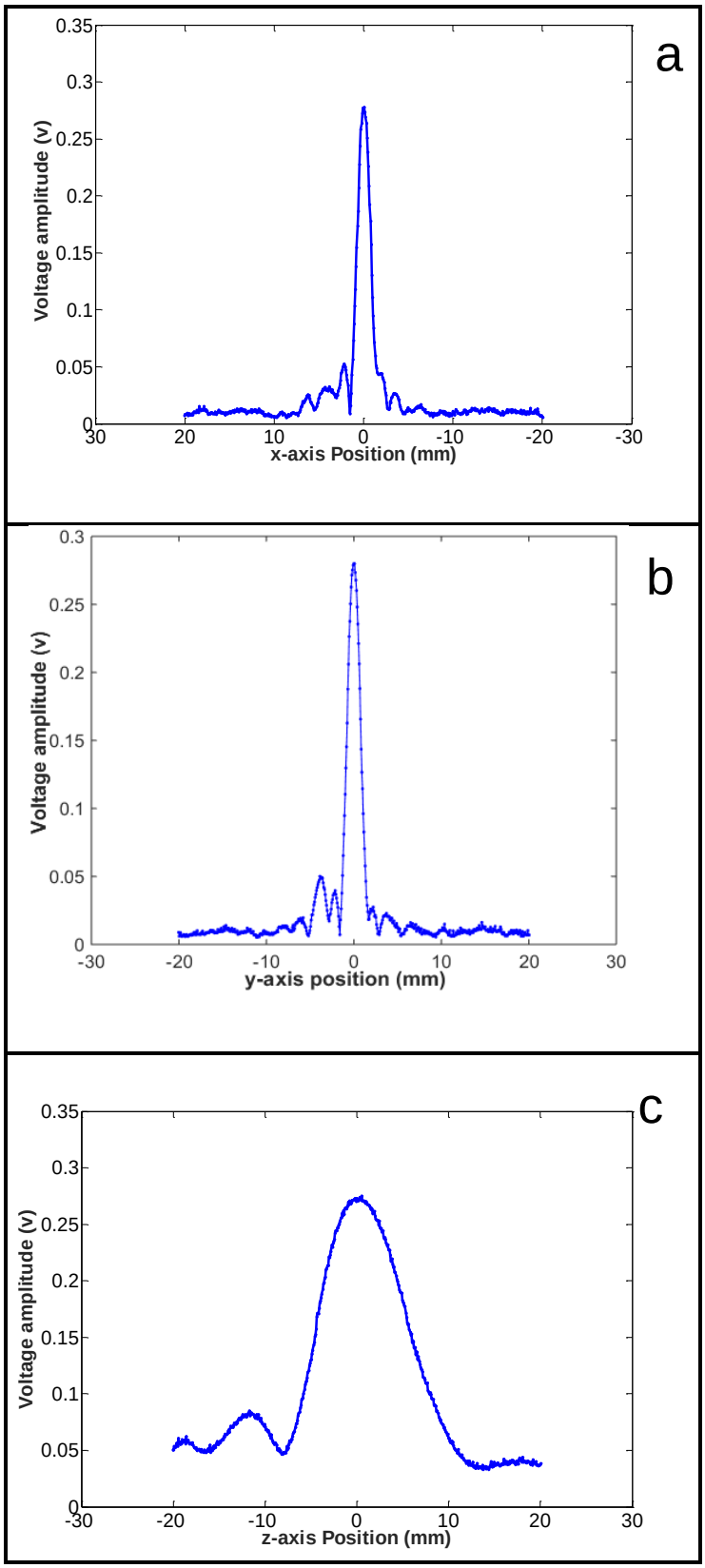
a
Voltage amplitude (v)
x-axis Position (mm)
b
Voltage amplitude (v)
y-axis position (mm)
c
Voltage amplitude (v)
z-axis Position (mm)

Figure 3.5: Characterization of the 1.21 MHz Sonostat transducer showing, (a) voltage amplitude in radial direction x, (b) voltage amplitude in radial direction y, (c) voltage amplitude in axial direction z.

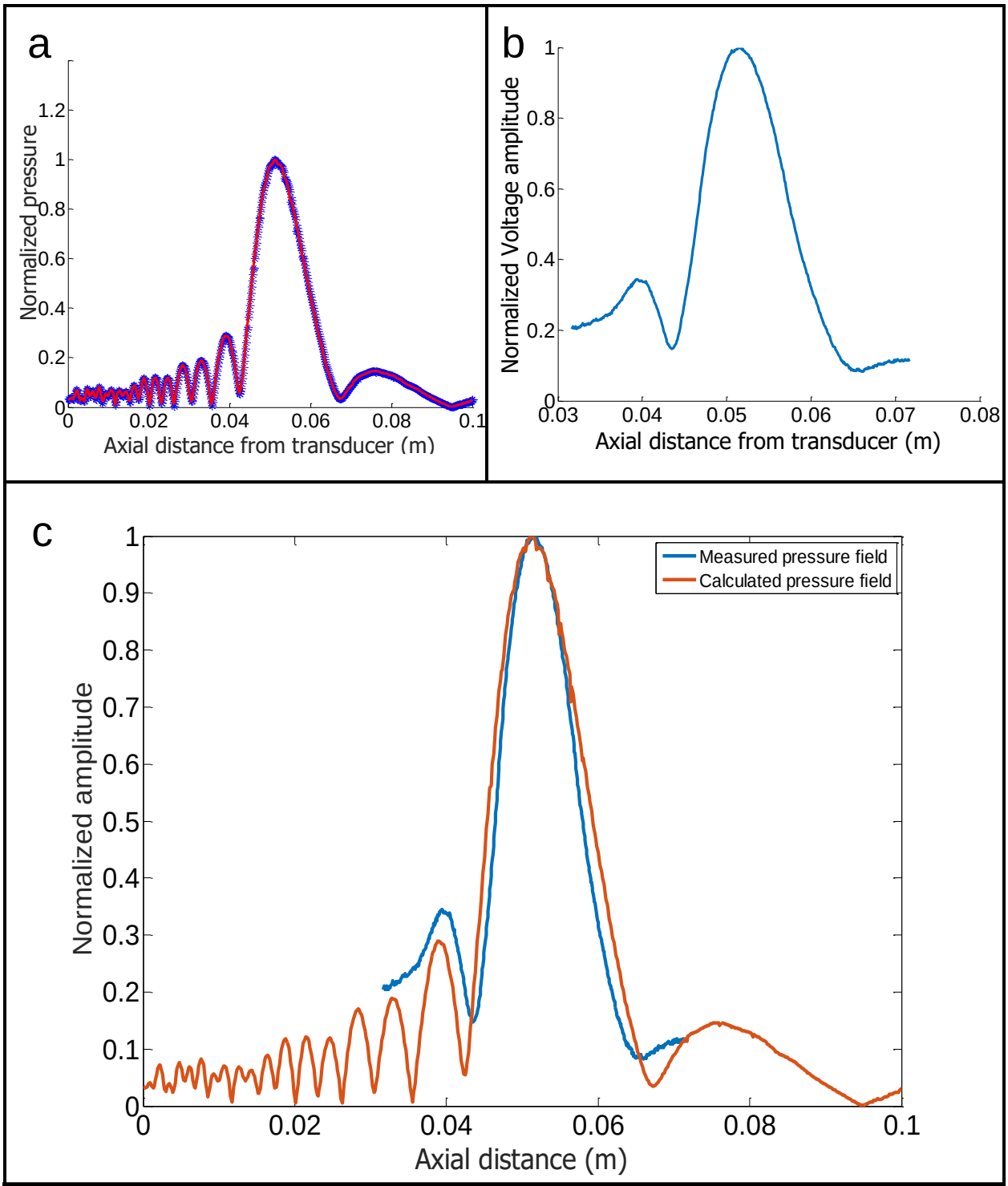

Figure.3.6: Characterization of the 1.21-MHz transducer-lens combination showing normalized calculated (a) and measured (b) positive peak pressure profiles in axial direction , and (c) a comparison of the normalized pressure profiles verses axial distance for the transducer obtained from calculation (using the code) and measurement (using the scan-tank).

In the following section, the experimental data collected during the experiment are presented. Figure. 3.7 contains four images shown the focal zone scans; the top left image (a) marked with the acoustic axis is the experimental data from the plane scan using the hydrophone. The bottom left image (b) marked with the positive value indicate the scan for the distance of 1 mm beyond the focal zone.

Other sets of data are shown in figures (c) and (d), which are the field measurements with a negative distance beyond the focal zone of transducer, respectively.

The images show millimeters on both axes, and the color adds a third dimension to the graph: the relative amplitude of the pressure field. The dark blue indicates lowest pressure, and the dark red indicates the highest pressure.

By comparing the color distribution in the experimental data and also the pressure amplitude for each graph, it is noticeable that whenever the hydrophone is beyond the center of the scan plane, in general, the amplitude of the pressure field (and therefore the electrical signal) captured by the oscilloscope decreases. The size of the signal can vary greatly over the scan plane.

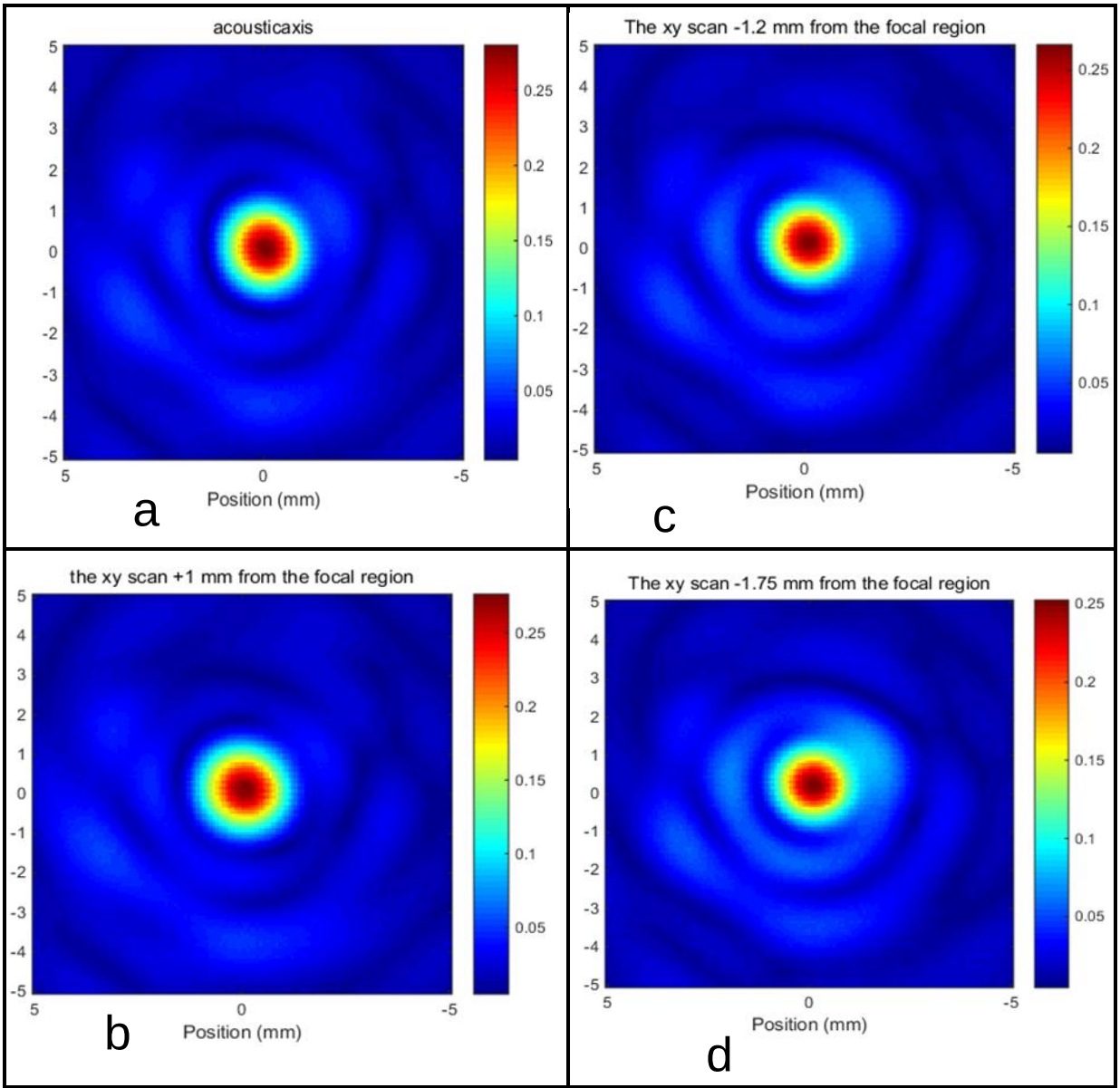

Fig.3.7: Pressure field pattern of transducer-lens, peak-to-peak voltage of: a) 275 mV at the focus ; b) 270.3 mV for 1mm beyond the focus; and c) 257.8 mV for -1.2mm beyond the focus ; and d) 248.5 mV at -1.75 mm beyond the focus

RESULTS OBTAINED FROM PRESSURE AND INTENSITY CALCULATIONS FOR 1 AND 3 MHZ IN WATER

Tables 3.3 and 3.4 illustrate the results from the intensity calculations in water at 1 and 3 MHz. As mentioned before, the goal of these intensity calculations was to compare them with the intensity numbers from the simulation to verify our numerical model and also use these values to determine the derated intensities in tissue, as explained in section 2.8.

Table 3.3: Intensity calculations for 1MHz frequency in water

Source pressure (kPa)	**Focal pressure (MPa)**	**Calculated Intensity** $\boldsymbol{I = \frac{p^2}{2\rho c}}$ $(\frac{\mathbf{W}}{\mathbf{cm^2}})$	**Pressure vs time at the position of the peak pressure (MPa)**	**Calculated Intensity** $\boldsymbol{I = \frac{1}{\rho c T}\int p^2 dt}$ $(\frac{\mathbf{W}}{\mathbf{cm^2}})$	**Simulated Intensity** $(\frac{\mathbf{W}}{\mathbf{cm^2}})$
10	0.77	20.15	0.77	20.16	23.5
20	1.57	82.26	1.57	82.26	94.5
30	2.40	189.3	2.40	189.30	213
40	3.21	343	3.21	343.50	381
50	4.06	550	4.06	550.00	559
60	4.92	810	4.93	810.00	871
70	5.82	1126	5.82	1130.00	1194
140	12.80	5461.3	12.80	5461.30	5560

ρ water $= 1000\ kg/m^3$ $\quad$ c water $= 1500$ m/s

Table 3.4: Intensity calculations for 3MHz frequency in water

Source pressure (kPa)	**Focal pressure (MPa)**	**Calculated Intensity** $\boldsymbol{I = \frac{p^2}{2\rho c}}$ $(\frac{\mathbf{W}}{\mathbf{cm^2}})$	**Pressure vs time at the position of the peak pressure (MPa)**	**Calculated Intensity** $\boldsymbol{I = \frac{1}{\rho c T}\int p^2 dt}$ $(\frac{\mathbf{W}}{\mathbf{cm^2}})$	**Simulated Intensity** $(\frac{\mathbf{W}}{\mathbf{cm^2}})$
10	2.23	167	2.23	167	188.61
20	4.60	705.02	4.65	720.75	777.72
30	7.09	1677	7.10	1684.12	1758.9
40	9.81	3212.33	9.78	3193.33	3238.7
50	12.67	5350.9	12.21	4969.47	4918.9
60	15.90	8427	15.75	8400.52	8239.2
70	19.40	12545	18.50	11433	12338
140	56.71	107200.80	56.71	107200.80	117230

ρ water $= 1000\ kg/m^3$ $\quad$ c water $= 1500$ m/s

Figure 3.8 shows the time-varying pressure waveforms at the location of the peak pressure (pressure at the focus) for series of source pressures from 10-70 kPa .The averaged peak positive pressure over several positions was found in the range of 0.77- 5.82 MPa at 1MHz as can be seen in fig (a), while the corresponding values of the averaged peak pressures at 3MHz were found in the range of 2.23- 18.5 MPa. These values were used to calculate the intensity numbers both at 1 and 3 MHz in water.

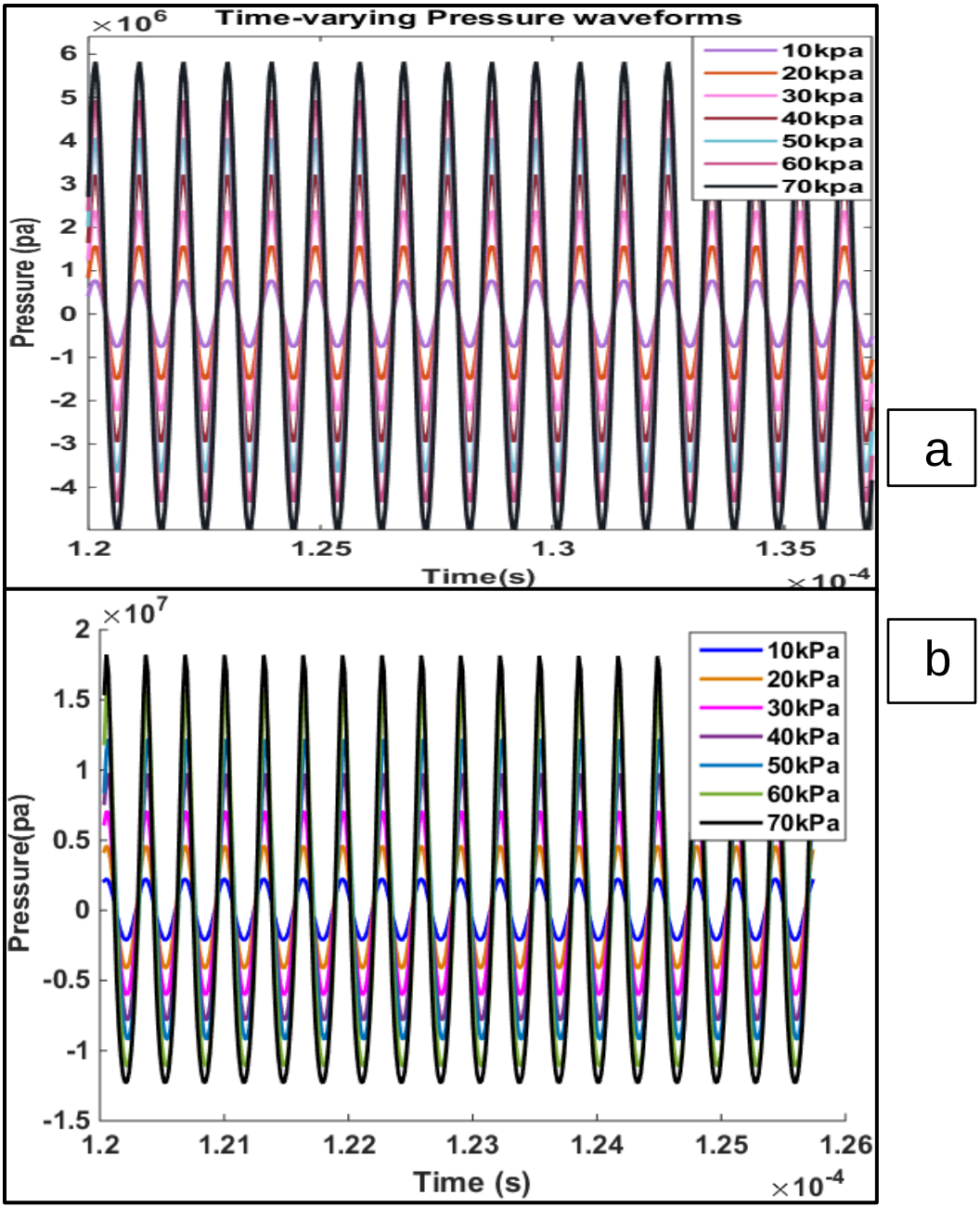

Fig.3.8: Time-varying pressure waveforms for a series of source pressure in water for (a) 1MHz and (b) 3MHz frequency

Figure 3.9 shows the comparison of the simulated intensities using the numerical FDTD code and calculated intensities from pressure waveforms integration. A good agreement between these two computations were found in order to verify our numerical model.

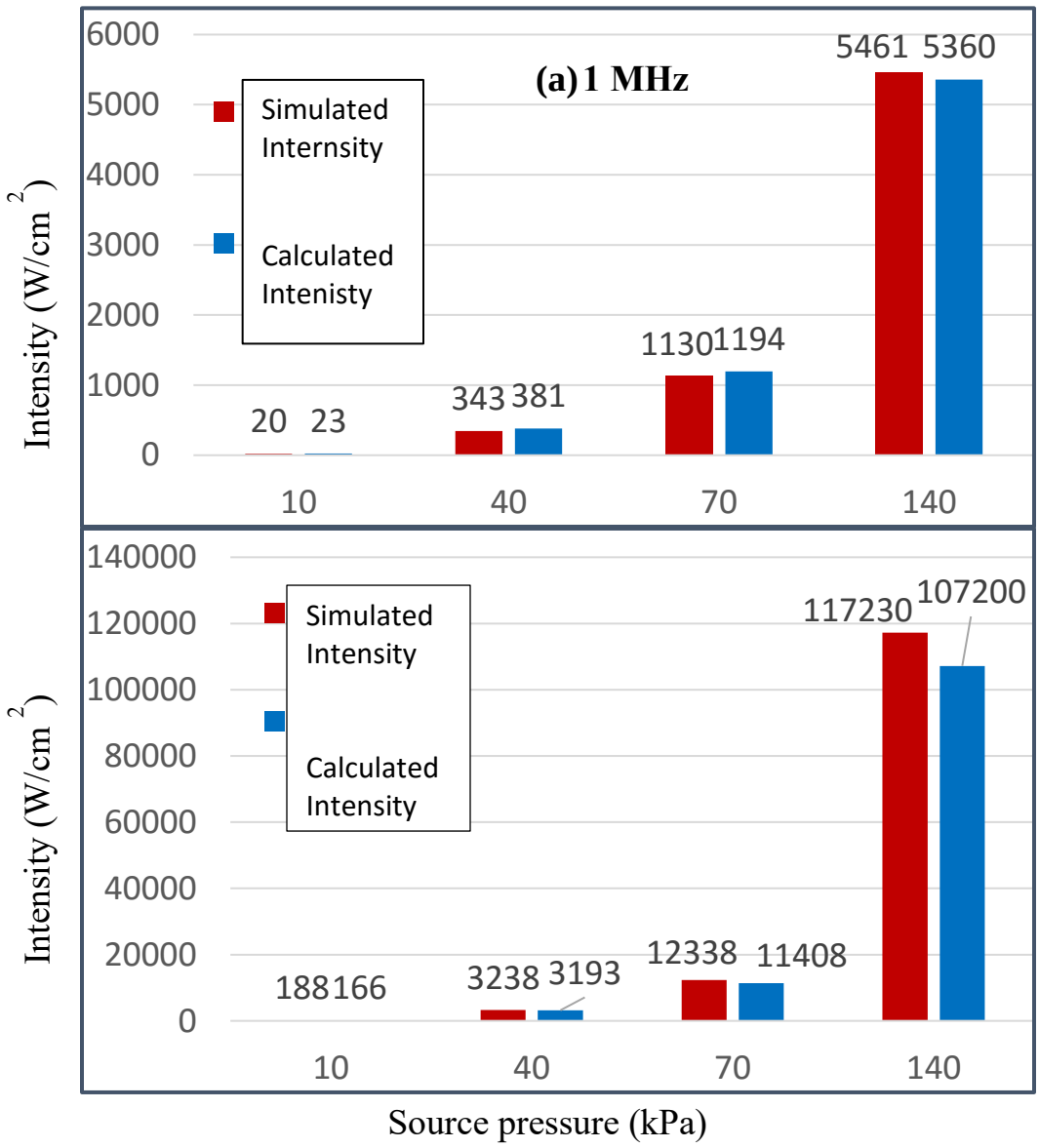

Figure 3.9: Comparison of simulated and calculated intensities in water vs. source pressure at (a) 1 and (b) 3MHz

RESULTS OBTAINED FROM 2D PRESSURE AND INTENSITY SIMULATION FOR 1 AND 3 MHZ FREQUENCIES IN TISSUE USING FDTD CODE

The pressure amplitudes in tissue were calculated with the same process used to calculate the pressure amplitudes in water. Table 3.5 shows the simulation parameters at 1 and 3 MHz frequencies for tissue obtained by Matlab scripts. Figure 3.10 shows the comparison of the pressure amplitude in water and tissue at both 1 and 3 MHz derived at 140 kPa. The black dashed line indicates the tissue region with a thickness of 3 cm. Looking through the data of figures 3.10 indicates that nonlinear distortion of the waveform accumulated differently in tissue and in water due to higher attenuation and thus less wave amplitude over the propagation path in tissue. It is clear that the actual acoustic focal length in tissue is shorter (12.21cm) than the actual focal length of water (12.3cm). This is due to the fact that the degree of refraction of the beam from the transducer surface depends on the speed of sound in the medium. This leads to less focal pressure amplitudes in the case of tissue than water. Moreover, it is clearly visible that a lower pressure amplitude is obtained in the focal region in tissue than in water due to the higher attenuation coefficient of tissue, which leads to more attenuated pressure amplitude and eventually less wave amplitude over the propagation path in tissue. The same behavior can be found at 3MHz with even more attenuated pressure amplitude in tissue. This is due to the fact that attenuation depends on frequency linearly; by increasing the frequency, attenuation will also increase, which leads to more attenuated pressure amplitude. Since by increasing the frequency, harmonics will grow, so the attenuation of the nonlinear distorted waves in tissue is also higher than predicted by the given equation in Dunn's paper [26]. This is because of the generation of higher harmonics that are absorbed more than fundamental frequency.

The positive and negative peak pressures for 1 and 3 MHz frequencies are shown respectively in Figure 3.11. Figure (a) shows the higher compressional pressures as 0.67, 2.76, 4.97, and 10.74 MPa corresponding to the source pressures of 10, 40, 70, and 140 kPa, respectively, at a distance of 10cm from the source, i.e., where the beam enters the tissue, to the nominal focus at 13cm (Tissue thickness 3cm), while figure (b) shows the corresponding lower rarefactional pressure at the peak values of 0.66, 2.58, 4.42, and 8.35 MPa with the same range of source pressures and the same distances at 1MHz. Similar results are given for 3 MHz in figures (c) and (d). Figure (c) shows the positive peak pressures as 1.40, 5.90, 11.00, and 27.5 MPa corresponding to the source pressures of 10. 40, 70 and 140 kPa, respectively, while figure (d) illustrates the negative peak pressures at 1.35, 5.11, 8.51, and 14.90 MPa. Herein for 1 and 3 MHz, like the water media, the pressure amplitude in the main focal lobe is significantly higher than in the pre-focal region, and the length of the focal region is much shorter than the geometric focal length. Under these conditions, it is hypothesized that the distortion of the waves increased mainly with increasing driving level and frequency, and the peak pressures also became larger with increases in source pressures. In addition, the 3MHz frequency shows higher pressure amplitudes than 1MHz.

The focal peak pressures and intensities were calculated in the tissue of various thicknesses of 3, 2, and 1 cm, when the distal surface of the tissue is at 13 cm, which is the geometric focus. The results of compressional and rarefactional peak pressures, calculated intensities using simulations, and derated intensities are indicated for both 1 and 3 MHz frequencies are shown in Tables 3.6 (a) and (b) respectively. From the results as shown in figures 3.12 and 3.13, it can be

concluded that that as source pressure increases, the calculated intensities are increased and derated intensities using the formula $I = I_0 \exp(-\mu d)$] agreed well with numerical simulation in tissue and derated (reduced) more compare to intensity numbers in water, as we expected. Moreover as tissue thickness increases from 1 to 3 cm, the intensities attenuate more as expected from the exponential relation between intensity and thickness of tissue. The same behavior can be found for both positive and negative peak pressure amplitudes at1 and 3 MHz.

For each value of derated intensity, the exposure time was computed using equation $t = \left(\frac{c'(f,T)}{I}\right)^2$ as shown in the last column of Table 3.6 (a) and (b). These numbers can be correlated with given exposure times in a log-log plot in the Dunn paper [26] which will discussed in next chapter.

Table 3.5 Simulation Parameters for 2-D pressure code at 1and 3 MHz frequencies in tissue

Simulation Parameters	**Values for 1MHz**	**Values for 3MHz**
Max distance in z-direction- zmaxP	15cm (0.15m)	15cm (0.15m)
Max distance in r-direction- rmaxP	6.5 cm (0.65m)	6.5 cm (0.65m)
Max distance in z-direction- zmaxT (temperature space)	14cm (0.14m)	14cm (0.14m)
Max distance in r-direction- zmaxT(temperature space)	6.35cm (0.635m)	6.35cm (0.635m)
Distance from front face of transducer to front surface of tissue – Iskin	10 cm (0.10m)	10 cm (0.10m)

Spatial step in z direction- dzp	1.5×10^{-4} m	5.0×10^{-5} m
Spatial step in r direction- drp	1.5×10^{-4} m	5.0×10^{-5} m
Time step- dtp	5×10^{-8} s = 0.05μs	1.6667×10^{-9} s = 0.0016μs
Number of acoustic cycles- Nptspercycle	20	20
Max index in z-direction- Imaxp	1001	3001
Max index in r-direction - Jmaxp	434	1301
Max index in z-direction temp- ImaxT	934	2801
Max index in r-direction temp- JmaxT	424	1271
Distance from front face of transducer to front surface of tissue – Iskin	668	2001
Coordinate of geometric focus of transducer in z-axis - Ifocusp	868	2601
Coordinate of geometric focus of transducer in r axis-Jfocusp (symmetry)	1	1
Tend to end time index	$2.0 \times 10^{+3}$ s	$5.9 \times 10^{+3}$ s
Max index in time- Nmaxp	2500 (each unit equivalent to 0.05μs)	6000 (each unit equivalent to 0.0016μs)

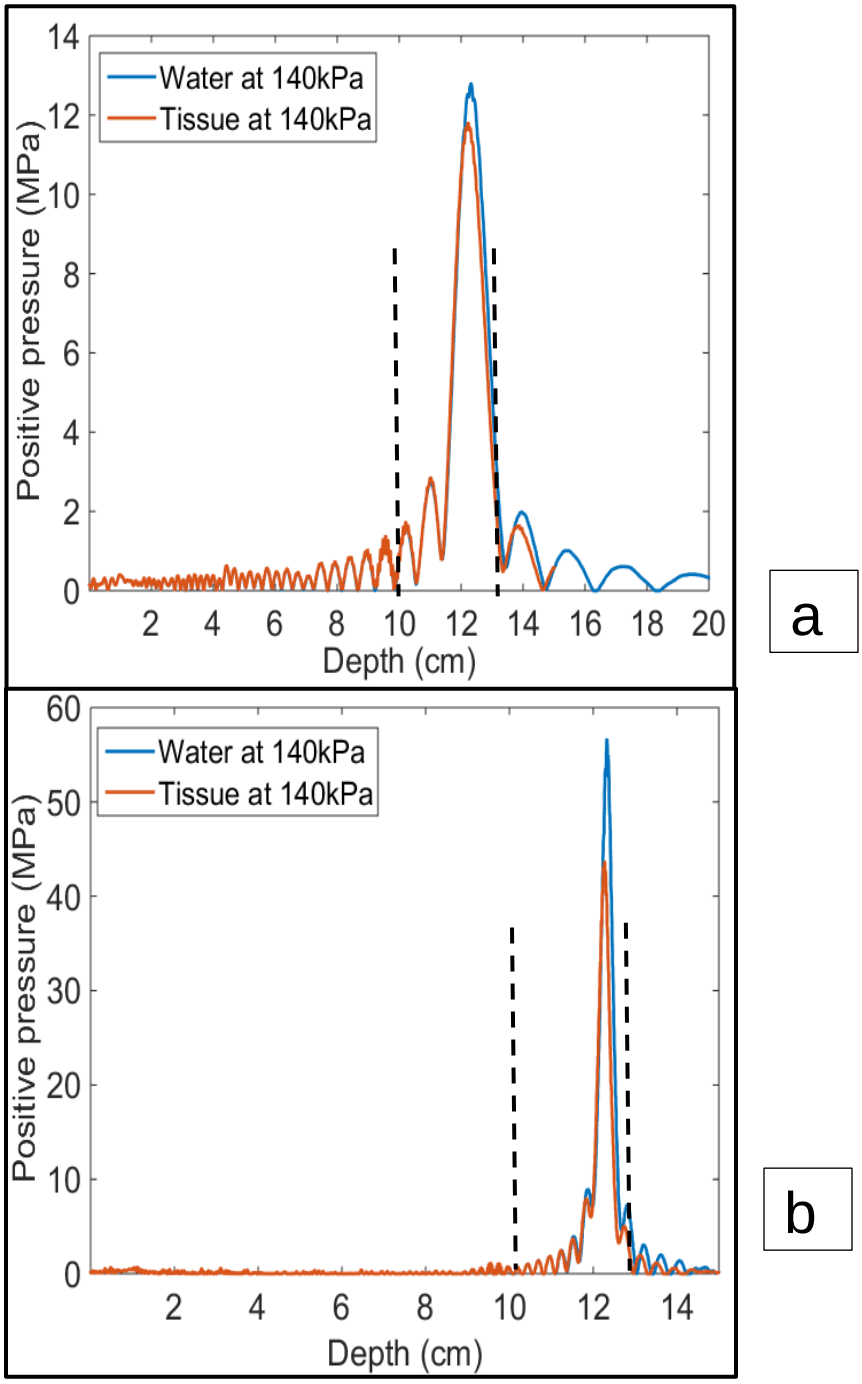

Figure3.10: Comparison of tissue and water pressure amplitudes at the focus at (a) 1 and (b) 3 MHz

Table 3.6 (a): Peak focal pressures and intensities in tissues of various thicknesses at 1 MHz

Tissue thickness 1cm (12-13 cm)

Source Pressure (kPa)	Positive Pressure (MPa)	Negative Pressure (MPa)	Intensity in tissue		Time (sec)
			Calculated (W/cm^2)	by derating (W/cm^2)	Exposure Time (sec)
10	0.77	0.75	17.93	16.50	376.12
40	3.20	2.95	286.84	281.23	1.29
70	5.80	5.04	965.25	925.16	0.11
140	12.72	9.53	3992.40	4471.33	0.005

Tissue thickness 2 cm (11-13 cm)

Source Pressure (kPa)	Positive Pressure (MPa)	Negative Pressure (MPa)	Intensity in tissue		Time (sec)
			Calculated (W/cm^2)	by derating (W/cm^2)	Exposure Time (sec)
10	0.72	0.70	15.80	13.51	561.03
40	2.98	2.76	237.11	230.25	1.93
70	5.40	4.70	778.50	757.46	0.17
140	11.81	8.80	3296.00	3660.87	0.007

Tissue thickness 3 cm (10-13 cm)

Source Pressure (kPa)	Positive Pressure (MPa)	Negative Pressure (MPa)	Intensity in tissue		Time (sec)
			Calculated (W/cm^2)	by derating (W/cm^2)	Exposure Time (sec)
10	0.67	0.66	13.42	11.06	837.12
40	2.76	2.58	223.61	188.51	2.88
70	4.97	4.42	686.87	620.15	0.26
140	10.74	8.35	2818.10	2997.22	0.011

"By derating" means use equation 2 from Dunn et al [24] [$I = I_0 \exp(-\mu d)$] with I_0 equal to the computed values for water, $\mu = 0.20f$ cm^{-1}, and d = 1, 2, 3 cm, (Distance from where the beam enters the tissue to the focus).

Table 3.6 (b): Peak focal pressures and intensities in tissue of various thicknesses at 3 MHz

Tissue thickness 1 cm (12-13 cm)

Source Pressure (kPa)	Positive Pressure (MPa)	Negative Pressure (MPa)	Intensity in tissue		Time (sec)
			Calculated (W/cm^2)	by derating (W/cm^2)	Exposure Time (sec)
10	2.14	2.02	143.73	91.65	10.71
40	9.50	7.37	2272.10	1752.53	0.02
70	19.07	11.81	6505.80	6274.56	0.002

Tissue thickness 2 cm (11-13 cm)

Source Pressure (kPa)	Positive Pressure (MPa)	Negative Pressure (MPa)	Intensity in tissue		Time (sec)
			Calculated (W/cm^2)	by derating (W/cm^2)	Exposure Time (sec)
10	1.72	1.65	83.94	50.30	35.57
40	7.41	6.18	1391.9	961.81	0.09
70	14.21	10.14	4640.30	3443.60	0.007
140	43.74	18.40	21406.00	32288.26	8.63×10^{-5}

Tissue thickness 3 cm (10-13 cm)

Source Pressure (kPa)	Positive Pressure (MPa)	Negative Pressure (MPa)	Intensity in tissue		Time (sec)
			Calculated (W/cm^2)	by derating (W/cm^2)	Exposure Time (sec)
10	1.40	1.35	54.68	27.60	118.14
40	5.90	5.11	886.32	527.85	0.32
70	11.00	8.51	2768.00	1889.90	0.02
140	27.5	14.90	12423.00	17720.17	2.86×10^{-4}

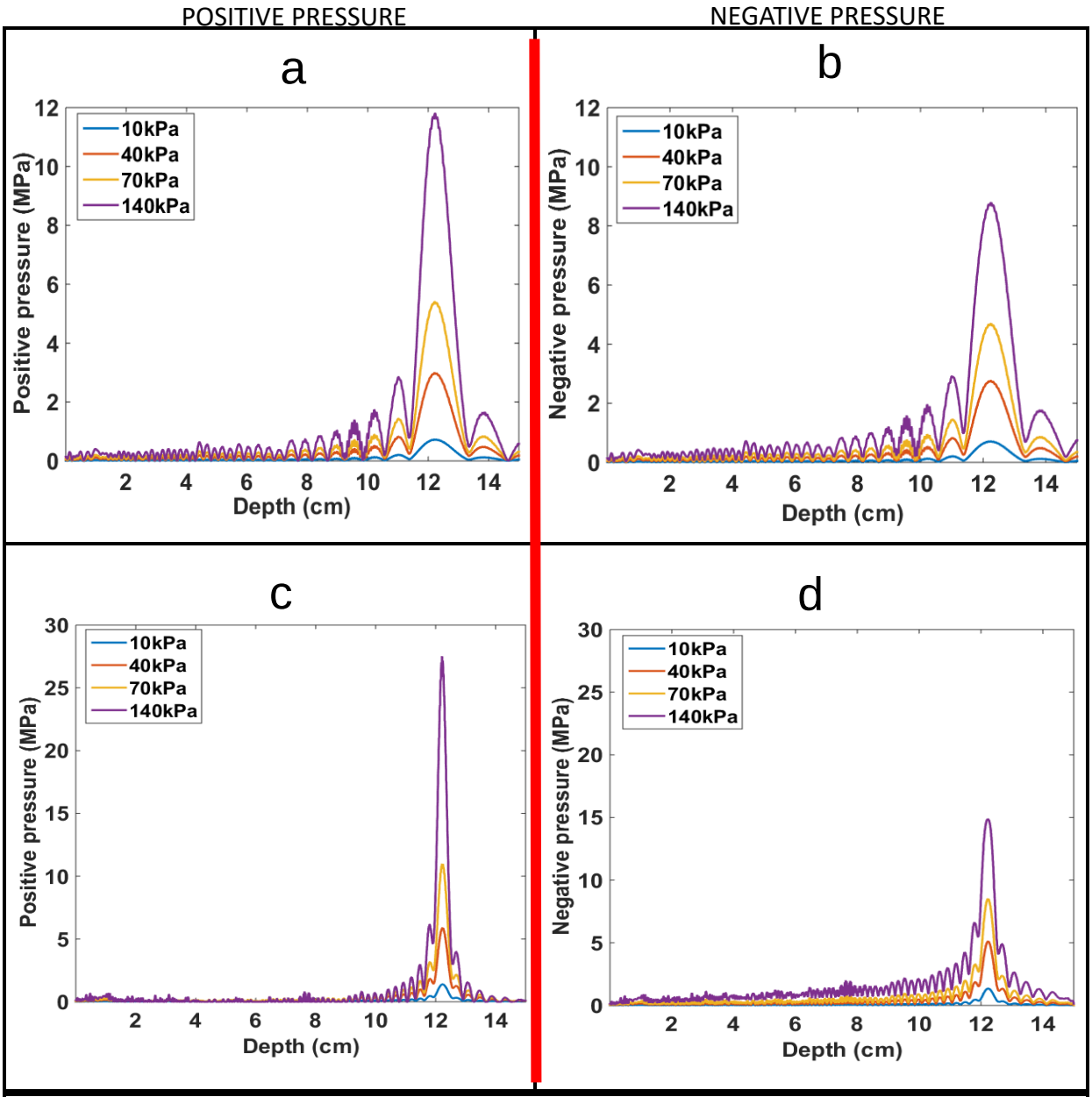

Fig 3.11: Characterization of 1 and 3 MHz transducer in tissue (depth 10-13cm) showing (a) steady-state compressional pressure vs. depth at 1MHz (b) steady state rarefactional peak pressure vs. depth at 1MHz (c) steady state compressional pressure vs. depth at 3MHz (d) steady state rarefactional peak pressure vs. depth at 3MHz.

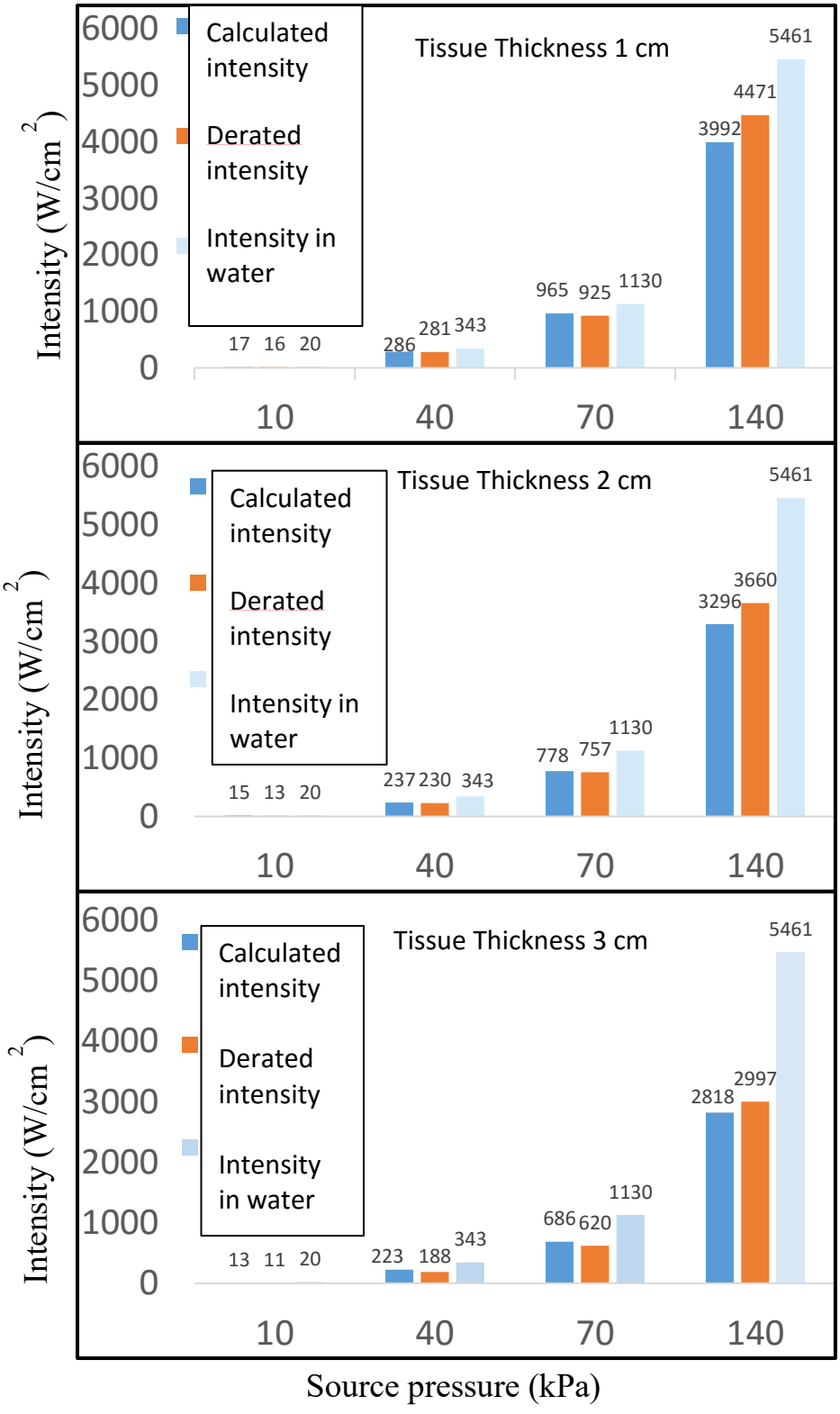

Figure 3.12: Results of peak focal intensities in tissue at 1MHz for various tissue thicknesses

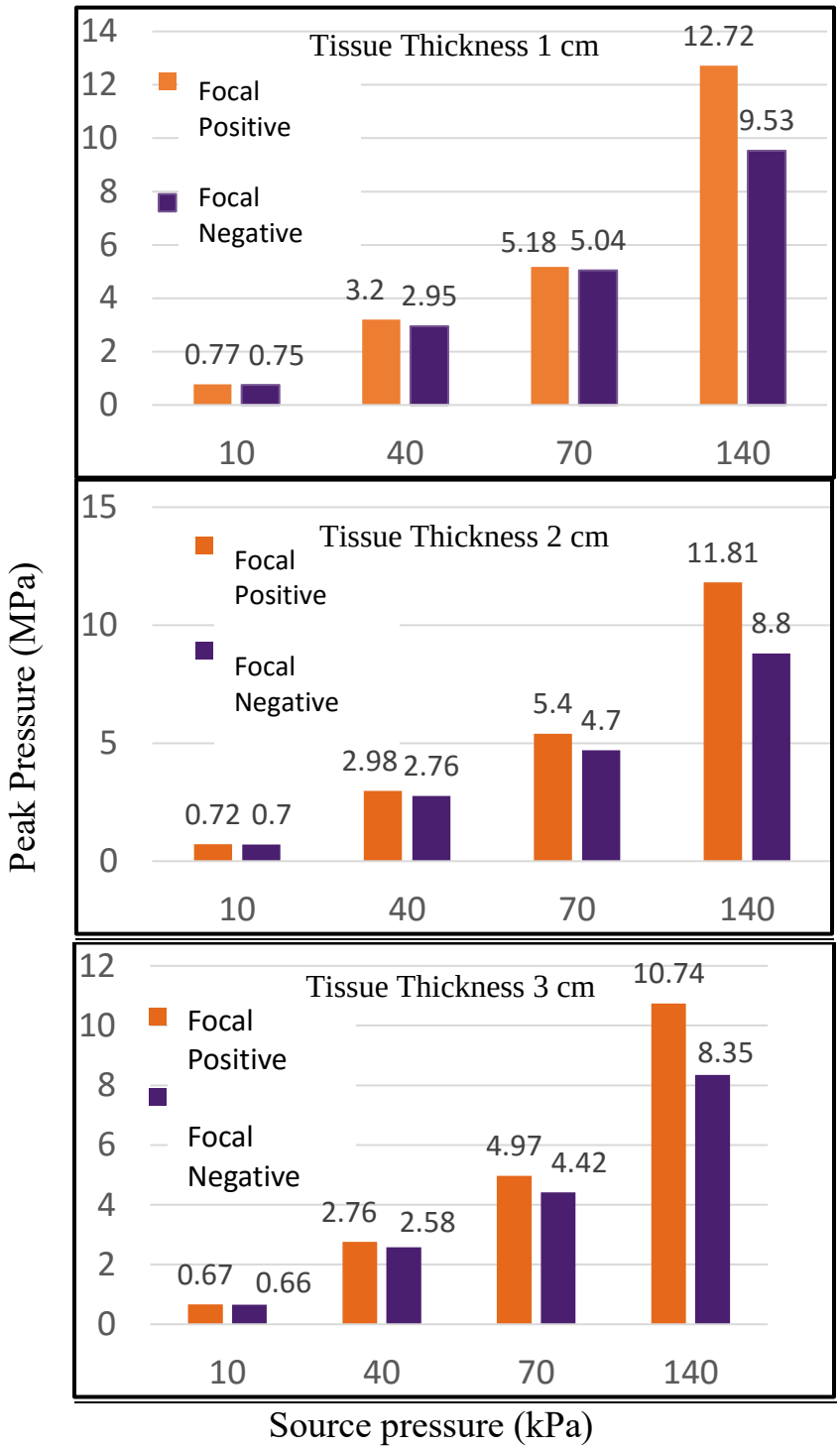

Figure 3.13: Results of peak focal pressures in tissue at 1MHz for various tissue thicknesses

Shown in figure 3.14 are the calculated intensities (y-axis) versus derated intensities for each tissue depth; the black dashed line is what the curve would look like if the two intensities were equal. The reason for making this plot was to find the proper exposure time for each depth. Then we made three graphs separately for 1 and 3 MHz as can be seen in figures 3.15 and 3.16, for the calculated values of intensity (a) along with its log-log plot (b), positive pressures (c) along with its log-log plot (d), and negative pressures (e) along with its log-log plot (f), all versus the exposure times (x-axis) that we just calculated for each tissue depth. The results of these figures could be correlated with the intensity numbers published in the previous paper at given exposure times [26] in which it has been suggested empirically that on a log-log plot in Figure 3.17 , intensity as a function of exposure time can produce lesions at three different regions, as discussed in section 2.5.

By looking into the data of the table 3.6 (a) and (b) and figures 3.15 and 3.16, the true shape of intensity curve vs exposure time can be estimated accordingly. We observed that, as an example, for tissue thickness of 3 cm at 1 MHz, intensity increases from 13.42 to 2818.10 W/cm^2 while the corresponding duration of exposure is decreased from 837.12- 0.011 sec. The same behavior can be observed for other tissue thicknesses at both 1 and 3 MHz.

We also observed that the positive and negative peak pressures are increased while the exposure time is decreased. An actual shape of the pressure curve vs the exposure time could also be estimated, as it is shown in figs 3.15 and 3.16. As can be seen in figures 3.15 and 3.16 (f), the threshold positive and negative pressures for various tissue thicknesses versus exposure time conditions are similar in the log-log plot and appear to increase with decreasing the pulse length as shown in figs 3.15 and 3.16 (e) , for both 1 and 3MHz. Moreover it can be seen from figures

3.15 and 3.16 (e) that the threshold peak pressures increase with increasing ultrasound frequency from 1 to 3MHz.

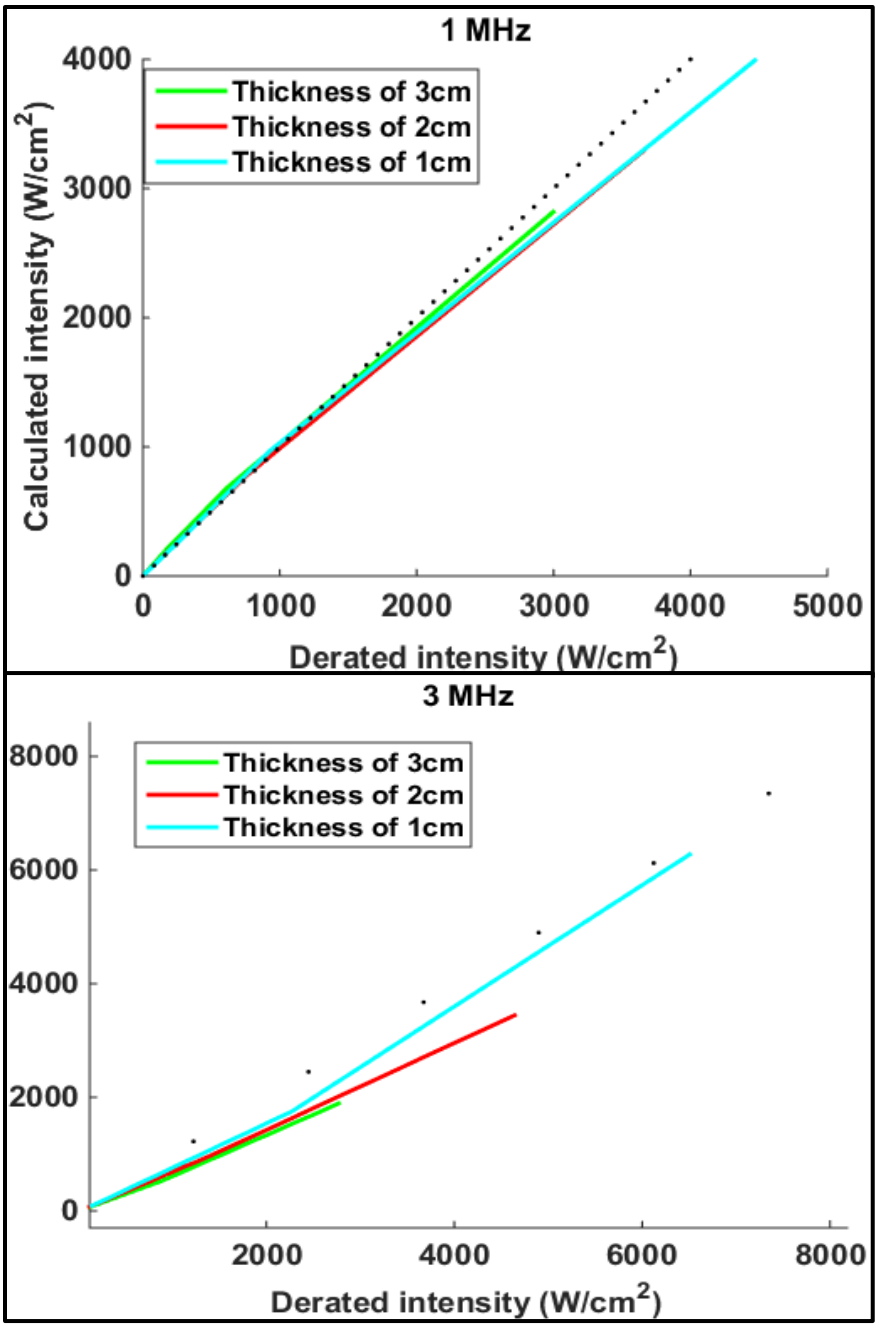

Figure 3.14: The calculated intensities using the simulation vs derated intensities using formula in the paper at 1 and 3 MHz frequencies for various tissue thicknesses

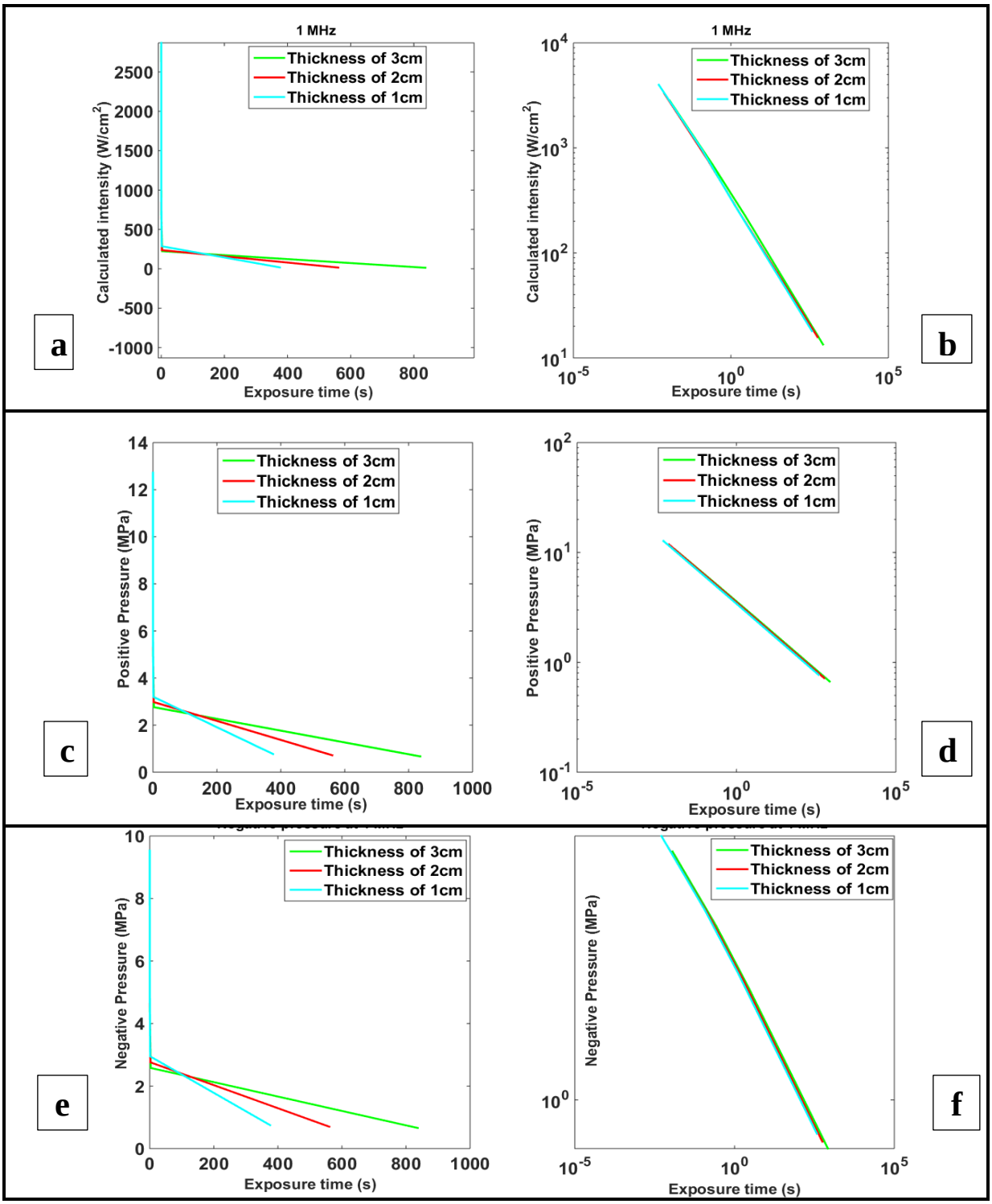

Figure 3.15: Calculated intensity (a), Positive pressure (c), and Negative pressure (e) vs exposure times at different tissue thicknesses at 1MHz along with their log-log plots (b), (d), and (f).

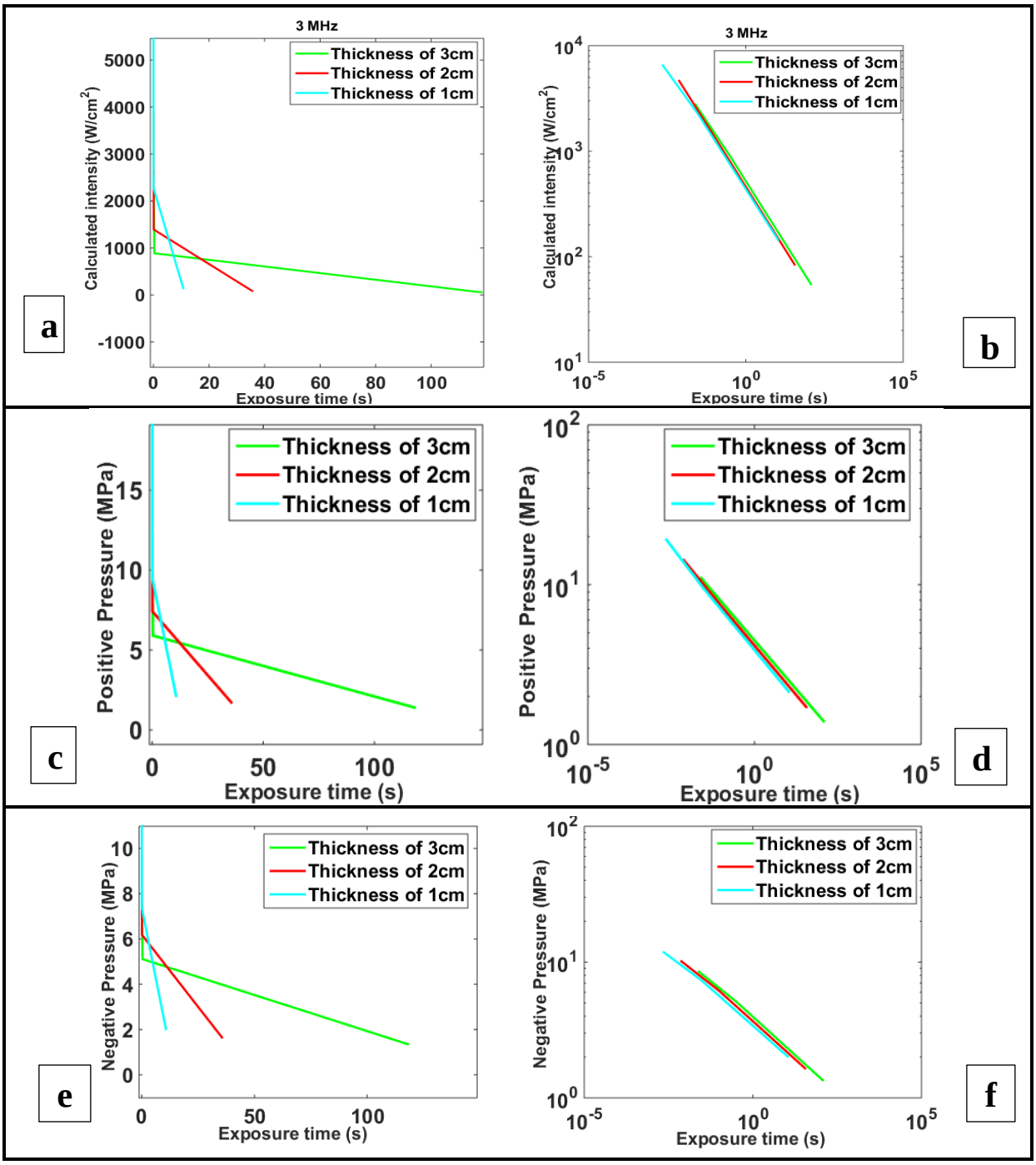

Figure 3.16: Calculated intensity (a), Positive pressure (c), and Negative pressure (e) vs exposure times at different tissue thicknesses at 3 MHz along with their log-log plots (b), (d), and (f).

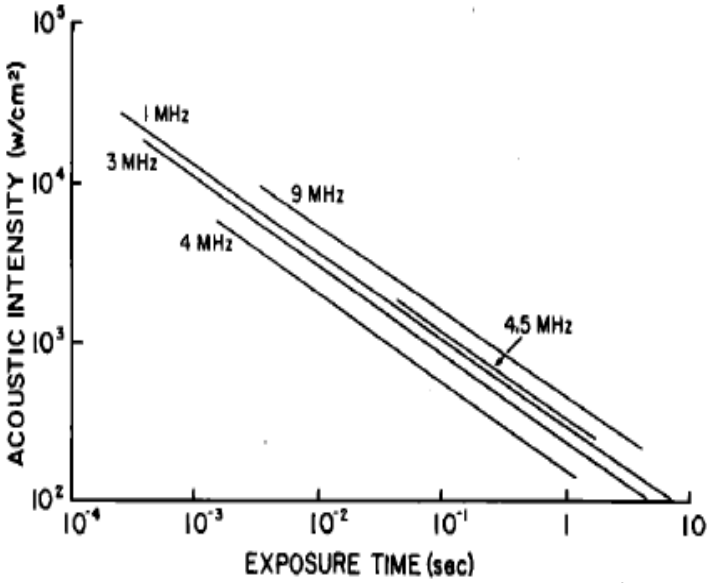

TABLE II. Statisitcally relevant data of Fig. 1.

f (MHz)	Number of threshold loci determining threshold curve	Slope† of threshold curve, $b \pm e$ (W/cm²/sec)	Threshold intercept function† $c = I_0 t_0^{b \pm e}$ (W/cm²/t^b)
1	7	−0.536 ± 0.059	320^{+90}_{-70}
3	12	−0.512 ± 0.035	300^{+52}_{-44}
4	6	−0.456 ± 0.064	248^{+61}_{-49}
4.5	4	−0.512 ± 0.343	347^{+114}_{-86}
9	12	−0.512 ± 0.037	489^{+96}_{-68}

Figure 3.17: Threshold acoustic intensity at the irradiation site versus duration required for a single pulse to produce a lesion in the mammalian brain, with relevant data of figure. [26]

CHAPTER IV:

CONCLUSION AND DISSCUSION

4.1 Remarks, Conclusions, and Dissuasions

In this work, we were able to compare the acoustic field measurements from a previous study to equivalent measurements made using modern techniques. Although it was difficult, we attempted to make use of the data from the previous study for the purpose of our research to make it convenient to support scientifically. In order to support the solutions for the problems we addressed in the motivation section, the study followed a 3-step process:

1. The acoustic pressure and intensity waveforms were calculated numerically using FDTD solutions to correlate with published experimental data of previous investigations.

2. The model was verified through comparison with experiments run in a water bath instrumented for *in situ* pressure measurement. Relevant physical properties were independently determined. The measurement and computations agreed very well to support the model of field experiment done by Dunn et al [26].

3. This verified numerical model was used to investigate the true shape of the curves for threshold pressure and intensity versus exposure time to estimate the true cavitation threshold and possibly other mechanisms.

As indicated above, in order to better understand the simulation process in water-tissue media, we used a model that coupled ultrasound propagation based on an inhomogeneous wave equation derived from the basic equations of fluid mechanics and thermodynamics for a thermoviscous fluid, keeping terms up to second order; it is thus appropriate for simulating the propagation of finite amplitude sound in biological media. The equation accounts for the combined effects of diffraction, inhomogeneity, absorption, and nonlinearity. The model also captured nonlinearity which has been found to play an essential role on the generation of harmonics in an

ultrasonic beam, in particular, from a strongly focusing source. The model equations were numerically solved via a finite difference method imposing appropriate initial and boundary conditions given all acoustical and physical properties for water and tissue with three different tissue thicknesses.

The result was a 2-D numerical simulation of the pressure and intensity in both water and tissue coupled to a 2-D nonlinear acoustic propagation model. For the purpose of our numerical model, we assumed all tissue inhomogeneity was weak, (to avoid any significant impedance mismatches) and the only parameters used in our model were density, speed of sound, nonlinearity parameter, and attenuation coefficient, and that the pressure and intensity calculations could be run in 2-D.

In order to verify the model, we undertook a series of *in vitro* experiments in a water scan tank. This experiment was designed only to provide a verification of the mathematical model's predictions as well as the model of field experiment done by Dunn et al. Good agreement between experimental data and numerical model predictions was found over a range of values for acoustic source pressure and insonation time.

We then conducted a series of simulations that address two types of wave propagation of interest: the linear and nonlinear wave propagation using lower and higher driving level. We employed water-tissue (cat brain) properties while neglecting the blood vessels and ventricles. We considered a 2-D geometry for our simulation. The results showed that the pressure and intensity waveforms at water and tissue behaved almost the same, except for a slight difference at pressure and intensity amplitude in tissue due to the higher attenuation coefficient and more distorted waves because of harmonic generation, as explained in detail above.

The results may be summarized in the following conclusions: both linear and non-linear wave propagation successfully explained the behavior of the computed pressure waveforms at low and higher source pressures and the focal intensities were matched with experimentally determined values from previous study reported in the range of $10^2 - 2 \times 10^4\ \mathrm{W/cm^2}$,as described in literature review. For higher source pressures typically used in therapeutic medical applications, the focal field parameters (peak pressures and intensities) derated more compare to water, as we expected, and agreed well with numerical simulation in tissue. Results of derated intensities helped us to compute the pulse lengths, time duration of exposures which have a significant impact on cavitation threshold using published relation ($I = \frac{c(f,T)}{\sqrt{t}}$) to estimate the true shape of the curve for cavitation threshold.

In order to solve the difficulties of previous study scientifically, we placed this work in the context of the modern scheme. As described in the objective and motivation section, the previous study was not focused primarily on studying cavitation in tissue, at least not the type of cavitation the Mechanical Index was designed to predict. That is there were no measurements of acoustics emissions specific to inertial cavitation; there were no search for the lesions expected to be produced by inertial cavitation at threshold exposures.

The mechanical index (MI) is the magnitude of the negative acoustic pressure divided by the square root of the frequency of an ultrasonic field, $MI = P_{\mathrm{r}}/\sqrt{f}$ [51]. The MI provides an estimate of the likelihood of mechanical damage in tissue.

As described in the literature review, the data from the previous study suggest that the duration of excitation has a significant impact on the cavitation threshold. From a mechanistic point of view and from the University of Illinois suggest that the probability that exposure to

diagnostic ultrasound will induce cavitation in tissue (not containing pre-existing cavitation nuclei) is essentially zero [1], [25], [26], [51]. Based on their results, the pulse durations were found to be only in the range of $2.5 - 5 \times 10^{-4}\ sec$, while in our calculations, particularly, for 10 kPa, the values of exposure times are longer than those results from Dunn measurements and even longer than any other cases for 40, 70, and 140 kPa we made in our calculations. Therefore, only shortest duration of exposures were considered in our calculations. The same behavior can be seen for intensity numbers.

In order to estimate the true shape of the cavitation threshold in our current study, the rarefactional peak pressures (negative peak pressures) as a function of exposure times was considered since the negative pressures are the natural places that we can talk about cavitation. The data in Table 3.6 (a) and (b) and the plot of the negative pressure picks as a function of exposure time is given in figures 3.15 and 3.16 (e) and (f). The values for all tissue thicknesses of 1, 2, and 3 cm are shown in blue, red, and green curves, respectively, for the cat brain. As can be seen in figures 3.15 and 3.16 (f), the threshold negative pressures for various tissue thicknesses versus exposure time conditions are similar in the log-log plot and appear to increase with decreasing the pulse length as shown in figs 3.15 and 3.16 (e), for both 1 and 3MHz. Moreover it can be seen from figures 3.15 and 3.16 (e) that the threshold peak pressures increase with increasing ultrasound frequency from 1 to 3MHz.

By looking through the values of MI at 1 MHz, ranging from 0.66 to 9.53 compared to 3 MHz, ranging from 0.79 to 11.82, in can be concluded that the range of MI at 3 MHz are much more higher than 1MHz, thus the threshold for inertial cavitation is predicted to increase with frequency as mentioned and expected by previous study.

Negative pressure data of table 3.6 (a) shows the threshold of the negative pressure for 3 cm thickness is about 4.42 MPa (source pressure 70kPa) occurs at frequency of 1MHz, which corresponds to MI of about 4.42; this is above the usual diagnostic frequency range. The lowest value in the diagnostic range, 5MPa, is found at 1 MHz, or MI= 5.0, or more than 2 ½ times the current maximum MI in the guidance on substantial equivalent from the US FDA. (Based on FDA, MI maximum was found to be 1.9) [51]. Thus it be can concluded that the values of MI from the pressure threshold and from the diagnostic range, are both higher than the equivalent theoretical values for the cavitation threshold values suggest that this tissue may not contain pre-existing gas bubbles. Therefore, there should exist a limitation for acoustic pressure threshold in the medium to provide a safety margin. Likewise at 3 MHz, the MI corresponds to about 4.91, which shows the same fact as 1MHz. The summary of these data given in Table 4.1 reveals a wide range of pressure threshold values which could be attributed to cavitation detection method.

Table 4.1 (a): Summary of the calculations determined cavitation threshold in tissue at 1MHz

Tissue thickness 1cm (12-13 cm)

Source Pressure (kPa)	**Negative Pressure (MPa)**	**Exposure Time (sec)**	**MI** $(\frac{p}{\sqrt{f}})$
10	0.75	376.12	0.75
40	2.95	1.29	2.95
70	5.04	0.11	5.04
140	9.53	0.005	9.53

Tissue thickness 2 cm (11-13 cm)

Source Pressure (kPa)	**Negative Pressure (MPa)**	**Exposure Time (sec)**	**MI** $(\frac{p}{\sqrt{f}})$
10	0.70	561.03	0.70
40	2.76	1.93	2.76
70	4.70	0.17	4.70
140	8.80	0.007	8.80

Tissue thickness 3 cm (10-13 cm)

Source Pressure (kPa)	Negative Pressure (MPa)	Exposure Time (sec)	MI $(\frac{p}{\sqrt{f}})$
10	0.66	837.12	0.66
40	2.58	2.88	2.58
70	4.42	0.26	4.42
140	8.35	0.011	8.35

Table 4.1 (b): Summary of the calculations determined cavitation threshold in tissue at 3 MHz

Tissue thickness 1 cm (12-13 cm)

Source Pressure (kPa)	Negative Pressure (MPa)	Exposure Time (sec)	MI $(\frac{p}{\sqrt{f}})$
10	2.02	10.71	1.17
40	7.37	0.02	4.25
70	11.81	0.002	6.81

Tissue thickness 2 cm (11-13 cm)

Source Pressure (kPa)	Negative Pressure (MPa)	Exposure Time (sec)	MI $(\frac{p}{\sqrt{f}})$
10	1.65	35.57	0.95
40	6.18	0.09	3.57
70	10.14	0.007	5.85
140	18.40	8.63×10^{-5}	10.62

Tissue thickness 3 cm (10-13 cm)

Source Pressure (kPa)	Negative Pressure (MPa)	Exposure Time (sec)	MI $(\frac{p}{\sqrt{f}})$
10	1.35	118.14	0.77
40	5.11	0.32	2.95
70	8.51	0.02	4.91
140	14.90	2.86×10^{-4}	8.60

4.2 Suggestion for future study

Many more simulations could be performed based on the current numerical model. The current version of the finite difference software had a lot of problems with computations. Some of these were because we had to go to a very small spatial step size and we also needed a large spatial domain since we had a long focal length transducer. This caused many failures. There were also large spaces that do not really need small step sizes.

There are several components to the model, each of which may be individually improved. One solution to these problems would be to dynamically assign some of the integration parameters or to divide the space into different regions where different step sizes can be used. This would be really time-saving. In that case, we would not need to go through all of the current steps such as input files into Matlab, compute the indices, go to the code, enter the parameters, make sure these build properly, and check to see that it all works. Although such a code may not be totally user-friendly, it will reduce runtime errors, and therefore the software would be a more flexible FDTD code that we could use for more general purposes. Such studies remain for the next student to perform.

BIBLIOGRAPHY

[1] Dunn, F. and Fry, F. J. *Ultrasonic Threshold dosages for the mammalian central nervous system*. IEEE Trans. Biomed. Engr. 1971.

[2] Nick Joyce. David B.Baker. *The Galton Whistle*. Asso. Pysh. Scie. Vol22, No.3 March 2009.

[3] Novelline, R. Squire's .*Fundamentals of Radiology (5th Ed.).* Harvard University Press. pp. 34 35. *ISBN 0-674-83339-2*. 1997.

[4] Fry, W. J. *Intense ultrasound in investigations of the central nervous system. I*n advances in medical and biological physics, PP281-348, Ed by J. H Lawrence and C.A .Tobias, NY.1958.

[5] Wesley L. Nyberg. *Biological Effect of Ultrasound: Development of Safety Guidelines, Part I: Personal Histories.* Physics Department, University of Vermont, Burlington, VT 05405, USA.

Biological effects of ultrasound: Development of safety guidelines. Part II: General review. Ultrasound Med Biol 2001; 27:301–33.

[6] F. J. Fry and F. Dunn. *Threshold ultrasound dosages for the structural changes in the Mammalian brain.* J. Acoustic. Soc. Amer., vol. 48, 1970, pp. 1413-1417.

[7] Douglas Miller, Nadine Smith. *Overview of Therapeutic Ultrasound Applications and Safety Conditions.* J Ultrasound Med. 2012 Apr; 31(4): 623-634.

Ozgur Erdogan, Emin Esen, *Biological Aspect and Clinical Importance of Ultrasound Therapy*. American Institute of Ultrasound in Medicine. J Ultrasound Med 2009; 28:765-776.

[8] Dunn, F. and O'Brien, W. D. *Ultrasonic Biophysics.* Vol. 7, 1976.

[9] Robison, T. C. and Lele, P. P. *An analysis of lesion development in the brain and in plastics by high-intensity focused ultrasound at low-megahertz frequencies*. J. Acous. Soc. 1972.

[10] Chou et al. *Cochlear micro-phonics generated by microwave pulses*. J Microwave Power 10:361–367. 1975.

[11] Taylor E.M, Ashleman B.T. *Analysis of central nervous system involvement in the microwave auditory effect*. Brain Res; 1974, 74:201–208.

[12] Guy et al. *Microwave induced acoustic effects in mammalian auditory systems and physical materials*. Ann NY Acad Sci 247: 1975, 194–215.

[13] Lin J. C. *Microwave-induced hearing: Some preliminary theoretical observations*. J Microwave Power; 1976a, 11:295–298.

[14] Floyd Dunn, *Ultrasound Bio effects and Clinical Diagnostic Relevance*. Jpn. J. Appl. Phys. Vol. 36. Pp.2946-4950. 1997

[15] Asha M.L, Rajarathinam, Arun Kumar G, Poulomi Dey. *Ultrasound in Dentistry- A Review of Literature.* American Journal of Oral Medicine and Radiology. 2015; 2(4):234-239.

[16] Langevin P, inventor; French patent No. 505, 703. , 1920

[17] F. J. Fry, P. D. Wall, D. Tucker. *The Use of High Intensity Ultrasound in Experimental Neurology.* J. Acoust. Soc. Am., 25:2, 1952.

[18] Harvey E. N: *Biological effects of ultrasonic waves: A general survey*. Biol Bull 1930; 59:306

[19] *Safety standard for diagnostic ultrasound equipment*. J Ultrasound Med 1983; 2:S1–50.

[20] Lehmann, J. F. *The biological mode of action of biologic and therapeutic ultrasound reactions*. J. Acoust. Soc. Am., 25:17-25, 1953.

[21] Herrick, J. F. *Temperature produced in Tissue by Ultrasound: Experimental Study Using Various Technics.* J. Acoust. Soc. Am., 25:12-16, 1953.

[22] W. J. Fry, F. J. Fry, W. H. Mossberg. *The central nervous system with Ultrasound.* Bioacoustics Lab, University of Illinois, Urbana, Illinois, 1954.

[23] J. W. Barnard, W. J. Fry, F. J. Fry. *Effect of High Intensity Ultrasound on the Central Nervous System of the Cat.* Bioacoustics Lab, University of Illinois, Urbana, Illinois, 1955.

[24] W. J. Fry. *Brain Surgery by Sound*. Office of Naval Research, Dep. Of. The. Navy. Washington, D. C. 1953.

[25] F. J. Fry and F. Dunn. *Threshold ultrasound dosages for the structural changes in the Mammalian brain.* J. Acoustic. Soc. Amer., vol. 48, 1970, pp. 1413-1417

[26] F. J. Fry and F. Dunn, *"Frequency dependence of threshold ultrasonic dosages for irreversible structural changes in mammalian brain,"* J. Acoustic. Soc. Amer., vol. 58, 1975, pp. 512-514.

[27] W. J. Fry, V. J. Wulff, D. Tucker, and, F. J. Fry. *Physical Factors involved in ultrasonically Induced Changed in Living System: I. Identification of Non-Temperature Effects.* J. Acoustic. Soc. Amer., vol. 22:6. 1950.

[28] W. J. Fry, V. J. Wulff, D. Tucker, and, F. J. Fry. *Physical Factors involved in ultrasonically Induced Changed in Living System: I. Amplitude Duration Relations and Effect of Hydrostatic Pressure for Nerve Tissue.* J. Acoustic. Soc. Amer., vol. 23:3. 1950.

[29] W.J. Fry, J. W. Barnard, F. J. Fry. *Ultrasonic Lesions in the Mammalian Central Nervous System*. Amer. Assoc. Advancement. Science. Vol. 122, No.3168, 1955.

[30] W J. Fry and Ruth Baumann Fry, *Determination of Absolute Sound Levels and Acoustic Absorption Coefficients by Thermocouple Probes. Experiment,* J. Acoustic. Soc. Amer., vol. 26:3. 1953. & W J. Fry and Ruth Baumann Fry, *Determination of Absolute Sound Levels and Acoustic Absorption Coefficients by Thermocouple Probes. Theory.* J. Acoustic. Soc. Amer., vol. 26:3. 1953

[31] R. M. Lerner, E. L. Carstensen, F. Dunn. *Frequency dependence of thresholds for ultrasonic production of thermal lesion in tissue.* Vol.54, No2 1973.

[32] W J. Fry and Ruth Baumann Fry. *Temperature Changes Produced in Tissue during Ultrasonic Irradiation.* J. Acoustic. Soc. Amer., vol. 25, No.1, 1952.

[33] T. F. Hueter, H. T. Ballantine, Jr., and, W. C. Cotter. *Production of Lesions in the Central Nervous System with Focused Ultrasound: a Study of Dosage Factors.* J. Acoustic. Soc. Amer., vol. 28:2. 1955.

[34] W. J. Fry. *Action of Ultrasound on Nerve Tissue- a Review.* J. Acoustic. Soc. Amer. Vol. 25, No.1. 1955.

[35] Wells P.N. *Ultrasonic in medicine and biology.* Phys Med Biol, Vol 22:629–669, 1977.

[36] Burgess SE, Silverman RH, Coleman DJ, et al. *Treatment of glaucoma with high-intensity focused ultrasound.* Ophthalmology; 1986.

[37] Kremkau F.W. *Cancer therapy with ultrasound: a historical review.* J Clin Ultrasound; 1979 7:287–300.

[38] Samulski TV, Grant WJ, Oleson JR, et al. *Clinical experience with a multi-element ultrasonic hyperthermia system: analysis of treatment temperatures.* Int J Hyperthermia; 1990 6:909–922.

[39] Francis J. Fry, Robert F. Heimburger, Larry Gibbons, Reginald C. Eggleton. *Ultrasound for Visualization and Modification of Brain Tissue*. IEEE Transaction on sonic and ultrasonic, Vol.SU-17, No.3, July 1970.

[40] Thomas D. Rossing. *Handbook of Acoustics*. 2nd Ed. Springer. USA

[41] William R. Hendee, E. Russell Ritrnour. *Medical Imaging Physics*, NY, 2002, 4ed. Chap.19.

[42] C. R. Hill, *Physical Principle of Medical Ultrasound*. 2nd Ed. England, 1986.

[43] A. D. Pierce. Acoustics: *An Introduction to Its Physical Principle and Applications.* Acoustical Society of America, NY, 1994.

[44] I. M. Hallaj. *Nonlinear Acoustics in Underwater and Biomedical Applications: Array Performance Degradation and Time Reversal Invariance*, Ph.D. Dissertation, University of Washington, 1999.

[45] C. Labuda. *Enhanced High Intensity Focused Ultrasound Heat Deposition for More Efficient Hemostasis*. Ph.D. Dissertation, University of Mississippi, 2008.

[46] Jinlan Huang. *Heating in Vascular Tissue and Flow-Through Tissue Phantoms Induced By Focused Ultrasound*, Ph.D. Dissertation, Boston University, College of Engineering, 2002.

[47] X. Fan, and K. Hynynen. *Ultrasound surgery using multiple sonications —Treatment time considerations*. Ultrasound in Medicine and Biology, 22(4): 471-482, 1996.

[48] G. Mur. *Absorbing boundary conditions for the finite-difference approximation of the time-domain electromagnetic-field equations*. IEEE Transactions on Electromagnetic Compatibility, EMC-23(4): 377-382, 1981.

[49] Christopher W. Conner, *Simulation Methods and Tissue Property Models for Non-Invasive Transcranial Focused Ultrasound Surgery*. Ph.D. Dissertation, Massachusetts Institute of Technology, 2003.

[50] Duck F. *Physical Properties of Tissue*: A Comprehensive Reference Book. New York, NY: Academic Press; 1990.

[51] Church CC, *Conditionally increased acoustic pressures in non-fetal, non-contrast agent diagnostic ultrasound: a preliminary assessment*. J Ultrasound Med. 2015 Jul 34 (7):1-41.

LIST OF APPENDICES

APPENDIX A

Error Analysis

For the purpose of this thesis, we take the term “error” to refer any form of uncertainty, be it systematic or statistic. First we can say error exists in the simulation due to simplifying model assumptions which affects the accuracy and also uncertainty in the input parameters which affects both accuracy and precision. Because in the FDTD simulation technique, we used discrete time and space that can be one of the limitation for our calculations.

In addition, in practical point, our ability to calculate the intensity and the exposure time values in tissue as shown in Table 3.6 (a) and (b) in Chapter III, is going to be about the precision amounts as shown in Table A1 below. In our calculations, two decimal digits and three significant figures were kept, also in the Mechanical Index calculations, as shown in Table 4.1 (a) and (b), three significant figures were considered, however the relevant values with our model can be reported by maybe the next decimal place or another order of magnitude beyond that to be really meaningful for using this to match to the real data.

APPENDIX B

Finite-Difference Time- Domain Code: Pressure Solution

The following code was used to calculate the pressure and intensity field in the water-tissue domain.

```
            program pressure_nonlinear
c ********************************************************************
c x is transducer axial direction, r is radial
c Imaxp,Jmaxp: specifies the x,r limits of the total simulation space.
c Narray: no. of coords in bowlarray file with coords of transducer surf
c Ntrain: no. of discrete points in source waveform file wtrn10001.trn
c Nmaxp: time index specifying total HIFU on time. Time=Nmaxp*dtp
c ifocusp,jfocusp: Coords. of real focus of transducer. j=1 cyl. symmetry
c ImaxT,JmaxT: specifies the x,r limits for temp space; defined by phantom
size
c Iskin: Distance from front face of transducer to phantom front surface
        implicit none
        integer Imaxp,Jmaxp,Narray,Ntrain,Nmaxp,ifocusp,jfocusp
     & ,ImaxT,JmaxT,Iskin
c ********************************************************************
        parameter(Imaxp=3001,Jmaxp=1301,Narray=1271,Ntrain=18000
     & ,Nmaxp=6000,ifocusp=2601,jfocusp=1,ImaxT=2801
     & ,JmaxT=1271,Iskin=2001)
c ********************************************************************
c drp,dxp,dtp: Discrete spatial and time steps; set in input file
bowl_press.in
c t,timep: t is simulation time, timep is time for pressure calculations;
same value
c cp,rhop,alphap,Betap: speed of sound, density, atten coeff, nonlin.
parameter dummy variable
c xshock,xtarget,xmaxp: axial dist where shock occurs, axial pos of geometric
focus,max x distance in simulation space
c rtarget,rmaxp: radial position of geometric focus, max radial distance in
simulation space
c tmaxp: total simulation time
c pi,period,freq,omega,kwave,lambda: pi,inout wave period,input freq,input
angular freq,wave number,wavelength
c tendtoend,Umax,Mach,train,trainmult: travel time across sim space,max
particle velocity,Mach no,normalized source pressure,pressure amplitude
c Umax,Mach,train,trainmult: max particle velocity, Mach no,input source
wave,pressure amplitude
c pn,pnplus1 etc: pressure and pressure time derivatives as specified in
discretization of equations for FDTD (see Jinlan these pg 40)
c cH2Op,rhoH2Op,alphaH2Op,BetaH2Op: sound speed, density, attenuation
coeff,nonlinearity parameter for water
c ctissuep,rhotissue,aplhaptissue,Betatissue: same parameters as above for
phantom or tissue
c cbloodp,rhoblood,alphablood,Betablood: same parameters as above for blood
or blood mimic
c cvesselp,rhovessel,alphavessel,Betavessel: same parameter as above for
vessel wall
```

```
c Qn,Q,Qmax,pfocusmax,pfocusmin: time indexed intensity, max intensity,max
positive pressure at focus,max negative pressure at focus
c power: acoustic power from source
c H,SA: height of spherical cap formed by transducer bowl,surface area of
transducer
c iradius,oradius,RoC: inner radius of transducer,outer radius of
transducer,radius of curvature of transducer(geometric focus)
        doubleprecision drp,dxp,dtp,t,timep(Nmaxp),cp(Imaxp,Jmaxp)
     & ,rhop(Imaxp,Jmaxp),alphap(Imaxp,Jmaxp),Betap(Imaxp,Jmaxp)
     & ,xshock,xtarget,xmaxp,rtarget,rmaxp,tmaxp,pi,period,freq,omega
     & ,kwave,lambda,tendtoend,Umax,Mach,train(Ntrain),trainmult
     & ,pnplus1(Imaxp,Jmaxp),pn(Imaxp,Jmaxp),pnminus1(Imaxp,Jmaxp)
     & ,pnminus2(Imaxp,Jmaxp),pnminus3(Imaxp,Jmaxp),q1,q2,q3,q4
     & ,cH2Op,rhoH2O,alphaH2O,BetaH2O,ctissuep,rhotissue,alphatissue
     & ,Betatissue,cbloodp,rhoblood,alphablood,Betablood,cvesselp
     & ,rhovessel,alphavessel,Betavessel
     & ,Qn,Q(ImaxT,JmaxT),Qmax,pfocusmax,pfocusmin
     & ,pxmax(Imaxp),pxmin(Imaxp),prmax(Jmaxp),prmin(Jmaxp),power
     & ,H,SA,iradius,oradius,RoC
c ****************************************************************
c i,j: index used for x direction, index used for r direction
c itargetp,jtargetp:
c Nptspercycle: number of points per acoustic cycle in source waveform
c nendtoend,ielement,jelement: travel time index from end to end of sim
space,x-coordinate of transducer surface, r-coordinate of transducer surface
c xorder,Naverage:
c maxvalip,maxvaljp,minvalip,minvaljp
c i0,j0: origin of intensity simulation space (phantom region)
c maxvaliQ,maxvaljQ
        integer i,j,n,m,itargetp,jtargetp,Nptspercycle,decimspace
     & ,decimtime,nendtoend,ielement(Narray),jelement(Narray)
     & ,xorder,Naverage,maxvalip,maxvaljp,minvalip,minvaljp
     & ,i0,j0,maxvaliQ,maxvaljQ
c ****************************************************************
c infile,trainfile,ptracefile,arrayfile: input parameters file,source wave
file,output pressure field file,file with coordinates of transducer surface
c icflag: flag F indicates only water present T indicates phantom present
c Qfile,Qcoordsfile: output intensity field no coordinates file,output
intensity field with coordinates file
c xamplitude,ramplitude: output steady state pressure along x-axis
file,output pressure along radial axis file
c parameters: output file to which some simulation parameters are written
        character*50 infile,trainfile,ptracefile,arrayfile,icflag,Qfile
     & ,Qcoordsfile
     & ,xamplitude,ramplitude,parameters
c ****************************************************************
c infile: input file specifying simulation parameters
        data infile/'bowl_press.in.Sonostat'/
c ****************************************************************
c subroutine: reads in input parameters from infile
        call readparams(drp,dxp,dtp,Nptspercycle,Naverage,xorder
     & ,RoC,oradius,iradius
     & ,trainmult,cH2Op,rhoH2O,alphaH2O,BetaH2O,ctissuep,rhotissue
     & ,alphatissue,Betatissue,cbloodp,rhoblood,alphablood,Betablood
```

```
     & ,cvesselp,rhovessel,alphavessel,Betavessel
     & ,decimspace,decimtime,icflag,infile,trainfile,ptracefile
     & ,arrayfile,Qfile,Qcoordsfile,xamplitude,ramplitude,parameters)
c ****************************************************************
c subroutine: specifies bounding coordinates of simulation space regions;
water, phantom, vessel
        call icfiles(cp,rhop,alphap,Betap,cH2Op,rhoH2O,alphaH2O
     & ,BetaH2O,ctissuep,rhotissue,alphatissue,Betatissue
     & ,cbloodp,rhoblood,alphablood,Betablood,cvesselp,rhovessel
     & ,alphavessel,Betavessel,Imaxp,Jmaxp,Iskin,icflag
     & ,ImaxT,JmaxT)
c ****************************************************************
c subroutine: initializes all parameters to be computed in the program to
zero
        call initialize(dtp,timep,Nmaxp,Imaxp,Jmaxp,pn,pnplus1
     & ,pnminus1,pnminus2,pnminus3,Q,ImaxT,JmaxT,pxmax,pxmin
     & ,prmax,prmin)
c ****************************************************************
c subroutine: reads in input source waveform
        call readtrain(train,n,Ntrain,trainfile)
c ****************************************************************
c subroutine: reads in coordinates of points on transducer surface
        call cylarray(Narray,arrayfile,ielement,jelement
     & ,itargetp,jtargetp)
c ****************************************************************
c subroutine: calculates a set of basic parameters
        call calcparams(rmaxp,drp,Imaxp,Jmaxp,xmaxp,dxp,tmaxp,dtp
     & ,Nmaxp,pi,period,Nptspercycle,freq,omega,lambda,kwave
     & ,tendtoend,nendtoend,trainmult,cH2Op,rhoH2O,BetaH2O
     & ,itargetp,jtargetp,rtarget,xtarget,q1,q2,q3,q4
     & ,xorder,xshock,Umax,Mach,power,SA,H,oradius,RoC)
c ****************************************************************
c writes parameters from calcparams to output file parameters
        print*,'opening output parameters file'
        open(unit=9,file=parameters,form='formatted',status='unknown')
        call displayparams(drp,dxp,dtp,freq,lambda,kwave
     & ,cH2Op,rhoH2O,BetaH2O,Umax,Mach,tmaxp,tendtoend
     & ,xshock,xorder,Nptspercycle,Nmaxp,nendtoend,Imaxp,Jmaxp
     & ,decimtime,rmaxp,xmaxp,itargetp,jtargetp,rtarget,xtarget
     & ,parameters,power,SA,H,RoC,oradius,iradius,trainmult)
        close(9)
c ****************************************************************
c initializes pfocusmax and pfocusmin to zero
        pfocusmax=0.d0
        pfocusmin=0.d0
c ****************************************************************
c opens the ptracefile file:
        print*,'opening ',ptracefile
        open(1,file=ptracefile,form='formatted',status='unknown')
c ****************************************************************
        print*,' ------ start time-stepping ------ '
c time stepping starts here
        t=0.d0
c ****************************************************************
```

```
c loops through time using time index n
        do 11 n=1,Nmaxp
c ********************************************************************
c multiplies input wave train by pressure amplitude; sets source pressures at
points specified by array coordinates
        if (n.le.Ntrain) then
        do 15 m=1,Narray
        pn(ielement(m),jelement(m))=trainmult*train(n)
15        continue
        end if
c ********************************************************************
c subroutine: calculates pressure field using fdtd equations
c        print*, 'Calling fdtd2s2t'
        call fdtd2s2t(pn,pnplus1,pnminus1,pnminus2,pnminus3
     & ,q1,q2,q3,q4,drp,dxp,dtp,Imaxp,Jmaxp
     & ,cp,rhop,alphap,Betap,omega,Narray,ielement,jelement)
c ********************************************************************
c finds pressure amplitude at the real focus at the last cycle
        if (Nmaxp-n.le.Nptspercycle)then
         if (pn(ifocusp,jfocusp).gt.pfocusmax)then
         pfocusmax=pn(ifocusp,jfocusp)
         end if
         if (pn(ifocusp,jfocusp).lt.pfocusmin)then
         pfocusmin=pn(ifocusp,jfocusp)
         end if
        end if
c ********************************************************************
c finds pressure amplitude on axis at the last cycle
        if (Nmaxp-n.le.Nptspercycle)then
        do 13 i=1,Imaxp
         if (pn(i,1).gt.pxmax(i))then
         pxmax(i)=pn(i,1)
         end if
         if (pn(i,1).lt.pxmin(i))then
         pxmin(i)=pn(i,1)
         end if
13      continue
        do 14 j=1,Jmaxp
         if (pn(ifocusp,j).gt.prmax(j))then
         prmax(j)=pn(ifocusp,j)
         end if
         if (pn(ifocusp,j).lt.prmin(j))then
         prmin(j)=pn(ifocusp,j)
         end if
14        continue
        end if
c ********************************************************************
c output pressure snapshot at tendtoend
       if (n.eq.Nmaxp-1) then
         do 1000 i=1,Imaxp
           write(1,110)i,(i-1)*dxp,pn(i,1)
1000   continue
       end if
c outputs pressure at real and geometric focus
```

```
c       if (MOD(n,2).eq.0)then
c        write(1,110)t,pn(ifocusp,jfocusp),pn(itargetp,jtargetp)
c        end if
c ********************************************************************
110   format(3(G12.4, 1x))
c ********************************************************************
c calculates steady-state power in last ten cycles
c z=0 for intensity field output set at phantom edge on z-axis. origin
shifted to i0=i+Iskin where Iskin is the z-coordinate of the phantom edge
        if (n.ge.(Nmaxp-Naverage).and.n.lt.Nmaxp)then
       do 20 j=1,JmaxT
         do 30 i=1,ImaxT-Iskin+1
         i0=i+Iskin-1
         Qn=((3.d0*pn(i0,j)-4.d0*pnminus1(i0,j)+pnminus2(i0,j))
     &   /(2.d0*dtp))**2/(omega*omega*rhop(i0,j)*cp(i0,j))
         Q(i,j)=Q(i,j)+Qn
30       continue
20        continue
        end if
c ********************************************************************
c updates pressure time arrays in time
        call updatep(Imaxp,Jmaxp,pn,pnplus1,pnminus1
     & ,pnminus2,pnminus3)
c ********************************************************************
c prints time index to screen and steps through time by time step unit dtp
c        print*,'n=',n
        if (mod(n,100).eq.0) then
        print*,'timestep=',n
        end if
        t=t+dtp
11     continue
c ********************************************************************
        close(1)
        print*,'finish pressure calculation'
c ********************************************************************
c calculates steady-state intensity field from power
        do 40 j=1,JmaxT
         do 45 i=1,ImaxT
         Q(i,j)=Q(i,j)/DBLE(Naverage)
45         continue
40        continue
c ********************************************************************
c writes steady-state pressure amplitude along x and r to files
xamplitude,ramplitude
        open(3,file=xamplitude,form='formatted',status='unknown')
        do 48 i=1,Imaxp
        write(3,110) (i-1)*dxp,pxmax(i),pxmin(i)
48        continue
        close(3)
        open(4,file=ramplitude,form='formatted',status='unknown')
        do 49 j=1,Jmaxp
        write(4,110) (j-1)*drp,prmax(j),prmin(j)
49        continue
        close(4)
```

```
c ********************************************************************
c writes steady-state intensity field to files Qfile and Qcoordsfile
        open(5,file=Qfile,form='formatted',status='unknown')
        open(15,file=Qcoordsfile,form='formatted',status='unknown')
        do 50 j=1,JmaxT
         do 55 i=1,ImaxT
         write(5,*) Q(i,j)
         write(15,110) (i-1)*dxp,(j-1)*drp,Q(i,j)
55         continue
50        continue
        close(5)
        close(15)
c ********************************************************************
c finds location of maximum intensity
            call maxQ(Q,ImaxT,JmaxT,Qmax,maxvaliQ,maxvaljQ)
c ********************************************************************
c displays the pressure at focus
        print 111,trainmult,pfocusmax,pfocusmin
111   format ('P0=',e14.7,' pfocusmax=',e14.7,' pfocusmin=',e14.7)
c ********************************************************************
c displays where the maximum intensity is:
        print 112,trainmult,Qmax,maxvaliQ,maxvaljQ
112   format ('P0=',e14.7,' Qmax=',e14.7,' @ (',I4,' ',I4,')')
c ********************************************************************
        print*,'......closed acoustic tracefile',ptracefile
        print*,'time now= ',t*1.d6,' microseconds'
c ********************************************************************
        print*,'%%%%%%%%%%%%%%%%%%%%%% DONE
     &%%%%%%%%%%%%%%%%%%%%%%'
          end
c++++++++++++++++++++++++++++++++++++++++++++++++++++++++++++++++++++
c++++++++++++++++++++++++++++++++++++++++++++++++++++++++++++++++++++
        subroutine readparams(drp,dxp,dtp,Nptspercycle,Naverage,xorder
     & ,RoC,oradius,iradius
     & ,trainmult,cH2Op,rhoH2O,alphaH2O,BetaH2O,ctissuep,rhotissue
     & ,alphatissue,Betatissue,cbloodp,rhoblood,alphablood,Betablood
     & ,cvesselp,rhovessel,alphavessel,Betavessel
     & ,decimspace,decimtime,icflag,infile,trainfile,ptracefile
     & ,arrayfile,Qfile,Qcoordsfile,xamplitude,ramplitude,parameters)
c ********************************************************************
        implicit none
c ********************************************************************
        doubleprecision drp,dxp,dtp,trainmult,RoC,oradius,iradius
     & ,cH2Op,rhoH2O,alphaH2O
     & ,BetaH2O,ctissuep,rhotissue,alphatissue,Betatissue
     & ,cbloodp,rhoblood,alphablood,Betablood,cvesselp,rhovessel
     & ,alphavessel,Betavessel
c ********************************************************************
        integer Nptspercycle,xorder,decimspace,decimtime,Naverage
c ********************************************************************
        character*50 infile,trainfile,ptracefile,arrayfile,icflag,Qfile
     & ,Qcoordsfile
     & ,xamplitude,ramplitude,parameters
c ********************************************************************
```

```
        print*,'===called SUBROUTINE READPARAMS'
c read the pressure's input parameters from input file
        open(unit=1,file=infile,status='unknown')
        print*,'opened input file ',infile
        read(1,*)drp,dxp,dtp,Nptspercycle,xorder
        read(1,*)RoC,oradius,iradius
        read(1,*)trainfile
        read(1,*)ptracefile
        read(1,*)trainmult
        read(1,*)icflag,arrayfile
        read(1,*)cH2Op,rhoH2O,alphaH2O,BetaH2O
        read(1,*)ctissuep,rhotissue,alphatissue,Betatissue
        read(1,*)cbloodp,rhoblood,alphablood,Betablood
        read(1,*)cvesselp,rhovessel,alphavessel,Betavessel
        read(1,*)decimspace,decimtime,Naverage
        read(1,*)Qfile
        read(1,*)Qcoordsfile
        read(1,*)xamplitude
        read(1,*)ramplitude
        read(1,*)parameters
        close(1)
        print*,'closed input file ',infile
        print*,'Ending subroutine readparams'
c ***********************************************************************
        return
        end
c+++++++++++++++++++++++++++++++++++++++++++++++++++++++++++++++++++++++
c+++++++++++++++++++++++++++++++++++++++++++++++++++++++++++++++++++++++
c SUBROUTINE ICFILES
c ***********************************************************************
        subroutine icfiles(cp,rhop,alphap,Betap,cH2Op,rhoH2O,alphaH2O
     & ,BetaH2O,ctissuep,rhotissue,alphatissue,Betatissue
     & ,cbloodp,rhoblood,alphablood,Betablood,cvesselp,rhovessel
     & ,alphavessel,Betavessel,Imaxp,Jmaxp,Iskin,icflag
     & ,ImaxT,JmaxT)
c ***********************************************************************
        implicit none
c ***********************************************************************
        doubleprecision cp(Imaxp,Jmaxp),rhop(Imaxp,Jmaxp)
     & ,alphap(Imaxp,Jmaxp),Betap(Imaxp,Jmaxp),cH2Op,rhoH2O
     & ,ctissuep,rhotissue,alphatissue,Betatissue
     & ,BetaH2O,alphaH2O,cbloodp,rhoblood,alphablood,Betablood
     & ,cvesselp,rhovessel,alphavessel,Betavessel
c ***********************************************************************
        integer i,j,Imaxp,Jmaxp,Iskin,ImaxT,JmaxT
c ***********************************************************************
        character*50 icflag
c ***********************************************************************
        print*,'>>>>>>>>> beginning subroutine icfiles'
        do 10 j=1,Jmaxp
         do 20 i=1,Imaxp
         cp(i,j)=cH2Op
         rhop(i,j)=rhoH2O
         alphap(i,j)=alphaH2O
```

```
         Betap(i,j)=BetaH2O
20         continue
10        continue
c ******************************************************************
c icflag value specifies if the simulation domain contains water only or if
it contains a tissue/phantom region
        if (icflag.eq.'F')then
        print*,'using homogen. H2O Ics'
        print*,'Properties of fluid (water):'
        print*,' cH2O= ',cH2Op
        print*,' rhoH2O= ',rhoH2O
        print*,' alphaH2O= ',alphaH2O
        print*,' BetaH2O= ',BetaH2O
        print*,'Ending subroutine icfiles'
        else
        print*,'using inhomogen. H2O,PPO,phantom,blood Ics'
c ******************************************************************
c specifices coordinates of tissue/phantom regions and tissue/phantom
properties in this region
        do 30 i=Iskin,2601
         do 60 j=1,JmaxT
         cp(i,j)=ctissuep
         rhop(i,j)=rhotissue
         alphap(i,j)=alphatissue
         Betap(i,j)=Betatissue
60         continue
30        continue
        print*,'Properties of fluid (tissue):'
        print*,' ctissuep= ',ctissuep
        print*,' rhotissue= ',rhotissue
        print*,' alphatissue= ',alphatissue
        print*,' Betatissue= ',Betatissue
        print*,'Ending subroutine icfiles'
c ******************************************************************
        end if
        return
        end
c+++++++++++++++++++++++++++++++++++++++++++++++++++++++++++++++++
c+++++++++++++++++++++++++++++++++++++++++++++++++++++++++++++++++
        subroutine initialize(dtp,timep,Nmaxp,Imaxp,Jmaxp,pn,pnplus1
     & ,pnminus1,pnminus2,pnminus3,Q,ImaxT,JmaxT,pxmax,pxmin
     & ,prmax,prmin)
c ******************************************************************
        implicit none
c ******************************************************************
        integer n,Nmaxp,i,j,Imaxp,Jmaxp,ImaxT,JmaxT
c ******************************************************************
        doubleprecision dtp,timep(Nmaxp),pn(Imaxp,Jmaxp)
     & ,pnplus1(Imaxp,Jmaxp),pnminus1(Imaxp,Jmaxp)
     & ,pnminus2(Imaxp,Jmaxp),pnminus3(Imaxp,Jmaxp),Q(ImaxT,JmaxT)
     & ,pxmax(Imaxp),pxmin(Imaxp),prmax(Jmaxp),prmin(Jmaxp)
c ******************************************************************
        print*,'===called SUBROUTINE INITIALIZE'
c ******************************************************************
```

```
        print*,'...initializing pressure timewise arrays'
        do 10 n=1,Nmaxp
        timep(n)=dtp*(n-1)
10      continue
c initialize pressure field to zero everywhere:
        print*,'...initializing press. fields'
        do 20 i=1,Imaxp
        pxmax(i)=0.d0
        pxmin(i)=0.d0
         do 30 j=1,Jmaxp
         pn(i,j)=0.d0
         pnplus1(i,j)=0.d0
         pnminus1(i,j)=0.d0
         pnminus2(i,j)=0.d0
         pnminus3(i,j)=0.d0
30         continue
20        continue
       do 40 j=1,Jmaxp
       prmax(j)=0.d0
       prmin(j)=0.d0
40       continue
c ***********************************************************************
       do 25 j=1,JmaxT
        do 35 i=1,ImaxT
        Q(i,j)=0.d0
35        continue
25       continue
c ***********************************************************************
       print*,'Ending subroutine initialize'
       return
       end
c+++++++++++++++++++++++++++++++++++++++++++++++++++++++++++++++
c+++++++++++++++++++++++++++++++++++++++++++++++++++++++++++++++
       subroutine readtrain(train,n,Ntrain,trainfile)
       implicit none
       doubleprecision train(Ntrain)
       integer n,Ntrain
       character*50 trainfile
       print*,'===called SUBROUTINE READTRAIN'
c read in wave train data file:
       print*,'...reading source condition ',trainfile
       open(unit=1,file=trainfile,status='unknown')
       do 10 n=1,Ntrain
       read(1,*) train(n)
10       continue
       close(1)
       print*,'......closed ',trainfile
       print*,'Ending subroutine readtrain'
       return
       end
c+++++++++++++++++++++++++++++++++++++++++++++++++++++++++++++++
c+++++++++++++++++++++++++++++++++++++++++++++++++++++++++++++++
c SUBROUTINE cylarray
c ***********************************************************************
```

```
      subroutine cylarray(Narray,arrayfile,ielement,jelement
     & ,itargetp,jtargetp)
c ****************************************************************
      implicit none
c ****************************************************************
      integer n,Narray,ielement(Narray),jelement(Narray)
     & ,itargetp,jtargetp
c ****************************************************************
      doubleprecision itargetp0,jtargetp0,ielement0,jelement0
c ****************************************************************
      character*50 arrayfile
c ****************************************************************
      print*,'>>>>>>>>>> CALLED SUBROUTINE cylarray'
c ****************************************************************
c line 1 of point source coordinates lists coordinates of geometric focus
c subsequent lines indicate coordinates of point sources on transducer
surface
      open(1,file=arrayfile,form='formatted',status='unknown')
      read(1,*) itargetp0,jtargetp0
      itargetp = INT(itargetp0)
      jtargetp=INT(jtargetp0)
      do 20 n=1,Narray
      read(1,*) ielement0, jelement0
      ielement(n)=INT(ielement0)
      jelement(n)=INT(jelement0)
20      continue
      close(1)
c ****************************************************************
      return
      end
c+++++++++++++++++++++++++++++++++++++++++++++++++++++++++++++++++
c+++++++++++++++++++++++++++++++++++++++++++++++++++++++++++++++++
      subroutine calcparams(rmaxp,drp,Imaxp,Jmaxp,xmaxp,dxp,tmaxp,dtp
     & ,Nmaxp,pi,period,Nptspercycle,freq,omega,lambda,kwave
     & ,tendtoend,nendtoend,trainmult,cH2Op,rhoH2O,BetaH2O
     & ,itargetp,jtargetp,rtarget,xtarget,q1,q2,q3,q4
     & ,xorder,xshock,Umax,Mach,power,SA,H,oradius,RoC)
c ****************************************************************
       implicit none
c ****************************************************************
       doubleprecision rmaxp,drp,xmaxp,dxp,tmaxp,dtp,pi,period,freq
     & ,omega,lambda,kwave,tendtoend,Umax,trainmult,Mach
     & ,xshock,rtarget,xtarget,cH2Op,rhoH2O,BetaH2O
     & ,q1,q2,q3,q4,power,SA,H,oradius,RoC
c ****************************************************************
       integer Imaxp,Jmaxp,Nmaxp,Nptspercycle,nendtoend
     & ,itargetp,jtargetp,xorder,i,j
c ****************************************************************
       print*,'===called SUBROUTINE CALCPARAMS'
c ****************************************************************
c calculate some basic run parameters:
       rmaxp=drp*DBLE(Jmaxp-1)
       xmaxp=dxp*DBLE(Imaxp-1)
       tmaxp=dtp*DBLE(Nmaxp-1)
```

```
        pi=ACOS(-1.d0)
        period=dtp*DBLE(Nptspercycle)
        freq=1.d0/period
        omega=2.d0*pi*freq
        lambda=cH2Op*period
        kwave=omega/cH2Op
        tendtoend=xmaxp/cH2Op
        nendtoend=INT(tendtoend/dtp)
        Umax = trainmult/(rhoH2O*cH2Op)
        Mach = Umax/cH2Op
        xshock = 1.d0/(BetaH2O*Mach*kwave)
        H=RoC*(1-COS(ASIN(oradius/RoC)))
        SA=2*pi*RoC*H
        power=trainmult*trainmult*SA/(2*rhoH2O*cH2Op)
c ****************************************************************
c calculate where all the x's are at:
        xtarget=dxp*DBLE(itargetp-1)
        rtarget=drp*DBLE(jtargetp-1)
c ****************************************************************
c these q values are used in the fdtd equations (see Jinlan thesis)
        q1=dtp*dtp/(drp*drp)
        q2=dtp*dtp/(2.d0*drp)
        q3=dtp*dtp/(dxp*dxp)
        q4=2.d0/(omega*omega*dtp)
c ****************************************************************
        print*,'Ending subroutine calcparams'
        return
        end
c++++++++++++++++++++++++++++++++++++++++++++++++++++++++++++++++
c++++++++++++++++++++++++++++++++++++++++++++++++++++++++++++++++
        subroutine displayparams(drp,dxp,dtp,freq,lambda,kwave
     & ,cH2Op,rhoH2O,BetaH2O,Umax,Mach,tmaxp,tendtoend
     & ,xshock,xorder,Nptspercycle,Nmaxp,nendtoend,Imaxp,Jmaxp
     & ,decimtime,rmaxp,xmaxp,itargetp,jtargetp,rtarget,xtarget
     & ,parameters,power,SA,H,RoC,oradius,iradius,trainmult)
c ****************************************************************
        implicit none
c ****************************************************************
        doubleprecision drp,dxp,dtp,freq,lambda,kwave
     & ,cH2Op,rhoH2O,BetaH2O,Umax,Mach
     & ,tmaxp,tendtoend,xshock,rmaxp,xmaxp,rtarget,xtarget,power,SA,H
     & ,RoC,oradius,iradius,trainmult
c ****************************************************************
        integer xorder,Nptspercycle,decimtime
     & ,Nmaxp,nendtoend,Imaxp,Jmaxp,itargetp,jtargetp

        character*50 parameters
c ****************************************************************
        print*,'===called SUBROUTINE DISPLAYPARAMS'
c ****************************************************************
        print*,'opened output parameters file'
        write(9,102) trainmult
102     format('Pressure amplitude=',ES11.4,' Pa')
        write(9,99) power
```

```
99      format('power',G12.4,'W')
        write(9,100) H
100     format('H',G12.4,'m')
        write(9,101) SA
101     format('Surface area',G12.4,'m')
        if (xorder.eq.4) then
        write(9,103) xorder
103     format('calculation is order',I8)
        else
        write(9,104) xorder
104     format('calculation is order',I8)
        end if
        write(9,10) dxp*1.d3
10        format(' ','dx =',G12.4,' mm')
        write(9,15) drp*1.d3
15        format(' ','dr =',G12.4,' mm')
        write(9,20) dtp*1.d6
20        format(' ','dt =',G12.4,' microsec')
        write(9,40) freq/1.d6
40        format(' ','frequency =',G12.4,' MHz')
        write(9,50) Nptspercycle
50        format(' ','no. of samples/period in time =',I8)
        write(9,60) INT(lambda/dxp)
60        format(' ','no. of samples/period in space =',I8)
        write(9,70) lambda*1.d3
70        format(' ','wavelength in 1500 water=',G10.4,' mm')
        write(9,80) kwave
80        format(' ','wave number k =',G10.4)
        write(9,84) cH2Op
84        format(' ','cH2O =',G12.4,' m/sec')
        write(9,86) rhoH2O
86        format(' ','rhoH2O =',G12.4,' kg/m^3')
        write(9,90) BetaH2O
90        format(' ','BetaH2O =',G12.4)
        write(9,200) Umax
200   format('max. particle velocity =',G12.4,' m/sec')
        write(9,210) Mach
210   format('source acoustic Mach no. is about ',G12.4)
        write(9,230) tendtoend*1.d6,nendtoend
230   format('signal can go from end to end in ',F8.4,' microsec'
     & ,' taking',I12,' steps')
        write(9,235) tmaxp*1.d6,Nmaxp
235   format('calculation tmax is at t =',G12.4,'microsec'
     & ,' and Nmax=',I8)
        write(9,240) xtarget*100.d0, itargetp
240   format('focus is at x =',G12.4,'cm and i=',I8)
        write(9,245) rtarget*100.d0, jtargetp
245   format('focus is at r =',G12.4,'cm and j=',I8)
        write(9,250) xmaxp*100.d0,Imaxp
250   format('calculation xmax is at x =',G12.4,'cm and i=',I8)
        write(9,260) rmaxp*100.d0,Jmaxp
260   format('calculation rmax is at r =',G12.4,'cm and j=',I8)
        write(9,270) xshock*100.d0,INT(xshock/dxp)
270   format('shock forms at x= ',G12.4,'cm at i=',I12)
```

```
        write(9,275) xshock*1.d6/cH2Op,INT((xshock/cH2Op)/dtp)
275   format('shock forms at tshock = ',G12.4,'microsec'
     & ,' at Nshock=',I12)
c ****************************************************************
        print*,'Ending subroutine displayparams'
        return
        end
c+++++++++++++++++++++++++++++++++++++++++++++++++++++++++++++++
c+++++++++++++++++++++++++++++++++++++++++++++++++++++++++++++++
        subroutine fdtd2s2t(pn,pnplus1,pnminus1,pnminus2,pnminus3
     & ,q1,q2,q3,q4,drp,dxp,dtp,Imaxp,Jmaxp
     & ,cp,rhop,alphap,Betap,omega,Narray,ielement,jelement)
c ****************************************************************
        implicit none
c ****************************************************************
        doubleprecision pn(Imaxp,Jmaxp),pnplus1(Imaxp,Jmaxp)
     & ,pnminus1(Imaxp,Jmaxp),pnminus2(Imaxp,Jmaxp)
     & ,pnminus3(Imaxp,Jmaxp),z1,z2,z3,z4,z5,z6,z7,drp,dxp,dtp
     & ,q1,q2,q3,q4,cp(Imaxp,Jmaxp),rhop(Imaxp,Jmaxp)
     & ,alphap(Imaxp,Jmaxp),Betap(Imaxp,Jmaxp),omega,r
c ****************************************************************
        integer i,j,Imaxp,Jmaxp,Narray,ielement(Narray)
     & ,jelement(Narray),I0
c ****************************************************************
c Puts in first order Mur BC's at r=rmax, ie, j=Jmax (see Jinlan these pg 43)
        do 310 i=1,Imaxp
        pn(i,Jmaxp)=pnminus1(i,Jmaxp-1)+((cp(i,Jmaxp)*dtp-drp)/
     &  (cp(i,Jmaxp)*dtp+drp))*(pn(i,Jmaxp-1)-pnminus1(i,Jmaxp))
310   continue
c ****************************************************************
c Puts in first order Mur BC's at x=xmax, ie, i=Imax (see Jinlan these pg 43)
        do 300 j=1,Jmaxp
        pn(Imaxp,j)=pnminus1(Imaxp-1,j)+((cp(Imaxp,j)*dtp-dxp)/
     &  (cp(Imaxp,j)*dtp+dxp))*(pn(Imaxp-1,j)-pnminus1(Imaxp,j))
300   continue
c ****************************************************************
c Puts in symmetric BC's at j=1, r=0, makes z2=0 and the 1/r problem vanishes
(see Jinlan these pg 43)
        do 25 i=2,Imaxp-1
        z1=2.d0*(pn(i,2)-pn(i,1))
        z3=pn(i+1,1)-2.d0*pn(i,1)+pn(i-1,1)
        z4=pn(i,1)-3.d0*pnminus1(i,1)+3.d0*pnminus2(i,1)-pnminus3(i,1)
        z5=pn(i,1)*(2.d0*pn(i,1)-5.d0*pnminus1(i,1)
     & +4.d0*pnminus2(i,1)-pnminus3(i,1))
        z6=(3.d0*pn(i,1)-4.d0*pnminus1(i,1)+pnminus2(i,1))**2
        z7=-2.d0*pn(i,1)+pnminus1(i,1)
        pnplus1(i,1)= (cp(i,1)*cp(i,1))*(q1*z1+q3*z3)
     & +cp(i,1)*alphap(i,1)*q4*z4+(2.d0*Betap(i,1)
     & /(rhop(i,1)*cp(i,1)*cp(i,1)))*(z5+z6/4.d0)-z7
25        continue
c ****************************************************************
c Puts in first order Mur BC's at i=ielement(Narray) & i=ielement(1)
        i=ielement(Narray)
        do 30 j=jelement(Narray)+1,Jmaxp-1
```

```
        pn(i,j)=pnminus1(i+1,j)+((cp(i,j)*dtp-dxp)/
     &  (cp(i,j)*dtp+dxp))*(pn(i+1,j)-pnminus1(i,j))
30        continue
c ********************************************************************
c fdtd equations inside cells (see JInlan thesis pg 40)
        do 10 j=2,Jmaxp-1
        r=(j-1)*drp
         if (j.lt.jelement(Narray)) then
         I0=ielement(j)+1
         else
         I0=ielement(Narray)+1
         end if
         do 20 i=I0,Imaxp-1
         z1=pn(i,j+1)-2.d0*pn(i,j)+pn(i,j-1)
         z2=pn(i,j+1)-pn(i,j-1)
         z3=pn(i+1,j)-2.d0*pn(i,j)+pn(i-1,j)
         z4=pn(i,j)-3.d0*pnminus1(i,j)+3.d0*pnminus2(i,j)-pnminus3(i,j)
         z5=pn(i,j)*(2.d0*pn(i,j)-5.d0*pnminus1(i,j)
     &  +4.d0*pnminus2(i,j)-pnminus3(i,j))
       z6=(3.d0*pn(i,j)-4.d0*pnminus1(i,j)+pnminus2(i,j))**2
         z7=-2.d0*pn(i,j)+pnminus1(i,j)
         pnplus1(i,j)=(cp(i,j)*cp(i,j))*(q1*z1+q2*z2/r+q3*z3)
     &  +cp(i,j)*alphap(i,j)*q4*z4+(2.d0*Betap(i,j)
     &  /(rhop(i,j)*cp(i,j)*cp(i,j)))*(z5+z6/4.d0)-z7
20         continue
10          continue
c       print*,'Ending subroutine fdtd2s2t'
        return
        end
c++++++++++++++++++++++++++++++++++++++++++++++++++++++++++++++++++++
c++++++++++++++++++++++++++++++++++++++++++++++++++++++++++++++++++++
        subroutine updatep(Imax,Jmax,pn,pnplus1,pnminus1
     & ,pnminus2,pnminus3)
c ********************************************************************
        implicit none
c ********************************************************************
        doubleprecision pn(Imax,Jmax),pnplus1(Imax,Jmax)
     & ,pnminus1(Imax,Jmax),pnminus2(Imax,Jmax),pnminus3(Imax,Jmax)
c ********************************************************************
        integer i,j,Imax,Jmax
c ********************************************************************
c UPDATES ARRAYS IN TIME AND WRITE PRESSURE TO OUTPUT DATA FILE:
        do 10 j=1,Jmax
         do 20 i=1,Imax
         pnminus3(i,j)=pnminus2(i,j)
         pnminus2(i,j)=pnminus1(i,j)
         pnminus1(i,j)=pn(i,j)
         pn(i,j)=pnplus1(i,j)
20         continue
10        continue
c ********************************************************************
        return
        end
c++++++++++++++++++++++++++++++++++++++++++++++++++++++++++++++++++++
```

```
c++++++++++++++++++++++++++++++++++++++++++++++++++++++++++++++++
        subroutine maxQ(Q,Imax,Jmax,Qmax,maxvali,maxvalj)
        doubleprecision Q(Imax,Jmax),Qmax
        integer i,j,Imax,Jmax,maxvali,maxvalj
        Qmax=Q(1,1)
        maxvalj=1
c finds maximum intensity along acoustic axis
        do 10 i=1,Imax
         if(Q(i,1).gt.Qmax)then
         Qmax=Q(i,1)
         maxvali=i
         end if
10        continue
        return
        end
c++++++++++++++++++++++++++++++++++++++++++++++++++++++++++++++++
c++++++++++++++++++++++++++++++++++++++++++++++++++++++++++++++++
```

APPENDIX C

Matlab code for generating the simulation indices parameters

```
%Calculates indices corresponding to spatial coordinates for FDTD
%pressure simulation domain based on size of spatial steps and size of
domain.

clear all;

%Frequency
frequency=input('Frequency (MHz): ');
frequency=frequency*1e6;
%Speed of sound in water
c=1500;
%Wavelength of source signal (m)
wavelength=c/(frequency);

%Number of spatial grid points per wavelength (10<N<12)
N=10;
%Calculated size of axial grid spacing
dxp=wavelength/N
%Size of axial grid spacing (1 sig fig, floored)
dxp=input('Based on the calculation, user selected (floored) dxp=? :');
%Calculated size of radial grid spacing
drp=wavelength/N
%Size of radial grid spacing (1 sig fig, floored)
drp=input('Based on the calculation, user selected (floored) drp=? :');

%CFL number, determines time step for simulation stability, 0.25>CFL<0.5
CFL=0.5;
%Calculated size of time step
dtp=CFL*dxp/c
%Size of time step (1 sig fig, floored)
dtp=input('Based on the calculation, user selected (floored) dtp=? :')
%Numberof points per cycle in source signal waveform
Nptspercycle=round(1/(dtp*frequency));

xmaxp=input('Max x coordinate of total simulation space (cm): ');
xmaxp=xmaxp*1e-2;
%Maximum i index (axial) of total simulation space
Imaxp=round(xmaxp/dxp)+1;
xmaxT=input('Max x coordinate of temperature space (cm): ');
xmaxT=xmaxT*1e-2;
%Maximum i index of temperature space
ImaxT=round(xmaxT/dxp)+1;
rmaxp=input('Max r coordinate of total simulation space (cm): ');
rmaxp=rmaxp*1e-2;
%Maximum j index (radial) of total simulation space
Jmaxp=round(rmaxp/drp)+1;
rmaxT=input('Max r coodinate of temperature space (cm): ');
rmaxT=rmaxT*1e-2;
%Maximum j index of temperature space
```

```
JmaxT=round(rmaxT/drp)+1;

xfocus=input('x coordinate of geometric focus (cm): ');
xfocus=xfocus*1e-2;
%i index of geometric focus
ifocusp=round(xfocus/dxp)+1;
rfocus=input('r coordinate of geometric focus (cm): ');
rfocus=rfocus*1e-2;
%j index of geometric focus
jfocusp=round(rfocus/drp)+1;

xskin=input('Distance from transducer to phantom surface (cm): ');
xskin=xskin*1e-2;
%i index of distance to phantom surface (axial)
Iskin=round(xskin/dxp)+1;

%Time for acoustic signal to travel through total simulation space
tendtoend=xmaxp/c;
%Index for tendendtoend
tendtoendindex=tendtoend/dtp;

%Frequency dependent attenuation (Np/m/MHz)
alphaw=14e-15*frequency^2;
if frequency==1.0e6
    alphap=0.025;
elseif frequency==3.0e6
    alphap=6.6;
elseif frequency==9.0e6
    alphap=59.4;
end


m=1:8;
n=1:4;

S=struct('dxp',dxp,'drp',drp,'dtp',dtp,'Nptspercycle',Nptspercycle,'Imaxp',Im
axp,'Jmaxp',Jmaxp,'ImaxT',ImaxT,'JmaxT',JmaxT,'Iskin',Iskin,'ifocusp',ifocusp
,'jfocusp',jfocusp,'tendtoendindex',tendtoendindex,'alphap',alphap,'alphaw',a
lphaw)
save simindicespressure.mat
```

Matlab code for generating the transducer coordinate indices

```
% the length unit here is mm
% r --- j; z --- i; array indexes (i, j) begin from 1

clear all;

%R - radius of curvature; a - transducer radius
R=130.0e-3; a=63.5e-3;
%dr - radial grid spacing; dz - axial grid spacing
dr=1.5e-4; dz=1.5e-4;
%N - number of coordinates on bowl surface cross section
N=round(a/dr)+1;
%transducer radius calculated from discretized variables
rtot=(N-1)*dr;

%Creates radial and axial coordinates of points of transducer surface
r=0:dr:rtot;
for n=1:N
    bowlarrayr(n)=r(n);
    theta(n)=asin(r(n)/R);
    bowlarrayz(n)=R-R*cos(theta(n));
end

bowlarrayj=(round(bowlarrayr/dr))'+1;
bowlarrayi=(round(bowlarrayz/dz))'+1;
focusr=0; focusz=R;
focusj=round(focusr/dr)+1; focusi=round(focusz/dz)+1;
arrayn=(1:N)';
%Creates variable with axial, radial indices of transducer surface coords
bowlarray=[focusi focusj
           bowlarrayi bowlarrayj];
plot(bowlarray(:,1),bowlarray(:,2),'bs','linewidth',1), axis equal, grid
hold on, plot(focusi, focusj,'r*'), hold off
text(focusi+30, focusj-30, 'FOCUS')
title('Cylindrical bowl configuration')
xlabel('z grid'), ylabel('r grid')
%Creates dat file with indices of focus in first line and indices of
%transducer surface coordinates following
save bowlarray_Sonostat.dat bowlarray -asc
```

Matlab code for generating the source waveforms

```
%Generates a set of discrete points producing sinusoidal wave

%Speed of sound in water (m/s)
c=1500;
%Maximum axial dimension of simulation space
%xmaxp=6e-2;
xmaxp=input('Maximum x dimension (axial) of total simulation space (cm)= ');
xmaxp=xmaxp*1e-2;
%Source signal frequency (Hz)
frequency=input('Frequency of source (MHz)= ');
frequency=frequency*1e6;
dtp=input('Time step= ');
%Source signal wavelength (m)
wavelength=c/frequency;
%Number of points per cycle in source signal waveform
Nptspercycle=round(1/(dtp*frequency));
%Total number of cycles (number of cycles filling space for CW signal)
T=xmaxp/wavelength;
%Total cycles
T=3*T
%Total number of discretized points for sinusoidal signal
M=Nptspercycle*T;
%Size of discretization
D=2*pi/(Nptspercycle-1);

%Angle in radians
theta(1)=0;
%Sine of angle in radians
train(1)=sin(theta(1));

%Generates discretized sinusoidal wave
for i=2:M
    theta(i)=theta(i-1)+D;
    train(i)=sin(theta(i));
end

Sineplot=figure;
plot(train);
title('Sinusoidal wave')
xlabel('Number of discrete points'), ylabel('Amplitude')
train=train';

i=1:M;
time=i*dtp;
spaceplot=figure
plot(time,train);

%Saves discretized waveform to file
save wtrn.trn train -ascii;
```

VITA

NAZANIN OMIDI

145 Hill Drive• NCPA, University, MS 38677 • (301) 366-1056 • nomidi@olemiss.edu

EDUCATION

MS., Physics, University of Mississippi, August 2016

Concentrations: Biomedical Acoustics

Thesis: Computation of Ultrasonic Pressure Field in Feline Brain

B.S., Atomic and Molecular Physics, Shiraz/Iran, Feb 2010

Thesis: Designing and Manufacturing Optical Lenses

TEACHING EXPERIENCE

- Graduate Teaching Assistant at University of Mississippi; Astronomy Laboratory (Jan 2014 - Present)
- Instructed Astronomy courses in Astrophysics Institute related to the Municipality of Shiraz/Iran (Jun-Aug 2013)
- Instructed Astronomy course in a private elementary school (April 2012-April 2013)
- Performed as Physics and Mathematics tutor. (2008-2010)

RESEARCH EXPERIENCE

- Graduate Research Assistant at the National Center for Physical Acoustics, Department of Physics and Astronomy, University of Mississippi, University, MS National Center for Physical Acoustics (June 2014-Present)

- Performing Master's project focuses on numerically calculation of ultrasound pressure waveforms in cat brain using FDTD simulation technique.
- Performed research in 'Ultrasound Imaging of Brain Injuries' using Terason Ultrasound Machine, develops an imaging method to detect brain injuries from the signals that could get back from Image.

HONORS and FELLOWSHIPS

- The top 20 winners at the 3 Minutes Thesis Competition, Graduate School, The University of Mississippi (October 2015)
- The fourth place winner in the Mississippi INBRE Graduate Scholars Symposium Poster Competition, University of Southern Mississippi (February 2016)

PUBLICATIONS and PRESENTATIONS

- Nazanin Omidi, Charles C. Church, Cecille Labuda , "Computation of Ultrasonic Pressure Fields in Feline Brain" The Journal of the Acoustical Society of America, JASA (April 2016)
- Nazanin Omidi, Charles C. Church, Cecille Labuda , "Computation of Ultrasonic Pressure Fields in Feline Brain" The Journal of the Mississippi Academy of Science, Issued Abstract (Feb 2014 and Feb 2015)

- First Annual UM-MSU Joint Physics Research Symposium (February 2016)
- The Mississippi IDeA Network of Biomedical Research Excellence (INBRE) Symposium, University of Southern Mississippi (February 2016)
- Annual Mississippi Academy of Science Meeting, University of Southern Mississippi (February 2016)
- 3 Minutes Thesis Competition, University of Mississippi (October 2015)
- 8th Annual Mississippi Regional Biophysical Consortium, Poster Presentation (June 2015)
- 5th On-Campus Graduate Research Forum, Thad Cochran Research Center (April 2015)
- Annual Mississippi Academy of Science, University of Southern Mississippi (February 2015)
- Colloquium at Rhodes Collage, Memphis, TN (February 2015)
- APS Conference for Undergraduate Women in Physics at the University of Mississippi (January 2015)